To the Graduate Council:

I am submitting herewith a dissertation written by Konstadia Lika entitled "Interactions of Predator–Prey Ecological Processes and Advective Movement in a Spatially Heterogeneous Environment". I have examined the final copy of this dissertation for form and content and recommend that it be accepted in partial fulfillment of the requirements for the degree of Doctor of Philosophy, with a major in Mathematics.

Thomas G. Hallam, Major Professor

We have read this dissertation
and recommend its acceptance:

Accepted for the Council:

Associate Vice Chancellor
and Dean of The Graduate School

# Interactions of Predator–Prey Ecological Processes and Advective Movement in a Spatially Heterogeneous Environment

A Dissertation
Presented for the
Doctor of Philosophy
Degree
The University of Tennessee, Knoxville

Konstadia Lika
December, 1996

*Στον Μιχαλη*

*και στους γονεις μου*

# ACKNOWLEDGEMENTS

First I must express my deepest thanks to my thesis advisor, Professor Thomas Hallam for his support and encouragement throughout my graduate studies and his kind patience and valuable guidance during the development of this thesis.

I would also like to express my special thanks to Professors Lou Gross, Mark Kot and Suzanne Lenhart for serving on my committee. The comments and feedback they provided and their intriguing questions they posed were invaluable in the development of this work. I wish to thank Professor Donald DeAngelis for serving on my oral examination committee. I wish to express my gratitude to Professor Nicholas Alikakos for the many discussions that have contributed to this work, and Professors Vassilios Dougalis and Georgios Akrivis for their guidance and encouragement during my undergraduate studies.

Special thanks go to my friends and colleagues in the Mathematical Ecology group for helping me through the hard times of graduate school and for the many useful discussions.

The Department of Mathematics and the U.S. Environmental Protection Agency are kindly acknowledged for their financial support during my graduate studies.

As ever I am indebted to my family in Greece, especially my parents Thomas and Erasmia Lika, whose love and understanding are always essential to my success. Finally to Michael, I thank him for his unquestioning love and support in times of happiness and in times of frustration.

# ABSTRACT

Spatial models have been developed based on predator–prey ecological interactions and on a prey–gradient driven movement of the predator. Moreover, the prey species is assumed to be immobile.

We begin by establishing the existence of traveling wave solutions for an aggregated model in which the predator and prey interactions are based on a modified Lotka–Volterra model with logistic growth of the prey. Each predator responds identically to changes in the prey density. The traveling wave solutions discussed here are waves that travel without change in shape and are not necessarily monotone. We find that traveling wave solutions can evolve from asymptotic initial conditions. We also find that steep waves that correspond to slow moving waves, eventually "break".

We numerically investigate the dynamics of an aquatic predator–prey system in a bounded linear habitat. The predator species is physiologically structured according to the age, lipid, and structure (protein and carbohydrates) of an individual. The response of the predator to changes in the prey density depends on physiological characteristics of the individual. The dynamics of the predator population are compared using two movement behaviors, one in which individuals move continuously in the direction of increasing prey and another in which energetic constraints are imposed. The model has been developed for a rainbow trout, *Oncorhynchus mykiss*, population feeding on a *Daphnia* population.

The model has been used to study the effects of nonpolar narcotic toxicants on the fish population which is exposed to a spatially varying toxicant and a dynamic resource. The exposure might occur through the environmental and/or the food pathways.

# Contents

**Overview** 1

**PART I**

**Existence of Traveling Wave Solutions of Reaction–Advection Models** 3

1 Introduction . . . . . 4

2 Single Species Reaction–Advection Model . . . . . 5

3 Predator–Prey Pursuit Model . . . . . 11

4 Phase Plane Analysis . . . . . 15

5 Discussion and future work . . . . . 26

References . . . . . 27

Appendix . . . . . 28

**PART II**

**Prey–Directed Movement for a Structured Fish Population** 53

1 Introduction . . . . . 54

2 Individual Model . . . . . 56

3 The Dynamic Predator–Prey Model . . . . . 63

4 Numerical Procedure . . . . . 66

5 Results . . . . . 68

6 Discussion and future work . . . . . 73
References . . . . . 74
Appendix I . . . . . 78
Appendix II . . . . . 81
Appendix III . . . . . 83

## PART III

**Modeling the Effects of Toxicants on a Fish Population in a Spatially Heterogeneous Environment: Lethal Effects** **107**

1 Introduction . . . . . 108
2 A Physiologically-based Individual Model . . . . . 109
3 Exposure–Effect Model . . . . . 111
4 A Dynamic Population Model . . . . . 114
5 Effects of Toxicants on Population . . . . . 117
6 Discussion . . . . . 120
References . . . . . 121
Appendix . . . . . 124

**Vita** **139**

# List of Figures

**PART I**


1 The vector field of the logistic equation with advection. . . . . 28

2 Profiles of the traveling wave of the logistic equation with advection. . 29

3 Solution of equation (1) starting from initial data (11) with $A = 0.2$, $x_0 = 100$, and $\alpha = 0.1$. . . . . 30

4 The analogue of Figure 3 but with $\alpha = 0.2$. . . . . 31

5 The analogue of Figure 3 but with $\alpha = 0.5$. . . . . 32

6 Stability of the wavefront solution for the logistic equation with advection 33

7 The isoclines for system (I) . . . . . 34

8 The vector field of system (II) on the singularity curve $S$. . . . . 35

9 Parameter domains of stability/instability of the positive steady state $(b, 1-b)$ for system (I). . . . . 36

10 The isoclines $f = 0$ and $g = 0$, and the singularity curve $S$ for $c^2 < b(1-b)$. . . . . 37

11 Schematic phase plane trajectory near the curve $\Gamma$, for the case where $h(u,v) > 0$ and $u' < 0$. . . . . 38

12 The vector field for system (I), and the local stable and unstable manifolds of the saddle points when $c^2 < b(1-b)$ and $ac^2 > b^2$. . . . . 39

13 Local behavior of the vector field for system (I) when $c^2 < b(1-b)$ and $ac^2 > b^2$. . . . . 40

14 The vector field for system (I) when $b < \frac{1}{2}$, $b(1-b) < c^2 < \frac{1}{4}$, and $ac^2 > b^2$. . . . . 41
15 Typical phase plane portrait for system (I) when $b > \frac{1}{2}$, $c > \frac{1}{2}$, $c^2 > 4a(1-b) - 2$, and $ac^2 \leq b^2$. . . . . 42
16 The analogue of Figure 15 but with $b \leq \frac{1}{2}$. . . . . 43
17 Typical phase plane portrait for system (I) when $\frac{1}{2} < b < 1$, $b(1-b) < c^2 \leq \frac{1}{4}$, and $c^2 > 4a(1-b) - 2$. . . . . 44
18 Typical phase plane portrait for system (I) when $b > \frac{1}{2}$, $c > \frac{1}{2}$, $c^2 > 4a(1-b) - 2$, and $ac^2 > b^2$. . . . . 45
19 The analogue of Figure 18 but with $b \leq \frac{1}{2}$. . . . . 46
20 Wavefront solutions of the predator–prey system with initial conditions (26). . . . . 47
21 The vector field for system (I) and the heteroclinic connection, $T$, between $(1,0)$ and $(b, 1-b)$ with $a = 2.5$, $b = 0.7$, and $c = 0.8$. . . . . 48
22 The analogue of Figure 21 but with $a = 4$. . . . . 49
23 The analogue of Figure 21 but with $a = 4.5$. . . . . 50
24 Parameter domains for existence/nonexistence of traveling wave solutions of system (I). . . . . 52

## PART II

1 Threshold boundaries between extinction and persistence for the fish population and resource. . . . . 86
2 Dynamic behavior of the fish population and resource for $a = 0.5$, $K = 10^4$ and $s = 0.1$. . . . . 88
3 Dynamics of the total fish and resource biomass for $\alpha = 0.5$ and $s = 0.1$. (a) $K = 10^3$, (b) $K = 5 \times 10^2$, (c) $K = 3 \times 10^2$. . . . . 90
4 Dynamics of the total fish and resource biomass for $K = 50$. (a) $\alpha = 2.2$, $s = 1.5$, (b) $\alpha = 1.5$, $s = 0.01$. . . . . 91

5 The dynamic fish population on the time interval from 5,000 to 7,000 $d$ as viewed through its (a) age distribution, (b) lipid distribution, and (c) structural distribution . . . . . 93

6 Age distribution of the fish population with $\alpha = 0.5$, $K = 10^4$, and $s = 0.1$ at times (a) $t = t_0$ , (b) $t = t_0 + 150$ , (c) $t = t_0 + P$, and (d) $t = t_0 + P + 150$. . . . . 95

7 The analogue of Figure 6 but for the lipid distribution . . . . . 97

8 Structural distribution of fish at time $t = 5,000$ ($\alpha = 0.5$, $K = 5 \times 10^2$) (a) $s = 1.5$, (b) $s = 0.03$ and (c) $s = 0.009$. . . . . 99

9 Cumulative fish biomass versus the characteristic velocity $s$ of the population ($\alpha = 0.5$). (a) $K = 3 \times 10^2$, (b) $K = 5 \times 10^2$, (c) $K = 10^3$, and (d) $K = 10^4$. . . . . 101

10 Dynamics of the total fish and resource biomass with $\alpha = 2$, $K = 10^3$, and $s = 1.5$. . . . . 102

11 Dynamics of the total fish and resource biomass with $\alpha = 2$, $K = 10^3$, and $s = 0.1$. . . . . 103

12 Dynamics of the total fish and resource biomass with $\alpha = 0.5$, $K = 10^4$, and $s = 0.1$. . . . . 104

13 Comparison of the dynamics of the total fish biomass for continuous movement versus movement based on energetic constraints. . . . . 106

## PART III

1 Relationship between $\log LC_{50}$ and $\log K_{ow}$. . . . . 125

2 Age, lipid, and structural distributions of the fish population with $\alpha = 0.5$, $K = 5 \times 10^2$, and $s = 0.04$ on day 5,000 of the simulation. . . . . 127

3 The analogue of Figure 2 but with $s = 0.05$. . . . . 129

4 Spatial distribution of a chemical with $K_{ow} = 10^5$. Chemical concentration varies from $0.45 \times 10^{-5}$ to $9.9 \times 10^{-5}$ $g/cm^3$ with an average value of $3.57 \times 10^{-5}$ $g/cm^3$. . . . . 130

5 Toxicant exposure case 1: Age, lipid, and structural distributions of the fish population with $s = 0.04$ after the termination of a 7-$d$ environmental exposure initiated on day 5,000. . . . . 132

6 The analogue of Figure 5 but with $s = 0.05$. . . . . 134

7 Age and lipid distributions of the fish population with $\alpha = 0.5$, $K = 5 \times 10^2$, and $s = 0.05$ on day 5,256 of the simulation. . . . . 135

8 Spatial distribution of a chemical with $K_{ow} = 10^5$. Chemical concentration varies from $0.15 \times 10^{-5}$ to $2.0 \times 10^{-5}$ $g/cm^3$ with an average value of $1.06 \times 10^{-5}$ $g/cm^3$. . . . . 136

9 Toxicant exposure case 2: Age and lipid distributions of the fish population with $s = 0.05$ after the termination of a 10-$d$ exposure initiated on day 5,256. . . . . 137

10 Toxicant exposure case 2: Dynamic behavior of the fish population and resource for $a = 0.5$, $K = 5 \times 10^2$ and $s = 0.05$. . . . . 138

# OVERVIEW

In natural environments, an ecological system has heterogeneous spatial structure. This has provided many problems for researchers interested in analyzing spatiotemporal processes and their influence on population dynamics. An important aspect of natural populations is the structural variation within a population which arises from differences in individuals. Partial differential equations are one of the major mathematical tools for incorporating spatiotemporal processes and individual processes simultaneously into equations governing population dynamics.

In this dissertation we use partial differential equations coupled with ordinary differential equations to model populations in which individual movement is dominated by advective processes. By an advective process we mean movement of individuals towards neighboring areas with higher quality, for example, areas where food density is larger.

In Part I, we show how traveling wave solutions occur in two aggregated models. A traveling wave is defined to be a wave which travels without change in shape. In mathematical terms, a solution of the form $u(x,t) = u(x+ct)$ is a traveling wave moving at constant speed $c$ in the negative direction on the $x$–axis. The first model considers a single species population in which the movement of the individuals is directed towards neighboring areas with fewer individuals. At any given spatial position, the population grows according to the logistic equation. This model provides some insight for the analysis of a predator-prey system in which the prey is immobile and predators move in the direction of increasing prey density. Each predator responds identically to changes in the prey density. The specific model we study is a modified Lotka–Volterra system with logistic growth of the prey. We find that traveling wave solutions can evolve from asymptotic initial conditions. We also find that steep waves that correspond to slow moving waves eventually "break".

In Part II, we study the dynamics of an aquatic predator-prey system in a bounded

linear habitat in which the predators move continuously towards the sessile and unstructed prey where the density is the largest. In the absence of predators, at any given spatial location the prey population grows according to the logistic equation and its dynamics are described by an ordinary differential equation. The predator population is structured according to the physiological variables age, lipid, and structure (protein and carbohydrates) and so an individual model is needed to model the dynamics of those physiological variables. The individual model has been developed to deal with rainbow trout, *Oncorhynchus mykiss*, and is based on energetic budget techniques. The movement behavior of the predators is a function of the physiological characteristics of the individual. The dynamics of the predator population are described by an equation of extended McKendrick–von Foerster type. This equation allows incorporation of the dynamics of the physiological variables and the movement of individuals into a dynamic population formulation. Numerical studies of the model show that the system exhibits asymptotically periodic solutions for parameter values that result in the coexistence of the two populations. Through the cost of swimming and feeding the predator population is affected by the characteristic velocity, $s$, of the population, in such a way that there is an optimal value for $s$ that maximizes the predator biomass. The dynamics of the population are compared using two movement behaviors, one in which individuals move continuously in the direction of increasing prey and another in which energetic constraints are imposed.

In Part III, the model developed in Part II is used to study the effects of nonpolar narcotic toxicants on a fish population which is exposed to a spatially varying toxicant and a dynamic resource. The exposure might occur through the environmental and/or the food pathways. We demonstrate in an assessment of mortality that the spatial heterogeneity can influence the physiological structure of the population and determine the survival or extinction of the population. These depend on the spatial pattern of the toxicant and resource, as related to the distribution of individuals in space, during the exposure.

# PART I

# EXISTENCE OF TRAVELING WAVE SOLUTIONS OF REACTION-ADVECTION MODELS

# 1 Introduction

Traveling waves make up an important class of solutions of both reaction-diffusion equations and nonlinear hyperbolic equations. These solutions of the form $u = u(x \pm ct)$, where the speed of the wave, $c$, is a positive constant, travel without changing shape (see [7, 8]). The pleasant mathematical feature associated with such solutions is that the problem often reduces from a partial differential equation setting to one of ordinary differential equations. A typical solution involves finding orbits that connect steady states.

Many phenomena arising in various physical or biological contexts can be modeled by traveling waves. Examples include shock waves, nerve impulses, and various oscillatory chemical reactions. Traveling wave bands have also been observed in oceanic plankton [9] and are common in the movement of microorganisms directed towards a resource. Fisher [4] found a traveling wave solution of a single species model for the spatial spread of a favored gene in a population. Dunbar [2, 3] has shown the existence of traveling wave solutions of a modified Lotka–Volterra system with logistic growth of the prey and with both predators and prey dispersing by diffusion. He has also found that the waves have damped oscillations on the aft side of the transition zone.

In this part, we study the possibility of existence of traveling wave solutions of a predator–prey system in which the predators move towards a sessile prey where the density is the largest. We assume that advection is the dominant movement force and diffusion is negligible in the dispersal of the populations. The specific model we study is a modified Lotka–Volterra system with logistic growth of the prey.

To understand the case of the predator–prey system, we shall first study a simple

equation that models a single species population whose movement depends on the local population density.

## 2 Single Species Reaction–Advection Model

Consider a single species whose movement is governed by an advective process and the population at any given spatial position grows according to the logistic equation. A simple case of a nonlinear advective process coupled with a population growth rate that is logistic can be described by the nondimensional equation

$$\rho_t - \rho\rho_x = \rho(1-\rho), \tag{1}$$

where subscripts denote partial derivatives, and $\rho = \rho(x,t)$ is the population density. The second term in the lefthand side of the equation describes the nonlinear advective process in which animals move to neighboring areas with lower densities.

In the spatially homogeneous situation, the steady states, $\rho = 0$ and $\rho = 1$, are unstable and stable, respectively. This suggests that we should look for traveling wave solutions to (1) for which $0 \leq \rho \leq 1$ (negative $\rho$ has no biological or physical meaning) and have the form

$$\rho(x,t) = w(z), \quad z = x + ct, \tag{2}$$

where $c > 0$ is the wave speed that must be determined. These type of wavefront solutions are waves moving to the left in the $z$-plane. Substituting this traveling wave form into (1), $w(z)$ satisfies

$$\frac{dw}{dz} = \frac{w(1-w)}{c-w}. \tag{3}$$

Note that there is a singularity at $w = c$. We require the traveling wavefront solution, $w$, to have limiting values, as $z$ tends to plus or minus infinity, equal to the two steady states and also to be monotone increasing. So here we have to determine the values of $c$ such that a nonnegative solution of (3) exists which satisfies

$$\lim_{z\to-\infty} w(z) = 0, \quad \lim_{z\to+\infty} w(z) = 1, \quad \text{and} \quad w'(z) > 0. \tag{4}$$

The steady states of equation (3) are $w = 0$ and $w = 1$, and their stability depends on $c$. Linearization of equation (3) about 0 and 1, shows that 0 is unstable for all $c > 0$, while 1 is stable for $c > 1$ and unstable for $0 < c < 1$. For $c = 1$, equation (3) is reduced into $w' = w$. Thus, $w$ increases exponentially and takes the value 1 at some finite $z$. Figures 1a and 1b [1] indicate the vector field of (3), for the two cases $0 < c < 1$ and $c > 1$. For $c < 1$, the vector field of (3) (Figure 1a) indicates that a trajectory leaving from the unstable steady state $w = 0$ cannot approach $w = 1$. In fact, we can show that the trajectory will reach $w = c$ in finite time.

Consider an $\epsilon$ (to be chosen) sufficient small and assume that a solution of (3) with $0 < c < 1$ has a point $z_0$ such that $|c - w(z_0)| = \epsilon$, i.e, the trajectory corresponding to that solution is $\epsilon$ distance away from $c$ at $z = z_0$. Without loss of generality, we assume that $z_0 = 0$ and $w(0) < c$. Then, there exists a positive constant $c_1$, independent of $\epsilon$, such that for $w \in (w(0), c)$

$$w' \geq \frac{c_1}{\epsilon}.$$

Integrating this inequality from 0 to $z$ we obtain

$$w(z) - w(0) \geq \frac{c_1}{\epsilon} z.$$

This implies that in time $\epsilon$, the trajectory moves at least $c_1$ units to the left towards $c$. Now, if we choose $\epsilon < c_1$, then the trajectory will hit $c$ at some finite $z$. This trajectory cannot pass the point $c$ because the vector field points towards $c$ from the right and an argument analogous to the above will show that the trajectory should return to $c$.

Thus, a solution of (3) starting at $w(0) \in (0, c)$, $c < 1$, will never get values larger than $c$ and it will reach the value $c$ with infinite slope at some point $z$.

To make this clear, consider the special case $c = \frac{1}{2}$. Integration of (3) with

[1] All Figures appear in Appendix.

$0 < w(0) < \frac{1}{2}$ yields the solution

$$w(z) = \frac{1}{2} - \frac{\sqrt{1 - 4w(0)[1 - w(0)]e^{2z}}}{2}. \tag{5}$$

From (5), $w = \frac{1}{2}$ for $z = z_s$, where $z_s = \frac{1}{2} \ln \frac{1}{4w(0)[1-w(0)]}$. For $z > z_s$, $w(z)$ is not defined.

In general, an integration in equation (3) yields the solution for $0 < w < 1$ in a closed form, given by

$$\ln \frac{w^c}{(1-w)^{c-1}} = z + C, \tag{6}$$

where $C$ is the constant of integration.

The solution given by equation (6) satisfies the boundary condition (4) at $-\infty$ for all $c > 0$ and any constant $C$. For $c > 1$, the boundary condition at $+\infty$ is satisfied by (6) for each constant $C$ while for $c < 1$ it is not satisfied for any $C$. For $c = 1$, $w$ increases exponentially and takes the value 1 at some finite $z$. Therefore, equation (6) with $c > 1$ gives the traveling wave solutions. Since the wave solutions are invariant to any shift in the origin of the coordinate system (i.e., the equation is unchanged if $z \to z +$ constant), let us take $z = 0$ to be the point where $w = \frac{1}{2}$, so that equation (6) becomes

$$\ln \frac{2w^c}{(1-w)^{c-1}} = z. \tag{7}$$

Utilizing the solution given by (7), profiles of the traveling wave, $w = w(z)$, corresponding to values of $c = 2$, $c = 5$, and $c = 10$ are shown in Figure 2. We note that the wave slope decreases as the wave speed increases.

Now we address the problem of how such a traveling wave solution might evolve from the partial differential equation (1) with given nonnegative initial data $\rho(x, 0) = \rho_0(x)$. This initial-value problem can be solved using the method of characteristics.

The characteristic equations are

$$\frac{dt}{d\tau} = 1, \quad \frac{dx}{d\tau} = -\rho, \quad \frac{d\rho}{d\tau} = \rho(1 - \rho).$$

The initial data can be parametrized in the form

$$t(s,0) = 0, \quad x(s,0) = s, \quad \rho(s,0) = \rho_0(s), \quad s \in R.$$

Integrating the equation for $t$ yields $t = \tau$. For $\rho$, after substituting $t$ for $\tau$, we find

$$\rho(s,t) = \frac{\rho_0(s)e^t}{1 + \rho_0(s)(e^t - 1)}. \tag{8}$$

Finally, we integrate the differential equation for $x$ to obtain

$$x = s - \ln[1 + \rho_0(s)(e^t - 1)]. \tag{9}$$

For any $s \in R$, equation (8) gives the evolution of the solution along the characteristic (9) starting at $(s,0)$.

Now we need to determine what initial conditions give rise to traveling wave solutions. One initial guess might be to start with a unit step initial data, i.e,

$$\rho_0(x) = \begin{cases} 0, & \text{if} \quad x < 0, \\ 1, & \text{if} \quad x \geq 0, \end{cases}$$

or, with

$$\rho_0(x) = \begin{cases} 0, & \text{if} \quad x \leq x_1, \\ 1, & \text{if} \quad x \geq x_2, \end{cases}$$

where $x_1 < x_2$ and $\rho_0(x)$ is continuous in $x_1 < x < x_2$. Starting with any of the above initial conditions, the characteristic curves will intersect immediately, because the slope, $\frac{dx}{dt}$, is zero for $x$ where $\rho$ is zero initially and negative otherwise. Therefore, initial conditions such that $\rho_0(x) = 0$ for $x \leq x_1$ and $\rho_0'(s) \geq 0$ will give rise to shocks, i.e. $\rho$ will be multivalued at some point $(x,t)$. Thus, the initial data cannot assume the zero value.

The above observation together with the nature of the traveling wave suggest that we should look for initial data of the form

$$0 < \rho_0(x) \leq 1, \quad 0 \leq \rho_0'(x) \leq \rho_0(x), \quad \forall x \in R.$$

To make clear why $\rho_0'(x)$ should be bounded above by $\rho_0(x)$ for all $x \in R$, we follow the values of the derivative $\rho_x$ along the characteristic (9). We find from (8) that

$$\rho_x = \frac{\rho_0(s)e^t}{1 + [\rho_0(s) - \rho_0'(s)](e^t - 1)}. \tag{10}$$

Hence, if $\rho_0'(s) > \rho_0(s)$, then $\rho_x$ becomes infinite at some positive time. Thus, even if we start with smooth initial data, solutions may steepen and "break".

On the basis of the above analysis, initial data of the form

$$\rho_0(x) = \begin{cases} Ae^{\alpha(x-x_0)}, & x \leq x_0, \\ A[2 - e^{-\alpha(x-x_0)}], & x > x_0, \end{cases} \tag{11}$$

with $0 < A < \frac{1}{2}$ and $0 < \alpha \leq 1$, are good candidates for initiation of traveling wave solutions of the form (2) with the boundary conditions (4). For $a > 1$, the denominator of equation (10) with the initial data (11) for $x \leq x_0$, which has the form

$$1 + (1 - \alpha)Ae^{\alpha(x-x_0)}(e^t - 1),$$

will be zero for some positive $t$.

Traveling wave solutions for equation (1) were numerically observed starting with the initial data given by equation (11) with different values of $\alpha \in (0, 1]$. The speed of the wave depends on the parameter $\alpha$ which determines the data at infinity. It has numerically been found that the wave speed, $c$, is inversely proportional to $\alpha$. Figures 3-5 show the development of the wavefront solution for $\alpha = 0.1$, 0.2, and 0.5 with speeds approximately equal to 10, 5, and 2, respectively. For $\alpha = 1$, the evolving wave corresponds to a steep wavefront with speed $c = 1$.

The dependence of the wave speed on the initial condition at infinity can be shown following a simple analysis suggested by Mollison [6] for Fisher's equation.

Consider the leading edge of the evolving wave (as $x \to -\infty$) where $\rho^2$ can be neglected since $\rho$ is small. We can also neglect the term $-\rho\rho_x$, since advection is very small at low densities. Then equation (1) becomes

$$\rho_t = \rho. \tag{12}$$

Consider now the initial condition $\rho(x,0) = Ae^{\alpha x}$ as $x \to -\infty$ and look for traveling wave solutions of (12) in the form

$$\rho(x,t) = Ae^{\alpha(x+ct)}.$$

Substitution of the last expression into (12) gives a relation between $c$ and $\alpha$; namely,

$$c = \frac{1}{\alpha}. \tag{13}$$

If $\alpha > 1$, we have shown above that the evolving traveling wave solution of (1) exhibits shocks at some positive time. Then, equation (13) implies that slow moving waves will break. If $\alpha = 1$, then $c = 1$ is the minimum speed of the waves that can be evolved without breaking. Finally, if $\alpha < 1$, then for large and negative $x$, $e^{\alpha x} > e^{x}$ and so the speed of propagation of waves with asymptotic initial data like (11) will depend on the leading edge of the wave, and the wave speed, $c$, is given by (13).

Similar dependence of the wave speed on the initial data at infinity was found for Fisher's equation (see [7] and references cited there in). Note that because the diffusion is absent in our model, initial conditions with compact support cannot evolve to a traveling wave, in contrast to the Fisher's equation for which initial conditions with compact support evolve to traveling wave solutions with the minimum speed.

We have given conditions on the initial data that evolve to traveling wave solutions of equation (1). The next question we ask is that of the stability of such wavefront solutions. The wavefront is said to be asymptotically stable if a small perturbation imposed on it at some time (say $t = 0$) eventually decays away and the wavefront returns to its original state. We saw above that the speed of propagation of the wavefront solutions depends on the behavior of the initial data at the leading edge. This implies that the wavefront is unstable to perturbations at $-\infty$. So we consider only small perturbations imposed on a finite domain of the moving frame of the wave.

To investigate the asymptotic stability on a finite domain of the traveling wave solutions, equation (1) was solved numerically starting from a wavefront with an

imposed finite domain perturbation. Figure 6 suggests that the initial perturbation dies out and thus the solution approaches, asymptotically, the original wavefront.

The above analysis for the single species population model gives some insight for the analysis of the more complicated predator–prey system which is the focus of this part. Because both systems are governed only by advective processes, singularities and shocks that are present in the single equation might have analogues in the more complicated system.

# 3 Predator–Prey Pursuit Model

Let us suppose that the prey ($N$) is sessile and that the predators ($P$) move in the direction where the prey density is larger. If the diffusion process is negligible compared with the advection effects, then equations that describe the spatial–temporal dynamics of the two populations in one space dimension are

$$\begin{aligned} &\frac{\partial N}{\partial t} = rN(1-\frac{N}{K}) - \gamma NP \ , \\ &\frac{\partial P}{\partial t} + k\frac{\partial}{\partial x}(P\frac{\partial N}{\partial x}) = eNP - \mu P \ , \end{aligned} \tag{14}$$

where $r, \gamma, e, \mu$, and $K$, the prey carrying capacity, are positive constants, and $k$ a positive parameter associated with the pursuit of the predators. In the homogeneous situation, system (14) takes the form of the Lotka–Volterra predator–prey system with a logistic growth limitation on the prey.

Before discussing the existence of traveling wave solutions, it is convenient to express equations (14) in dimensionless variables and parameters. We nondimensionalize the system by setting

$$\begin{aligned} &U = \tfrac{N}{K} \ , \qquad V = \tfrac{\gamma P}{r} \ , \quad t^\star = rt \ , \\ &x^\star = \sqrt{\tfrac{r}{kK}}x \ , \quad a = \tfrac{eK}{r} \ , \quad b = \tfrac{\mu}{eK} \ . \end{aligned}$$

System (14) becomes, after omitting the asterisks for notational simplicity,

$$
\begin{aligned}
&\frac{\partial U}{\partial t} = U(1-U-V) \ , \\
&\frac{\partial V}{\partial t} + \frac{\partial}{\partial x}(V\frac{\partial U}{\partial x}) = aV(U-b) \ ,
\end{aligned} \tag{15}
$$

where $a$ and $b$ are positive constants.

A simple phase plane analysis shows that the spatially independent system has three steady states: $(0,0)$, representing the absence of both species; $(1,0)$, representing the absence of predators and the prey at its carrying capacity; and $(b, 1-b)$ representing the coexistence of both species if $b < 1$. In terms of the original dimensional parameters this last steady state exists if the predator's death rate, $\mu$, is less than its maximum growth rate, $eK$. It is easy to show that both $(0,0)$ and $(1,0)$ are saddle points, and $(b, 1-b)$ is a stable node if $4a \leq b/(1-b)$ and a stable focus if $4a > b/(1-b)$. It can be shown, e.g. in [5], that $(b, 1-b)$ is globally asymptotically stable in the positive quadrant. This means that solutions of the spatially independent system, i.e. system (15) with $\frac{\partial}{\partial x} \equiv 0$, initially close to equilibrium, say $(1,0)$, approach the interior equilibrium $(b, 1-b)$. In ecological terms, this means that if the prey is near its carrying capacity, the introduction of even a small number of predators will drive the system to a new stable steady state characterized by the coexistence of both species.

This analysis motivates us to look for wavefront solutions of (15) connecting the steady state $(1,0)$ to $(b, 1-b)$.

If such solutions exist, they can be written in the form

$$
U(x,t) = u(z), \quad V(x,t) = v(z), \quad z = x + ct, \tag{16}
$$

where the wave speed $c$ is positive. Such solutions represent waves moving to the left in the $z$–plane. Although mathematically a spectrum of solutions may exist, we are only interested in nonnegative traveling waves with limiting values, as $z$ tends to plus or minus infinity, equal to the steady states $(b, 1-b)$ and $(1,0)$. In ecological terms, this means that if in a one dimensional habitat, e.g. a river, initially free of predators

and with prey uniformly distributed at its carrying capacity, we introduce a small number of predators we may observe a wave of invasion with prey and predator at the steady state $(b, 1-b)$ on the "tail" of the wave.

Substituting the traveling wave forms (16) into (15), we obtain the following system of differential equations

$$\begin{aligned} cu' &= u(1-u-v) \ , \\ cv' + (vu')' &= av(u-b) \ , \end{aligned} \tag{17}$$

where primes denote differentiation with respect to $z$. Substituting $u'$ from the first equation in (17) into the second, we can rewrite system (17) as a first order system

$$\begin{aligned} u' &= \frac{1}{c}u(1-u-v) \ , \\ v' &= \frac{v}{c}\ \frac{ac^2(u-b) - u(1-u-v)(1-2u-v)}{c^2 + u(1-u-2v)} \ , \end{aligned} \tag{I}$$

for $(u,v) \notin S$, where $S = \{(u,v) \in R_+ \times R_+ \mid h(u,v) \equiv c^2 + u(1-u-2v) = 0\}$ is the singularity set of the second equation in (I).

For $(u,v) \in S$, the vector field is described by the following system of equations

$$\begin{aligned} u' &= \frac{1}{2c}[u(1-u) - c^2] \ , \\ v' &= -\frac{u^2 + c^2}{4cu^2}[u(1-u) - c^2] \ . \end{aligned} \tag{II}$$

The isoclines for the system (I) are

$$u = 0, \ v = 0,$$

$$f(u,v) \equiv 1 - u - v = 0,$$

$$g(u,v) \equiv ac^2(u-b) - u(1-u-v)(1-2u-v) = 0,$$

which are sketched in Figure 7. System (I) has three steady states: $(0,0)$, $(1,0)$ and $(b, 1-b)$; we are, as noted above, only interested in the case $b < 1$. Depending on the parameters $a$, $b$, and $c$, the slope of the isocline $g = 0$ at the steady state $(b, 1-b)$ might be positive or negative. The slope, $\frac{ac^2}{b^2} - 1$, is positive if $ac^2 > b^2$ and negative

if $ac^2 < b^2$. It will also be helpful to know that for $u \geq b$ the graph of $g(u,v) = 0$ lies in the set $\{(u,v) \mid 1-u-v \leq 0,\ 1-2u-v \geq 0\}$, and for $u < b$ it lies in the set $\{(u,v) \mid 1-u-v > 0,\ 1-2u-v < 0\}$.

Solving the algebraic equation $h(u,v) = 0$, which describes the singularity curve $S$, for $v$ in terms of $u$ we obtain a decreasing function, $h_1$, of $u$ given by

$$h_1(u) = \frac{c^2 + u(1-u)}{2u}.$$

The singularity curve $S$ intersects the positive $u$-axis at $\frac{1+\sqrt{1+4c^2}}{2} > 1$, for all positive $c$. For $c > \frac{1}{2}$, $S$ is above the isocline $f = 0$. For $c < \frac{1}{2}$, $S$ intersects the line $f = 0$ at $(u_1^s, v_1^s)$ and $(u_2^s, v_2^s)$ where

$$(20) \qquad \begin{aligned} u_1^s &= \tfrac{1-\sqrt{1-4c^2}}{2}, \quad v_1^s = \tfrac{1+\sqrt{1-4c^2}}{2} \\ u_2^s &= \tfrac{1+\sqrt{1-4c^2}}{2}, \quad v_2^s = \tfrac{1-\sqrt{1-4c^2}}{2}. \end{aligned}$$

From the equations in (II), we can determine the flow on the singularity set $S$. Notice that $u'$ and $v'$ have opposite signs. In particular,

$$\begin{aligned} &u' < 0 \text{ and } v' > 0 \text{ if } c > \tfrac{1}{2}, \qquad u > 0, \qquad v > 0, \\ &u' > 0 \text{ and } v' < 0 \text{ if } c < \tfrac{1}{2}, \quad u \in (u_1^s, u_2^s), \quad v \in (v_1^s, v_2^s), \\ &u' < 0 \text{ and } v' > 0 \text{ if } c < \tfrac{1}{2}, \quad u \notin (u_1^s, u_2^s), \quad v \notin (v_1^s, v_2^s), \end{aligned}$$

where $(u_1^s, v_1^s)$ and $(u_2^s, v_2^s)$ are, respectively, the unstable and stable steady states of the system for $c < \frac{1}{2}$. The flow on $S$ is shown in Figures 8a and 8b.

A linear analysis of system (I) shows that the eigenvalues $\lambda$ for the critical points $(0,0)$ and $(1,0)$ are:

$$\begin{aligned} (0,0) \ &: \lambda_1 = \tfrac{1}{c} \quad \text{and} \quad \lambda_2 = -\tfrac{ab}{c} \quad \Rightarrow \text{saddle point;} \\ (1,0) \ &: \lambda_1 = -\tfrac{1}{c} \quad \text{and} \quad \lambda_2 = \tfrac{a(1-b)}{c} \quad \Rightarrow \text{saddle point.} \end{aligned}$$

The local stable and unstable manifolds of the origin are, respectively, the $v$ and $u$-axes, and that of $(1,0)$ the $u$-axis and the line $v = -[1 + a(1-b)](u-1)$.

The eigenvalues of the linearization of system (I) at the critical point $(b, 1-b)$ are:

$$\lambda_1, \lambda_2 = \frac{-bc \pm \sqrt{b^2c^2 - 4a(1-b)[c^2 - b(1-b)]}}{2[c^2 - b(1-b)]}.$$

If $c^2 > b(1-b)$ and $0 < a \leq a^*$, where $a^* = b^2c^2/4(1-b)[c^2 - b(1-b)]$, the eigenvalues are real and negative; thus the steady state is a stable node. If $c^2 > b(1-b)$ and $a > a^*$, the eigenvalues are complex conjugates with negative real parts, so the steady state is a stable focus. If $c^2 < b(1-b)$ the eigenvalues are real and distinct with opposite signs. In this case the steady state $(b, 1-b)$ is a saddle, hence unstable. Figure 9 illustrates the stability/instability domains of the steady state $(b, 1-b)$ in the $(b, c)$ space.

# 4 Phase Plane Analysis

The solutions of interest correspond to orbits in phase plane connecting the steady state $(1, 0)$ to $(b, 1-b)$. So we look for nonnegative solutions of (I) satisfying the boundary conditions

$$u(-\infty) = 1, \quad v(-\infty) = 0, \quad u(+\infty) = b, \quad v(+\infty) = 1 - b \ , \tag{21}$$

where $u(-\infty) = 1$ means $\lim_{z \to -\infty} u(z) = 1$ etc. Thus, we require a heteroclinic connection between the two steady states. We have determined the unstable and stable directions of the saddle point $(1, 0)$. The unstable manifold that emanates out of this steady state has a slope less than $-1$ for all positive $a$ and $b < 1$. This is consistent with the boundary conditions at $-\infty$. Whether or not a heteroclinic connection exists depends on the position of the steady state $(b, 1-b)$ relative to the singularity curve $S$.

In the next two theorems we give conditions for existence and nonexistence of traveling wave solutions. Theorem 1 proves that for values of $b$ and $c$ in a certain domain of the parameter space the heteroclinic connection between the two steady states does not exist. Thus, traveling wave solutions of interest do not exist. Theorem 2 gives sufficient conditions for the existence of the heteroclinic connection.

THEOREM 1 *Traveling wave solutions of system (I) which satisfy the boundary conditions* (21) *do not exist if*

(a) $c < \sqrt{b(1-b)}$,

(b) $0 < b < \frac{1}{2}$ *and* $\sqrt{b(1-b)} < c < \frac{1}{2}$.

To prove Theorem 1 we need the following Proposition. First, define

$$\Gamma = \{(u,v) \in S \mid g(u,v) > 0,\ b < u < 1,\ 0 < v < 1-b\},$$

$$N_\epsilon = \{Q \equiv (u,v) \mid g(u,v) > 0,\ b < u < 1,\ 0 < v < 1-b,\ \mathrm{dist}(Q,\Gamma) < \epsilon\},$$

and let $\partial N_\epsilon$ to be the boundary of $N_\epsilon$.

PROPOSITION 1 *Let* $c < \sqrt{b(1-b)}$. *For sufficient small* $\epsilon$, *a solution of (I) having a point* $z_0$ *such that* $(u(z_0), v(z_0)) \in \partial N_\epsilon \setminus \Gamma$, *will have* $(u(z), v(z)) \in N_\epsilon$ *for all* $z > z_0$. *Furthermore, for some finite* $z_s$ $(u(z), v(z)) \in \Gamma$ *for all* $z > z_s$.

*Proof.* Clearly if $c^2 < b(1-b)$, then $c < \frac{1}{2}$ and thus the singularity curve, $S$, intersects the isocline $f = 0$ at $(u_1^s, v_1^s)$ and $(u_2^s, v_2^s)$ given by (20). Consider a small $\epsilon$ (to be chosen). Figure 10 shows the $\epsilon$-strip, $N_\epsilon$, constructed to include part of the singularity curve $S$. The vector field in $\overline{N_\epsilon} \setminus \Gamma$ is well defined by (I). From the equations in (I), there are positive constants $c_1$ and $c_2$ independent of $\epsilon$ such that, for $(u,v) \in \overline{N_\epsilon} \setminus \Gamma$

$$|u'| \le c_1,\ \ v' \ge \frac{c_2}{\epsilon} \text{ if } v' > 0, \text{ and } v' \le -\frac{c_2}{\epsilon} \text{ if } v' < 0. \tag{22}$$

Note that above $\Gamma$, $v'$ is always negative, and below $\Gamma$, $v'$ is always positive.

Without loss of generality we assume that $z_0 = 0$. Then, integrating each inequality in (22) from 0 to $z$ we obtain

$$|u(z) - u(0)| \le c_1 z \text{ and } |v(z) - v(0)| \ge \frac{c_2}{\epsilon} z. \tag{23}$$

From (23), in time $\epsilon$, the trajectory moves at least $c_2$ units vertically (upwards if $h > 0$ or downwards if $h < 0$) and at most $c_1\epsilon$ units horizontally (right if $f > 0$ or left

if $f < 0$). Note that for small $\epsilon$, the trajectory moves faster in the vertical direction than in the horizontal direction. We now need to choose $\epsilon$ so that the trajectory moves into $N_\epsilon$ and hits $\Gamma$ in finite $z$.

From Figure 10, on $AF$, $DC$, $BC$ and $EF$ (except on the points $F$ and $C$) the trajectories clearly point inwards because of the sign of $f(u,v)$, $g(u,v)$, and $h(u,v)$ on them. It is not clear whether trajectories on $AB$ or $ED$ move into $N_\epsilon$.

We will analyze in detail the case where $(u(0),v(0)) \in AB$ and $u' < 0$. Figure 11 shows the motion of the trajectory in time $\epsilon$.

Because $h_1$ is a decreasing function of $u$, $h_1'(b) < h_1'(u) < 0$ for $b < u < 1$. A sufficient condition that guarantees that the trajectory enters the $\epsilon$-strip is that the slope of the vector $\vec{w}$, which in this case is negative, is less than $h_1'(b)$, or

$$\frac{c_2}{c_1\epsilon} > |h_1'(b)|. \tag{24}$$

For $(u(0),v(0)) \in ED$ and $u' > 0$, condition (24) should hold for the trajectory to point inwards. It is easy to see that if $(u(0),v(0)) \in AB$ and $u' > 0$ or $(u(0),v(0)) \in ED$ and $u' < 0$, then the trajectory always points into $N_\epsilon$.

From system (II) and Figure 8b, we see that the direction of the trajectory on the points $F$ and $C$ points into $N_\epsilon$.

Thus, we constructed a bounded domain so that the vector field points into the domain across the boundary which implies that any trajectory in $N_\epsilon$ cannot cross the boundary.

We will show that a trajectory in $N_\epsilon$ will hit the curve $\Gamma$ in finite $z$. From Figure 11, the vector $\vec{w}$ will intersect the curve $\Gamma$, if its projection on $l$, where $l$ is perpendicular to $\Gamma$ is larger than $\epsilon$, i.e., if $\cos\theta\sqrt{c_2^2 + c_1^2\epsilon^2} > \epsilon$. If (24) holds, then $0 < \theta < 90$. Thus, there exists a positive constant $\eta$ such that $0 < \eta < \cos\theta < 1$. Then, $\cos\theta\sqrt{c_2^2 + c_1^2\epsilon^2} > \eta c_2$.

Hence, if $\epsilon < \min\{\eta c_2, \frac{c_2}{c_1|h_1'(b)|}\}$, then $(u(z_s),v(z_s)) \in \Gamma$ for some finite $z_s$.

We will show that $(u(z_s),v(z_s)) \in \Gamma$ for all $z > z_s$. Suppose to the contrary that there is a fixed positive number $\delta$ and $z_\delta^1$, $z_\delta^2$ so that with $\vec{y}(z) = (u(z),v(z))$,

$\text{dist}(\vec{y}(z), \Gamma) \geq \delta > 0$ for $z_\delta^1 < z < z_\delta^2$.

As above we can choose $\epsilon$ arbitrary small ($\epsilon < \delta$) to construct an $\epsilon$-strip so that the vector field points inwards. From the above assumption, the trajectory leaves the $\epsilon$-strip. This is a contradiction.

Therefore the trajectory evolves on $\Gamma$. In particular, it evolves towards the stable steady state $(u_2^s, v_2^s)$ of system (II). □

Now we will use the result of Proposition 1 to prove Theorem 1.

*Proof of Theorem 1.* (*a*) For $c < \sqrt{b(1-b)}$ the steady state $(b, 1-b)$ is a saddle point. Linearization shows that the local stable manifold of $(b, 1-b)$ lies on the line given by $v = (1-b) + m(u-b)$ where

$$m = -[1 - \frac{bc^2 - c\sqrt{c^2b^2 - 4ab(1-b)[c^2 - b(1-b)]}}{2b[c^2 - b(1-b)]}].$$

Using elementary algebra, it can be shown that

$$0 < m < \frac{ac^2}{b^2} - 1 \qquad \text{if} \quad ac^2 > b^2,$$
$$-1 < \frac{ac^2}{b^2} - 1 < m < 0 \quad \text{if} \quad ac^2 < b^2,$$

where $\frac{ac^2}{b^2} - 1$ is the slope of the curve $g = 0$ at the steady state $(b, 1-b)$. A possible vector field is illustrated in Figure 12.

In order for the connection between the two saddle points $(1, 0)$ and $(b, 1-b)$ to exist, the trajectory in the phase plane that emanates out of the steady state $(1, 0)$ must lie on the stable manifold of the steady state $(b, 1-b)$.

Let

$$P = \{(u, v) \mid b < u < 1, v > 1 - b\},$$
$$Q = \{(u, v) \mid 0 < u < b, 0 < v < 1 - b\},$$
$$P' = \{(u, v) \mid b < u < 1, g(u, v) < 0\},$$
$$Q' = \{(u, v) \mid 0 < u < b, v > 1 - b\}.$$

Then the stable manifold of $(b, 1-b)$ lies in $P \cup Q$ if $ac^2 > b^2$ or in $P' \cup Q'$ if $ac^2 < b^2$.

The following shows that the trajectory that leaves the saddle point $(1,0)$ will never cross the boundaries of $P \cup Q$ or $P' \cup Q'$.

Indeed, the unstable separatrix that emanates out of the steady state $(1,0)$ lies in the triangular region $ABC$ (see Figure 12). On $AB$ (not including the endpoints),

$$u' = 0,$$

$$v' = \frac{acv(u-b)}{c^2 - u(1-u)} > 0,$$

so that the vector field points into the triangular region (Figure 13). On $BC$ (not including the endpoints), $u = 1$ and

$$\mathbf{n} \cdot (\frac{du}{dz}, \frac{dv}{dz}) = \frac{du}{dz} = -\frac{v}{c} < 0$$

where $\mathbf{n}$ is the outward unit normal on $BC$. So, the vector field also points into the triangular region (Figure 13).

Because there is no steady state in the interior of this region, the vector field indicates that the trajectory moves upwards, towards the singularity curve. Eventually, the trajectory will be arbitrarily close to the singularity curve, $S$, so we can construct an $\epsilon$-invariant strip around $S$. Then by Proposition 1, the trajectory will evolve towards the stable steady state $(u_2^s, v_2^s)$ of system (II). This point is neither in $P \cup Q$ nor in $P' \cup Q'$. That proves that the trajectory will not reach the local stable manifold of the steady state $(b, 1-b)$, and thus the connection between the two saddle points cannot be made.

$(b)$ The proof of part $(b)$ is similar to proof of part $(a)$. If $\sqrt{b(1-b)} < c < \frac{1}{2}$, then the problem is in the parameter space domain where the steady state $(b, 1-b)$ is stable and the singularity curve, $S$, intersects the isocline $f = 0$ at $(u_1^s, v_1^s)$ and $(u_2^s, v_2^s)$. In addition, if $b < \frac{1}{2}$, then $b < u_1^s$ and $1 - b > v_1^s$. The vector field of system (I) for the case where $ac^2 > b^2$ is shown in Figure 14. Note that the position of the steady states $(1,0)$ and $(b, 1-b)$ relative to the singularity curve does not allow a connection between them. □

THEOREM 2 *Traveling wave solutions of system* $(I)$ *which satisfy the boundary conditions* (21) *exist if*

$(a)$ $c > \frac{1}{2}$, $c^2 > 4a(1-b) - 2$, *and* $ac^2 \leq b^2$

$(b)$ $\frac{1}{2} < b < 1$, $\sqrt{b(1-b)} < c < \frac{1}{2}$, *and* $c^2 > 4a(1-b) - 2$.

*Proof.* The requirements in parts $(a)$ and $(b)$ assert that the steady state $(b, 1-b)$ is a stable node or focus. Numerical experiments have shown that if the singularity curve, $S$, does not intersect the isocline $g = 0$ at least for $u \leq 1$, then the connection between the two steady states always exists. The condition $c^2 > 4a(1-b) - 2$ asserts that $S$ lies above the curve $g = 0$ for $u \leq 1$. The reason we require only $u \leq 1$ is because, as we will prove later, the unstable separatrix that emanates out of $(1, 0)$ cannot cross the line $u = 1$. The condition $ac^2 \leq b^2$ asserts that the slope of the isocline $g = 0$ at the steady state $(b, 1-b)$ is zero or negative, and the graph of $g = 0$ is as it is shown in Figure 7b.

$(a)$ We will show that the unstable separatrix that leaves the steady state $(1, 0)$ will approach the steady state $(b, 1-b)$ asymptotically. To prove this, we will construct a simply connected domain that includes both steady states and the unstable separatrix that leaves the steady state $(1, 0)$ cannot cross the boundary of the domain. Then, we will show, using the Bendixson-Dulac criterion, that there are no closed trajectories in that region. Because the construction of the region depends on the values of the parameters, the proof consists of two cases.

*Case 1.* $b > \frac{1}{2}$. Consider the domain $\mathcal{D}$ defined by $ABCDE$ in the $(u, v)$-phase plane as it is shown in Figure 15. The sides of $ABCDE$ are defined as parts of the following curves:

$AB$ : $u = 1$,

$BC$ : $\{y \equiv (u, v) \mid h(u, v) > 0, \text{dist}(y, S) = \delta\}$,

$CD$ : $v = \frac{1}{2}$,

$DE$ : $u = \frac{1}{2}$,

$EA$ : $v = 0$,

where $\delta > 0$ is so small that the side $BC$ is above the isoclines $f = 0$ and $g = 0$.

It can be shown simply but tediously that if $\mathbf{n}$ denotes the outward normal to the boundary of $\mathcal{D}$, $\mathbf{n} \cdot (\frac{du}{dz}, \frac{dv}{dz}) < 0$ for all points on the boundary except the side $EA$. Note that $EA$ is part of the stable manifold of the saddle point $(1, 0)$. A trajectory will never hit this side unless it starts there.

On $BC$ and $CD$ the vector field clearly points inwards because of the signs of $f(u, v)$, $g(u, v)$, and $h(u, v)$. On $AB$,

$$(1, 0) \cdot (\frac{du}{dz}, \frac{dv}{dz}) = -\frac{v}{c} < 0,$$

so that the vector field points inwards. On $DE$ ($u = \frac{1}{2}$ and $v < \frac{1}{2}$),

$$(-1, 0) \cdot (\frac{du}{dz}, \frac{dv}{dz}) = -\frac{1}{2c}(\frac{1}{2} - v) < 0.$$

Therefore, the trajectory cannot cross the sides of the domain $\mathcal{D}$. Now we must show that there is no closed trajectory in the interior of $\mathcal{D}$. Bendixson-Dulac criterion (see e.g. [1]) implies that for the dynamical system $u' = F(u, v)$, $v' = G(u, v)$, there are no closed trajectories in a simply connected region where the expression

$$\frac{\partial(\Phi F)}{\partial u} + \frac{\partial(\Phi G)}{\partial v}$$

does not change sign; here $\Phi(u, v)$ is any function having continuous first partial derivatives and $F(u, v)$ and $G(u, v)$ are smooth in that region.

Consider the function $\Phi(u, v) = \dfrac{ch(u, v)}{uv}$. Then, for system (I)

$$\frac{\partial(\Phi F)}{\partial u} + \frac{\partial(\Phi G)}{\partial v} = \frac{1}{v}[(1 - 2u - v)(1 - u) - h(u, v)] < 0 \text{ in } M,$$

where $M = \{(u, v) \mid 0 < u < 1, h(u, v) > 0, 1 - 2u - v < 0\}$. In particular, $\frac{\partial(\Phi F)}{\partial u} + \frac{\partial(\Phi G)}{\partial v}$ does not change sign in $\mathcal{D} \subset M$.

Therefore, because the stable steady state $(b, 1 - b)$ is the only steady state in the interior of $\mathcal{D}$ and there is no closed orbit in $\mathcal{D}$, the trajectory that leaves the steady state $(1, 0)$ through the unstable separatrix evolves towards the stable steady state

$(b, 1-b)$. Hence, the heteroclinic connection between the two steady states exists in this case.

*Case 2.* $b \leq \frac{1}{2}$. As in *Case 1*, we construct a domain $\mathcal{D}$ defined by $ABCDEF$ (Figure 16), where its sides are defined as parts of the following curves:

$AB$: $u = 1$,

$BC$: $\{y \equiv (u,v) \mid h(u,v) > 0, \text{dist}(y,S) = \delta\}$,

$CD$: $v = 1 - \frac{m-2}{m-1}b$,

$DE$: $v = -m(u-b) + 1 - 2b$,

$EF$: $v = 1 - 2u$,

$FA$: $v = 0$,

where $\delta > 0$ is sufficiently small so that the side $BC$ is above the isoclines $f = 0$ and $g = 0$ and $m$ is a positive constant to be chosen satisfying the condition $2 < m < \infty$.

Similarly, as in *Case 1*, on $AB$, $BC$, $CD$, and $EF$ the vector field points into $\mathcal{D}$. On $DE$, the inner product between the outward normal to $DE$ and the vector field is

$$(-m,-1)\cdot(\frac{du}{dz},\frac{dv}{dz}) = -m\frac{u}{c}(1-u-v) - \frac{v}{c}\frac{g(u,v)}{h(u,v)}. \tag{25}$$

If this inner product is negative, then the vector field crosses into D. Note that on $DE$, $1-u-v > 0$ and $h(u,v) > 0$. We can choose $m$ to be very large so that the first term in (25) dominates the second term (in case $g(u,v) < 0$). Thus, the inner product is negative.

Because $\mathcal{D} \subset M$, we can apply Bendixson-Dulac criterion, using the function $\Phi$ defined in *Case 1*, to show that there is no closed orbit in $\mathcal{D}$. Therefore, the heteroclinic connection between the two steady states exists also in this case.

$(b)$ The proof of part $(b)$ is similar to proof of part $(a)$. In this case the construction of an invariant set is simpler. Figure 17 illustrates an invariant set $\mathcal{D}$ defined by $ABCD$, where its sides are defined as parts of the following curves:

$AB$: $u = 1$,

$BC$: $\{y \equiv (u,v) \mid h(u,v) > 0, \text{dist}(y,S) = \delta\}$,

$CD$: $u = \frac{1}{2}$,

$DA$: $v = 0$,

where $\delta > 0$ is so small that the side $BC$ is above the isoclines $f = 0$ and $g = 0$. □

Theorem 2 gives sufficient conditions on the parameter values for the existence of traveling wavefront solutions.

*Remark 1.* If, in part $(a)$ of Theorem 2, $ac^2 > b^2$, i.e., the slope of the curve $g = 0$ at $(b, 1-b)$ is positive, but not steep, then invariant domains may be constructed as above. Figures 18 and 19 illustrate possible phase portraits of system (I), where the invariant domains are contained in $M$. Hence, there are no closed orbits in the interior of those domains, and the trajectory leaving the $(1,0)$ steady state approaches $(b, 1-b)$.

For $ac^2 >> b^2$, i.e., slope of the curve $g = 0$ at $(b, 1-b)$ is very steep, a domain can be drawn about the steady state $(b, 1-b)$ such that the trajectory emanating out of $(1,0)$ does not leave that domain, but this domain is not necessarily included in $M$. At present, it has not been demonstrated that there are no closed orbits in the interior of the invariant domain; however, system (I) was numerically studied for different sets of parameters that result in this case, and no limit cycles were observed. Therefore, we conjecture that limit cycles do not exist and that the trajectory leaving the $(1,0)$ steady state approaches $(b, 1-b)$.

*Remark 2.* Recall that for $a \leq a^\star$, where $a^\star = b^2c^2/4(1-b)[c^2 - b(1-b)]$, the eigenvalues of the linearized system (I) are real and negative, and for $a > a^\star$ the eigenvalues are complex conjugates with negative real parts. Therefore, in addition to the conditions of Theorem 2 and Remark 1, if $a \leq a^\star$, the trajectory approaches $(b, 1-b)$ monotonically (see Figures 15-16), and if $a > a^\star$, the trajectory will spiral in towards $(b, 1-b)$ with damped oscillations (see Figures 18 and 19).

Next we briefly discuss the question of how such wavefronts evolve from the

predator–prey system (15).

Based on the analysis of the single species model, system (15) was numerically solved starting with asymptotic initial condition for the predator equation and the prey at its carrying capacity. The initial conditions are

$$U(x,0) = 1, \quad V(x,0) = \begin{cases} Ae^{\alpha(x-x_0)}, & x \le x_0, \\ A[2 - e^{-\alpha(x-x_0)}], & x > x_0. \end{cases} \tag{26}$$

Using the same initial data ($A = 0.1$ and $\alpha = 0.1$) system (15) was numerically solved, using a finite difference scheme, for different values of the parameters $a$ and $b$. Figure 20a shows the solution of the system at $t = 20$ with $a = 0.5$ and $b = 0.8$. The speed, $c$, at which the waves move was computed to be very close to 0.87. We see that the solutions $U$ and $V$ approach $b$ and $1 - b$, respectively, monotonically. Figure 20b shows the solution at $t = 20$ with $a = 4$ and $b = 0.75$. The wave speed, $c$, is 10 and we see that the solutions $U$ and $V$ approach $b$ and $1 - b$, respectively, in an oscillatory way. The speed of the wave depends on the behavior of the initial data of the predator at the leading edge (where $V$ is very small and $U = 1$) as well as on the parameters $a$ and $b$. An analysis analogous to that of the single species model gives the dispersion relation, that is a relation between $c$, $a$, $b$, and $\alpha$,

$$c = \frac{a(1-b)}{\alpha}. \tag{27}$$

For the parameter values used in Figure 20b equation (27) gives $c = 10$, which is the same as the computed speed. For the parameter values used in Figure 20a equation (27) gives $c = 1$, while the numerical scheme gives a wave speed of 0.87. The finite difference scheme used here cannot accurately predict speeds of slow moving waves. A more accurate numerical scheme has to be developed for such waves.

*Remark 3.* If the condition $c^2 > 4a(1-b) - 2$ of Theorem 2 or Remark 1, which asserts that the curve $S$ lies above the graph of $g(u,v) = 0$ for $u \le 1$, does not hold, then the trajectory that emanates out of the unstable manifold of the saddle point $(1,0)$ might either approach the stable steady state $(b, 1-b)$ asymptotically

(see Figures 21 and 22), or it might hit the singularity curve, $S$, in finite time (see Figure 23). Notice that for fixed values of $b$ and $c$ the slope of the trajectory emanating out of $(1,0)$ increases in absolute value as $a$ increases. Consequently, the trajectory moves towards the singularity curve $S$. The vector field points towards to $S$, for the portion of $S$ that lies in the domain of the first quadrant where $g > 0$, and away from it otherwise. Now using an argument similar to Proposition 1, we can find a small $\epsilon > 0$ such that if the trajectory $T$ is within a distance $\epsilon$ from $S$, then it will hit $S$ at some finite $z$ and evolve on $S$ at least as long as it is on the portion of $S$ where $g > 0$. The portion of $S$ that lies in the domain where $g < 0$ is "unstable", i.e., small perturbations from S will send the trajectory to infinity or to the steady state $(b, 1-b)$; but if the trajectory hits $S$ on the stable portion, it should remain on $S$ since $u'$ and $v'$ defined by (II) never become infinite. Thus, the trajectory $T$ in Figure 23 will never approach the steady state.

We now summarize the conclusions of Theorem 1, Theorem 2, and the Remarks following them. Let

$$\begin{aligned}
\Sigma_1 &= \{a,b,c>0 \mid b<1,\ c^2 < b(1-b)\},\\
\Sigma_2 &= \{a,b,c>0 \mid b<\tfrac{1}{2},\ b(1-b) < c^2 < \tfrac{1}{4}\},\\
\Sigma_3 &= \{a,b,c>0 \mid b<1,\ c>\tfrac{1}{2},\ c^2 > 4a(1-b)-2,\ ac^2 \le b^2\},\\
\Sigma_4 &= \{a,b,c>0 \mid \tfrac{1}{2}<b<1,\ b(1-b) < c^2 < \tfrac{1}{4},\ c^2 > 4a(1-b)-2\},\\
\Sigma_5 &= \{a,b,c>0 \mid b<1,\ c>\tfrac{1}{2},\ c^2 > 4a(1-b)-2,\ ac^2 > b^2\},\\
\Sigma_6 &= \{a,b,c>0 \mid b<1,\ c>\tfrac{1}{2},\ c^2 \le 4a(1-b)-2\},\\
\Sigma_7 &= \{a,b,c>0 \mid \tfrac{1}{2}<b<1,\ b(1-b) < c^2 < \tfrac{1}{4},\ c^2 \le 4a(1-b)-2\}.
\end{aligned}$$

For $(a,b,c) \in \Sigma_1 \cup \Sigma_2$, traveling waves do not exist. For $(a,b,c) \in \Sigma_3 \cup \Sigma_4$, we have shown analytically that traveling waves exist, while for $(a,b,c) \in \Sigma_5$, we have shown numerically that traveling waves exist. For $(a,b,c) \in \Sigma_6 \cup \Sigma_7$, traveling waves might exist. Figures 24a, 24b, and 24c illustrate the domains of existence/nonexistence of traveling waves in the $(b,c)$ space for different values of $a$.

# 5 Discussion and future work

In this part, we have studied a single species population model and a community predator–prey model in which the dominant movement force was an advection process. In the predator–prey model only the predators were mobile. The focus of the work was to study the existence of traveling wave solutions.

For the single species model, we have found that traveling wave solutions cannot evolve from initial conditions with compact support. Analytical and numerical techniques showed that the speed of the traveling waves with asymptotic initial data depends on the behavior of the initial data at the leading edge. We have also shown numerically that waves that do not "break" are stable to finite domain perturbations.

For the predator–prey model, we have found sufficient conditions for the existence of traveling wave solutions, and computed monotone and oscillatory traveling wave solutions for given initial conditions. The stability of those waves has not been proved here.

In the analysis of the single species model, we found that slow moving waves ($c < 1$) are steep and eventually "break". We conjecture that for the predator–prey model the solutions corresponding to trajectories on the phase plane that hit the singularity curve are slow moving traveling wave solutions that are steep and potentially they break.

For the steep waves a more accurate numerical scheme has to be developed so that the speed of the wave is more accurately predicted.

For both models, we assumed that diffusion process is negligible compared with the advection effects. As the gradient of the waves becomes steep and because the wave is moving slowly, just before breaking, the effects of diffusion might not be negligible.

# References


[1] C. W. CLARK, *Mathematical Bioeconomics. The optimal Management of Renewable Resources*, Wiley Interscience, New York, 2nd ed., 1990.

[2] S. R. DUNBAR, *Travelling wave solutions of diffusive Lotka-Volterra equations*, J. Math. Biol., 17 (1983), pp. 11–32.

[3] ——, *Travelling wave solutions of diffusive Lotka-Volterra equations: a heteroclinic connection in $R^4$*, Trans. Amer. Math. Soc., 268 (1984), pp. 557–594.

[4] R. A. FISHER, *The wave of advance of advantageous*, Ann. Eugenics, 7 (1937), pp. 335–369.

[5] M. HIRSCH AND S. SMALE, *Differential Equations, Dynamical Systems, and Linear Algebra*, vol. 60 of Pure and Applied Mathematics, Academic Press, New York, 1974.

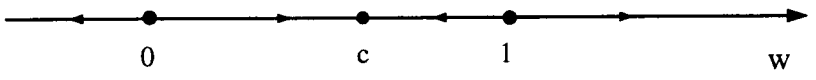
[6] D. MOLLISON, *Spatial contact models for ecological and epidemic spread*, J. Roy. Stat. Soc., B39 (1977), pp. 283–326.

[7] J. D. MURRAY, *Mathematical Biology*, Springer-Verlag, Berlin, Germany, 1989.

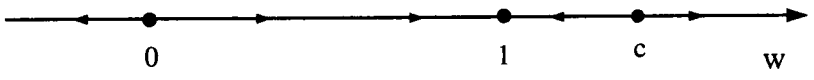
[8] J. SMOLLER, *Shock Waves and Reaction-Diffusion Equations*, Springer-Verlag, Berlin, 2nd ed., 1994.

[9] T. WYATT, *The biology of Oikopleara dioica and Fritillaria borealis in the Southern Bight*, Mar. Biol., 22 (1973), pp. 137–158.

# Appendix




(a)




(b)

Figure 1: The vector field of equation (1) for $0 < c < 1$ (a), and $c > 1$ (b).

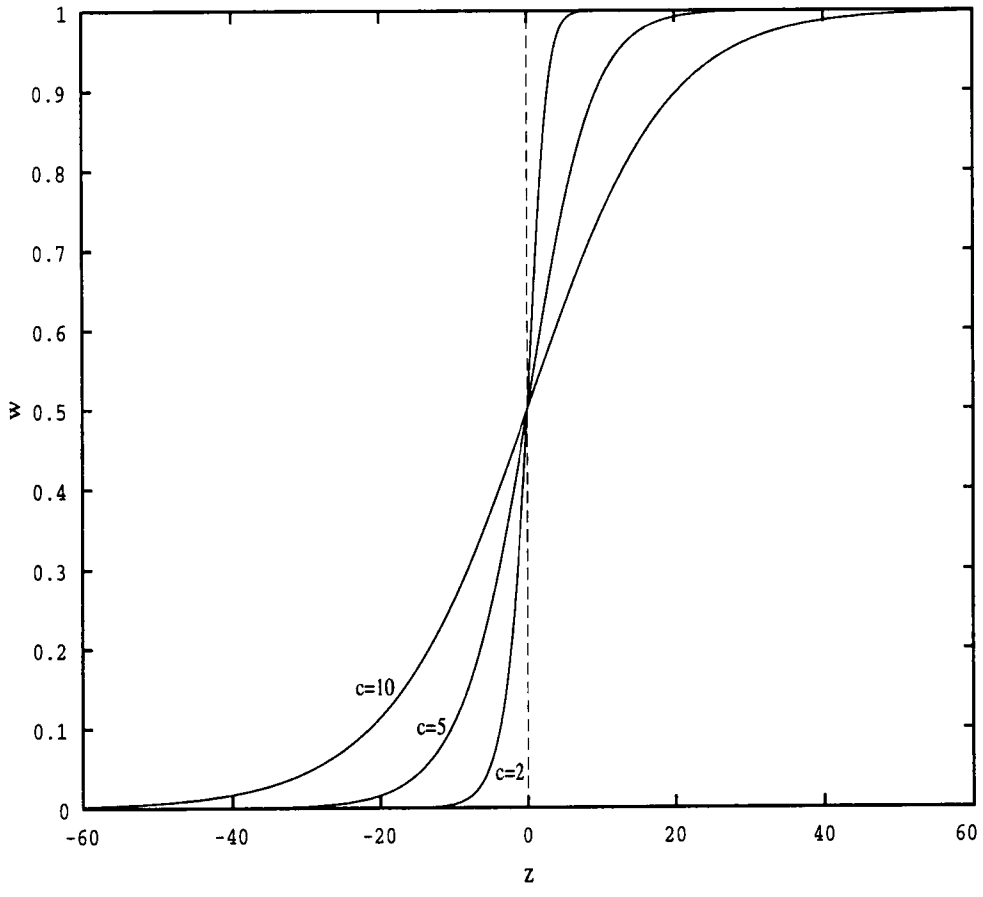



Figure 2: Profiles of the traveling wave of the logistic equation with advection.

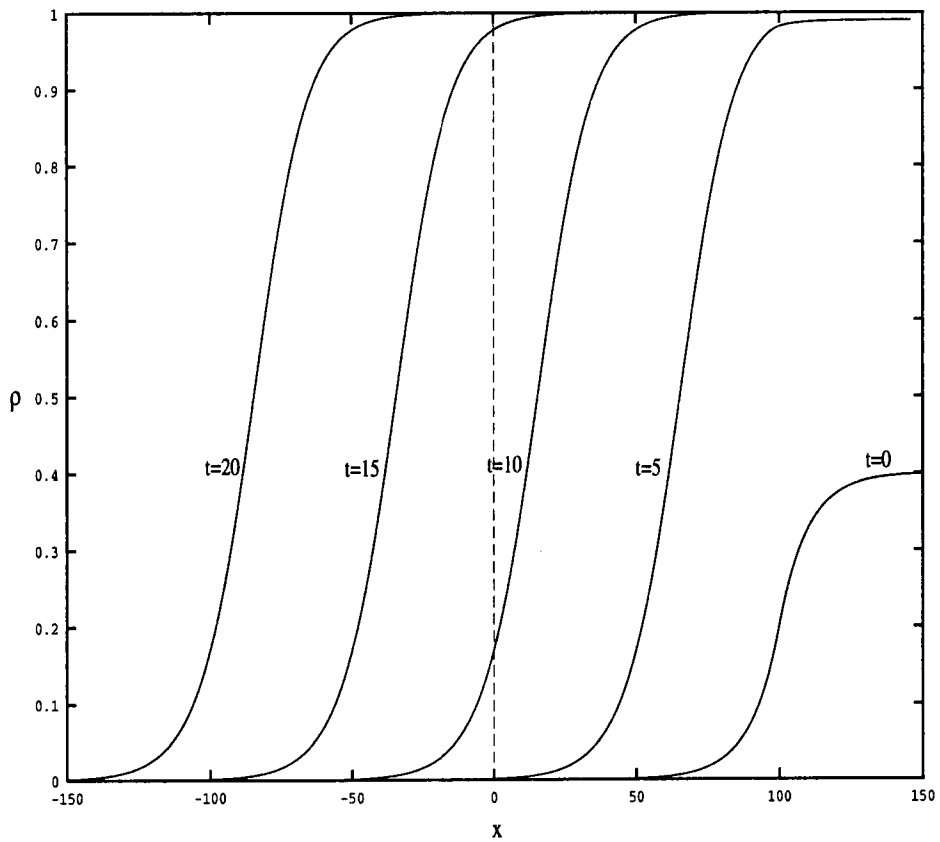



Figure 3: Solution of equation (1) starting from initial data (11) with $A = 0.2$, $x_0 = 100$, and $\alpha = 0.1$. Solutions are plotted on the same axes at $t = 0, 5, 10, 15, 20$.

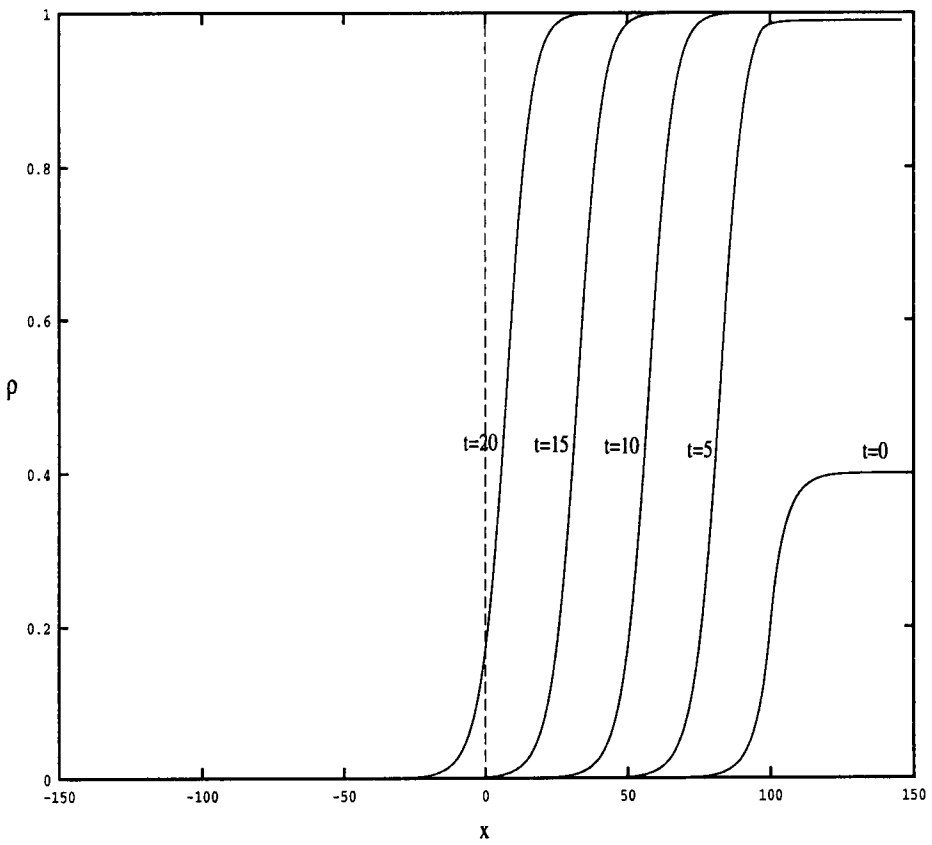



Figure 4: Solution of equation (1) starting from initial data (11) with $A = 0.2$, $x_0 = 100$, and $\alpha = 0.2$. Solutions are plotted on the same axes at $t = 0, 5, 10, 15, 20$.

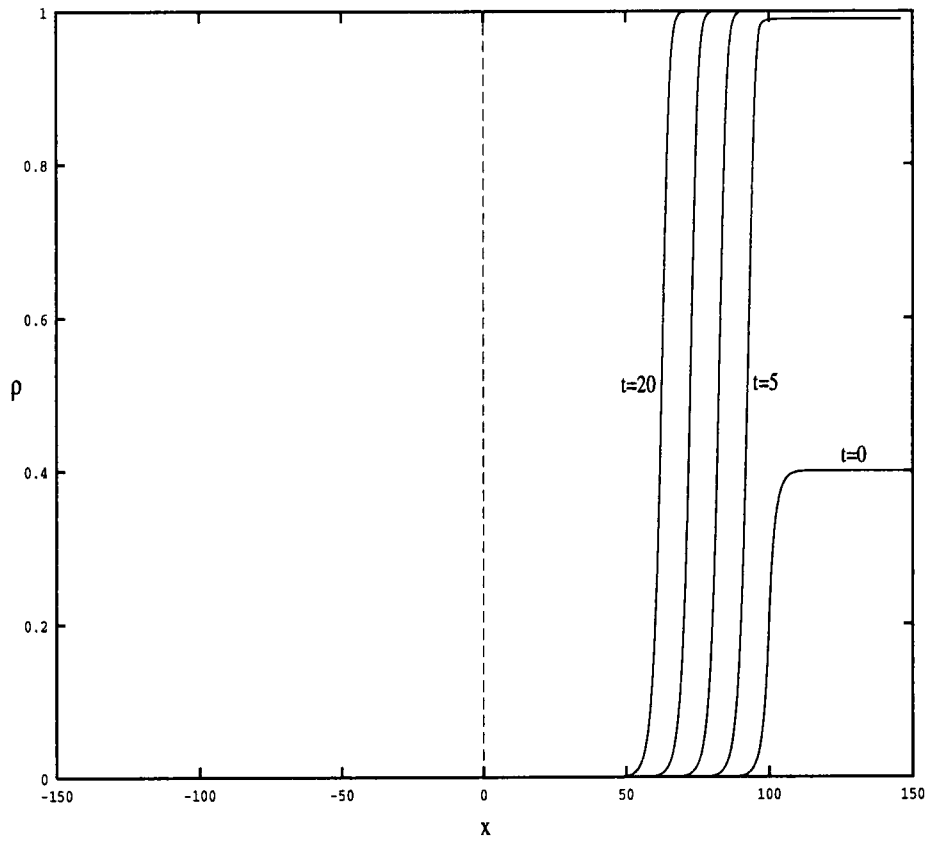



Figure 5: Solution of equation (1) starting from initial data (11) with $A = 0.2$, $x_0 = 100$, and $\alpha = 0.5$. Solutions are plotted on the same axes at $t = 0, 5, 10, 15, 20$.

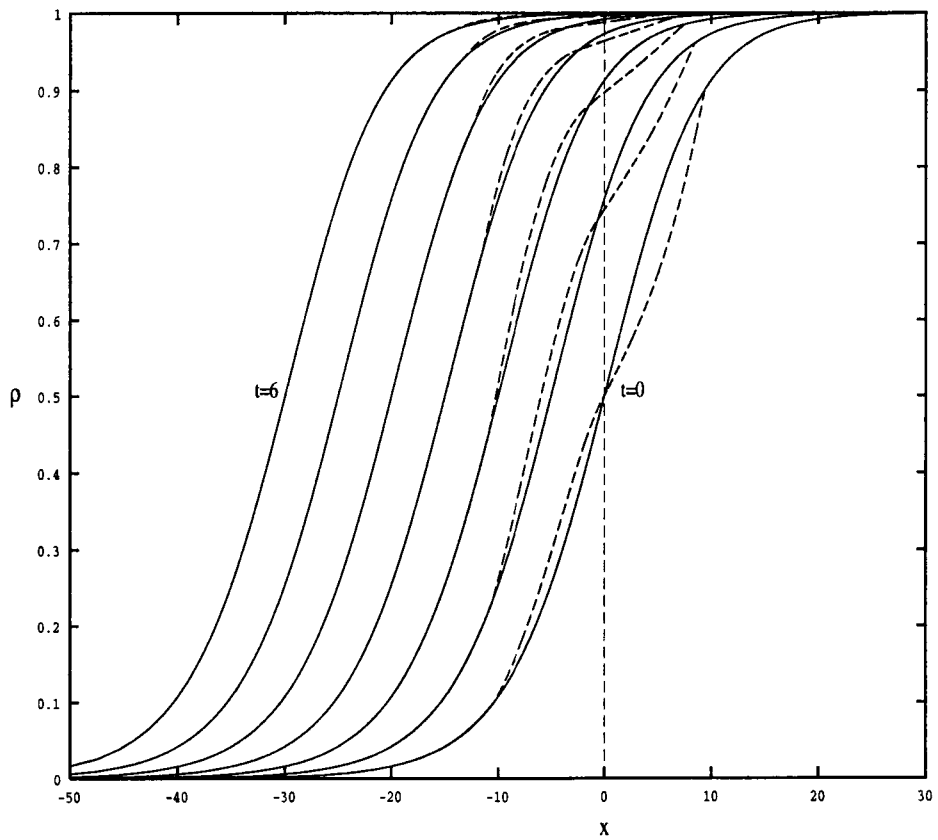
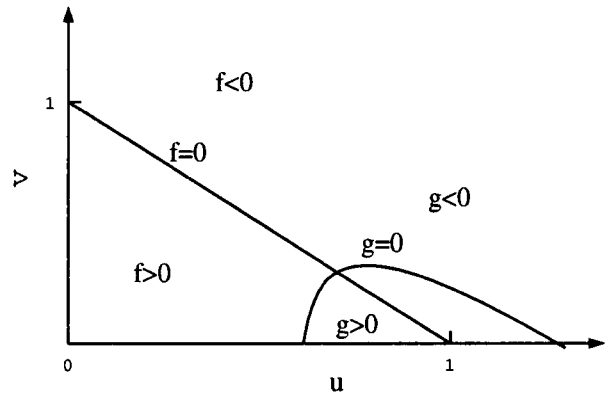
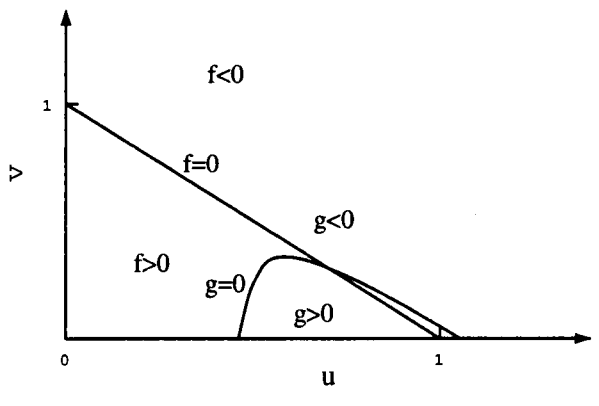



Figure 6: Solutions of equation (1) starting from the wavefront corresponding to $c = 5$ (—), and with an imposed small perturbation (– – –). Solutions are plotted on the same axes at $t = 0, 1, 2, 3, 4, 5, 6$.

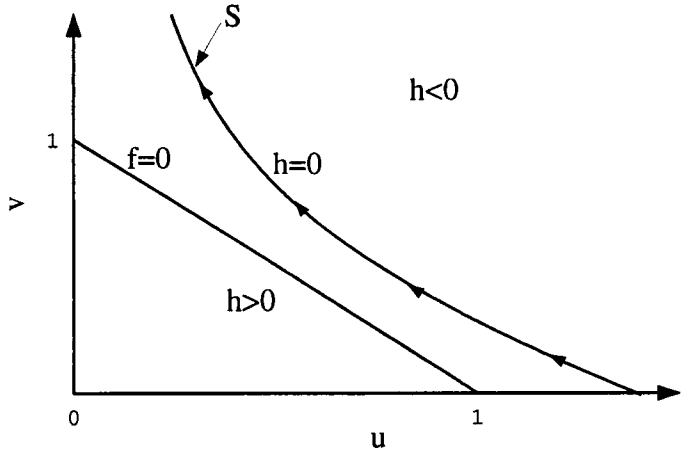



(a)

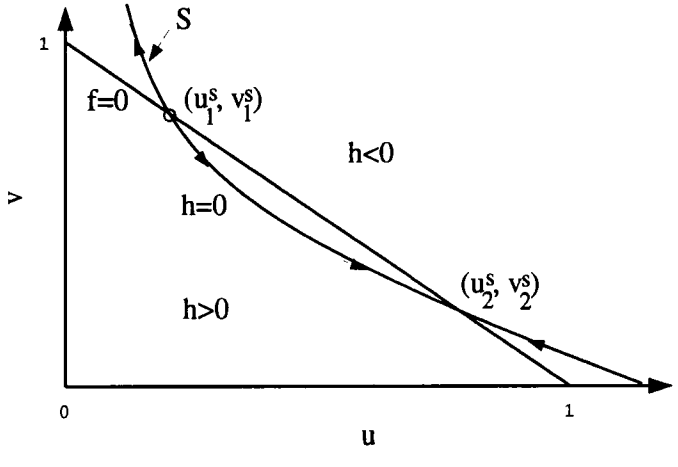



(b)

Figure 7: The isoclines $u = 0$, $v = 0$, $f(u,v) = 0$, and $g(u,v) = 0$ for system (I): $f(u,v) = 1 - u - v$ and $g(u,v) = ac^2(u-b) - u(1-u-v)(1-2u-v)$. (a) $ac^2 > b^2$, (b) $ac^2 < b^2$.




(a)




(b)

Figure 8: The vector field of system (II) on the singularity curve $S$: (a) $c > \frac{1}{2}$, (b) $c < \frac{1}{2}$.

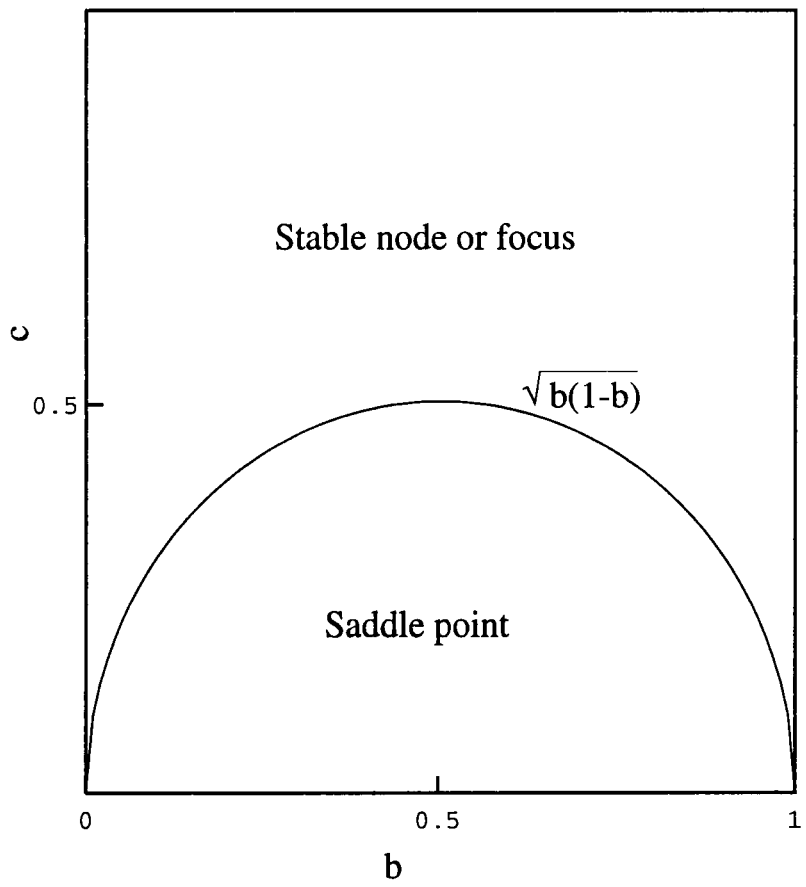



Figure 9: Parameter domains of stability/instability of the positive steady state $(b, 1-b)$ for system (I). For any positive value of $a$, the domain of instability is finite. As the point in parameter space crosses the curve $c = \sqrt{b(1-b)}$, the steady state changes stability.

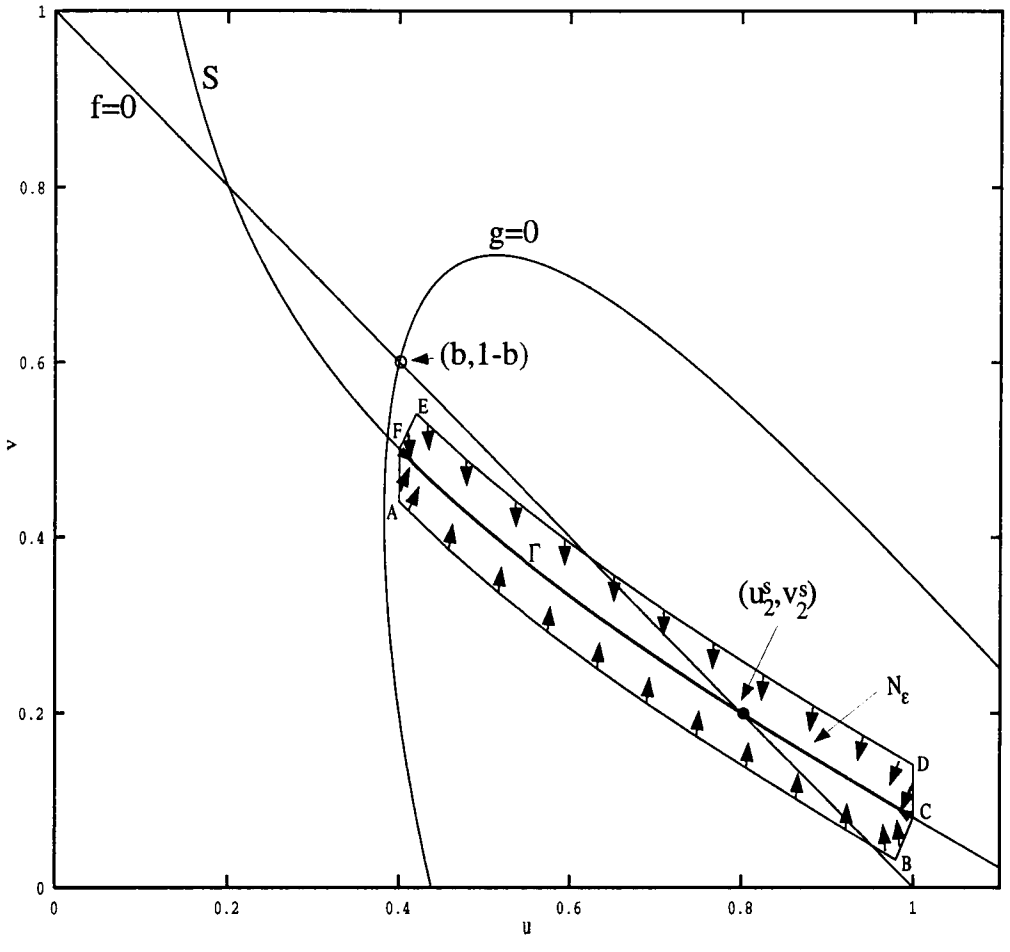



Figure 10: The isoclines $f = 0$ and $g = 0$, and the singularity curve $S$ for $c^2 < b(1-b)$. $ABCDEF$ is the boundary of the $\epsilon$-strip, $N_\epsilon$, around the curve $\Gamma$, on which the trajectories all point inwards.

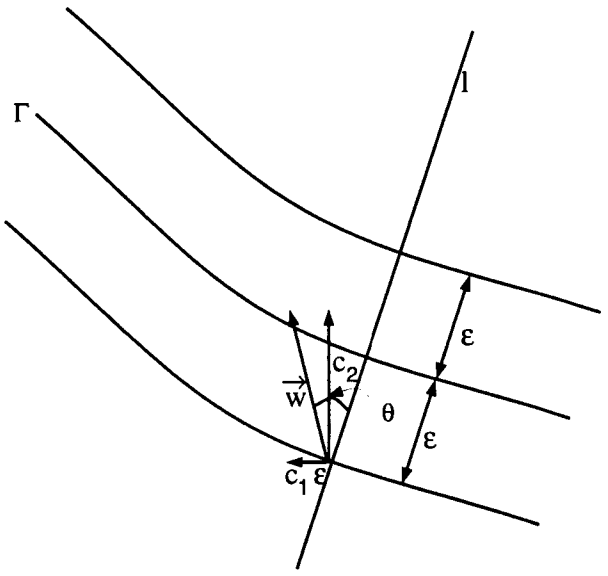



Figure 11: Schematic phase plane trajectory near the curve $\Gamma$, for the case where $h(u,v) > 0$ and $u' < 0$.

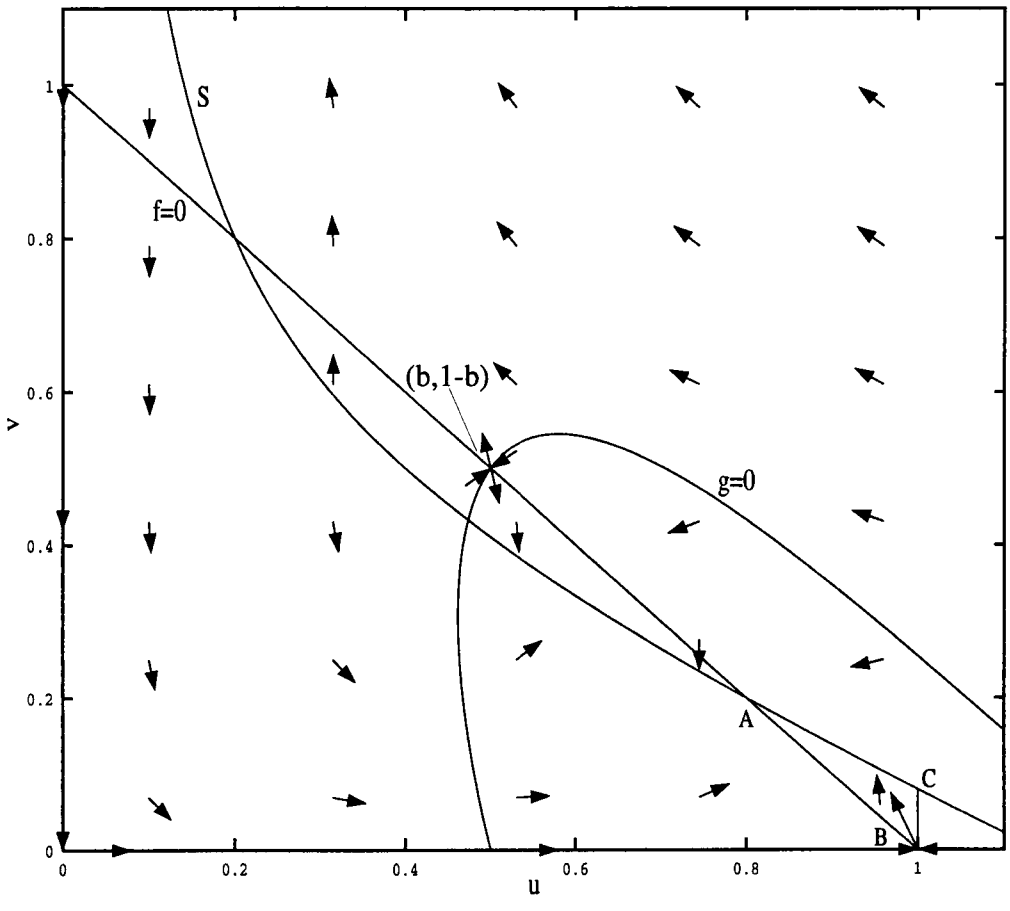



Figure 12: The vector field for system (I), and the local stable and unstable manifolds of the saddle points when $c^2 < b(1-b)$ and $ac^2 > b^2$.

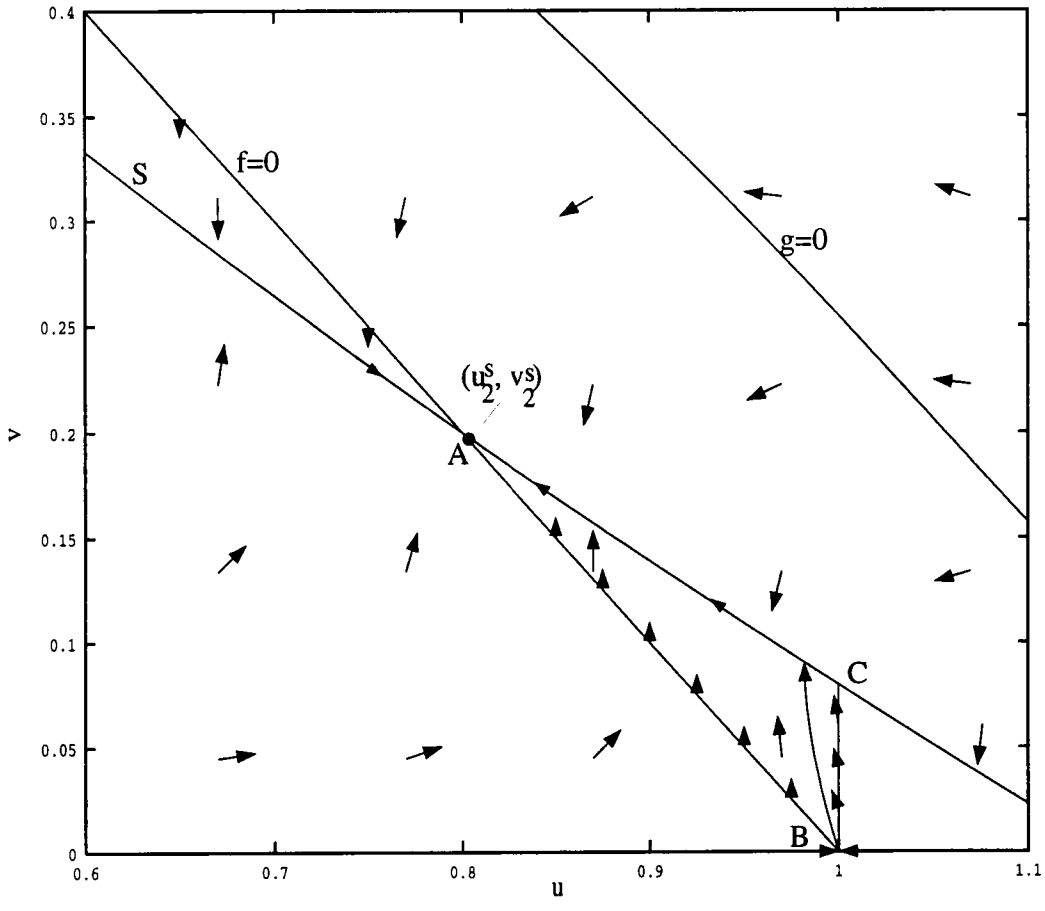



Figure 13: Local behavior of the vector field for system (I) when $c^2 < b(1-b)$ and $ac^2 > b^2$. Note that the trajectory $T$ that leaves the saddle point $(1,0)$ hits the singularity curve in finite time.

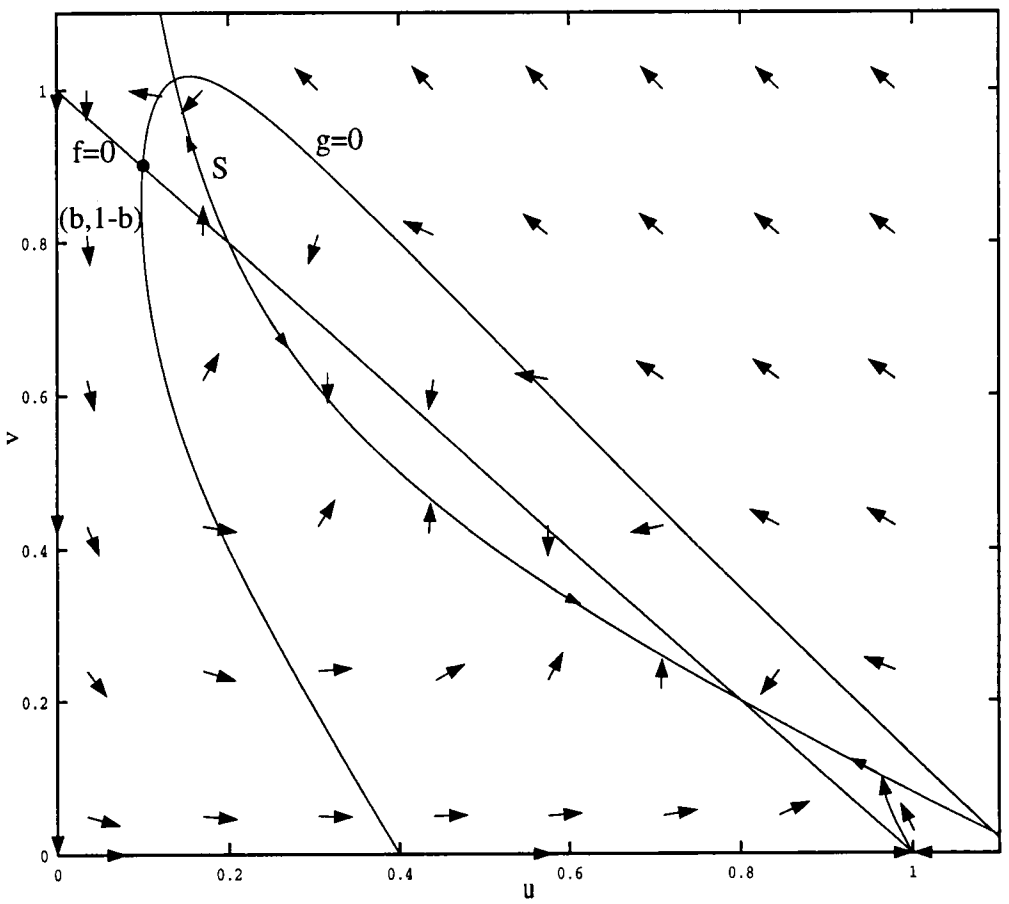



Figure 14: The vector field for system (I) when $b < \frac{1}{2}$, $\sqrt{b(1-b)} < c < \frac{1}{2}$, and $ac^2 > b^2$. Note that the trajectory $T$ that leaves the saddle point $(1,0)$ hits the singularity curve in finite time.

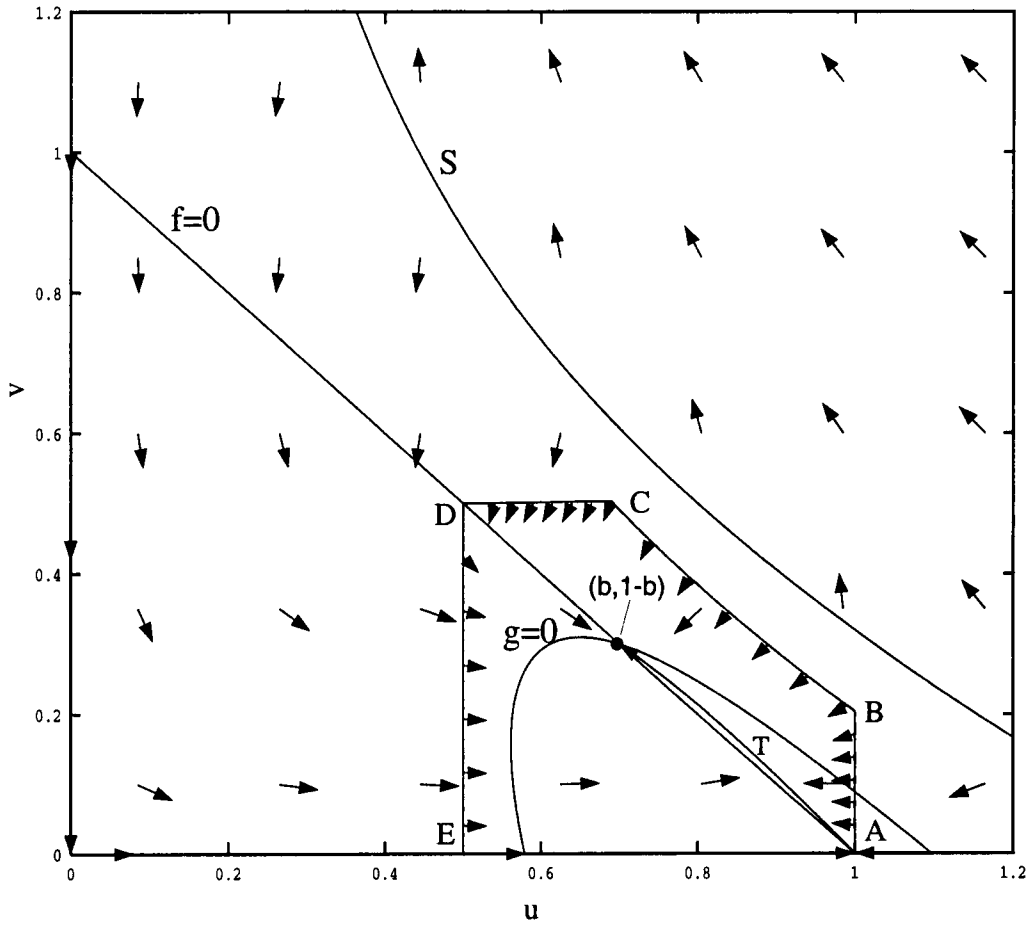



Figure 15: Typical phase plane portrait for system (I) when $b > \frac{1}{2}$, $c > \frac{1}{2}$, $c^2 > 4a(1-b) - 2$, and $ac^2 \leq b^2$. $ABCDE$ is the boundary of the invariant set about $(b, 1-b)$. Parameters are $a = 0.5$, $b = 0.7$, and $c = 0.8$.

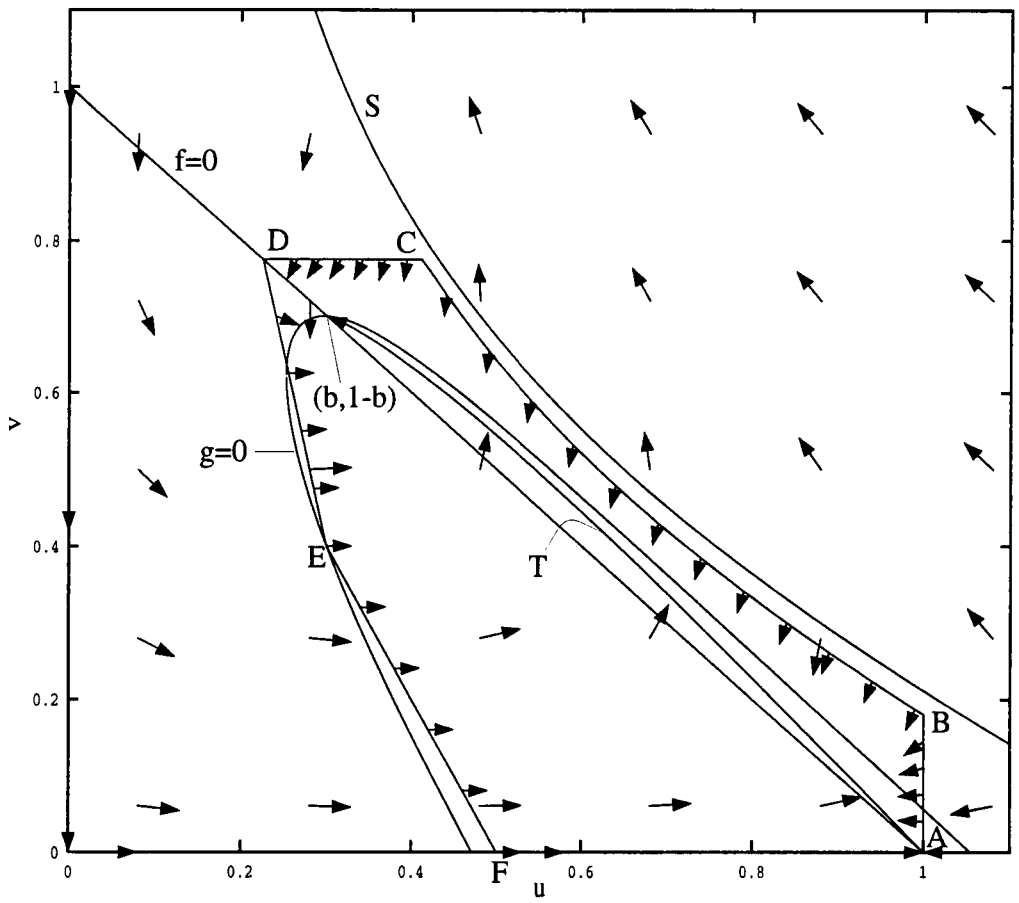



Figure 16: Typical phase plane portrait for system (I) when $b \leq \frac{1}{2}$, $c > \frac{1}{2}$, $c^2 > 4a(1-b) - 2$, and $ac^2 \leq b^2$. $ABCDE$ is the boundary of the invariant set about $(b, 1-b)$. Parameters are $a = 0.2$, $b = 0.3$, and $c = 0.65$.

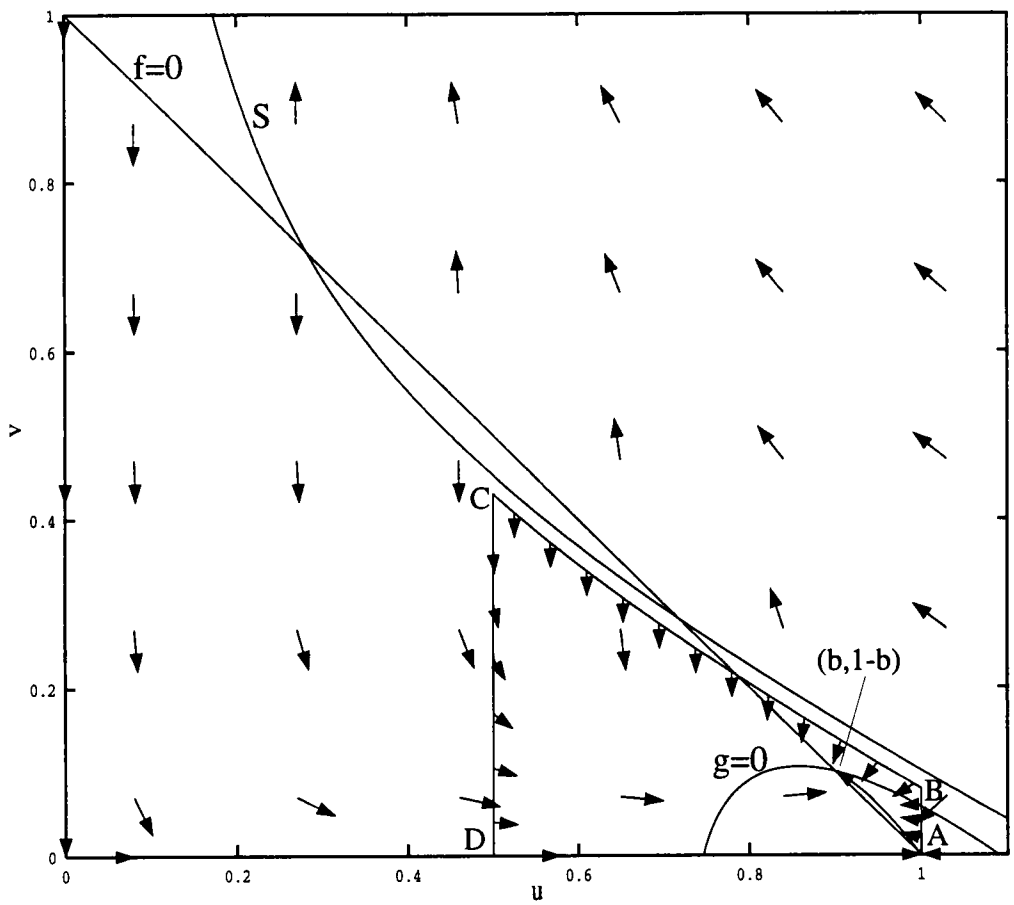



Figure 17: Typical phase plane portrait for system (I) when $\frac{1}{2} < b < 1$, $\sqrt{b(1-b)} < c \leq \frac{1}{2}$, and $c^2 > 4a(1-b) - 2$. $ABCD$ is the boundary of the invariant set about $(b, 1-b)$. Parameters are $a = 3$, $b = 0.9$, and $c = 0.45$.

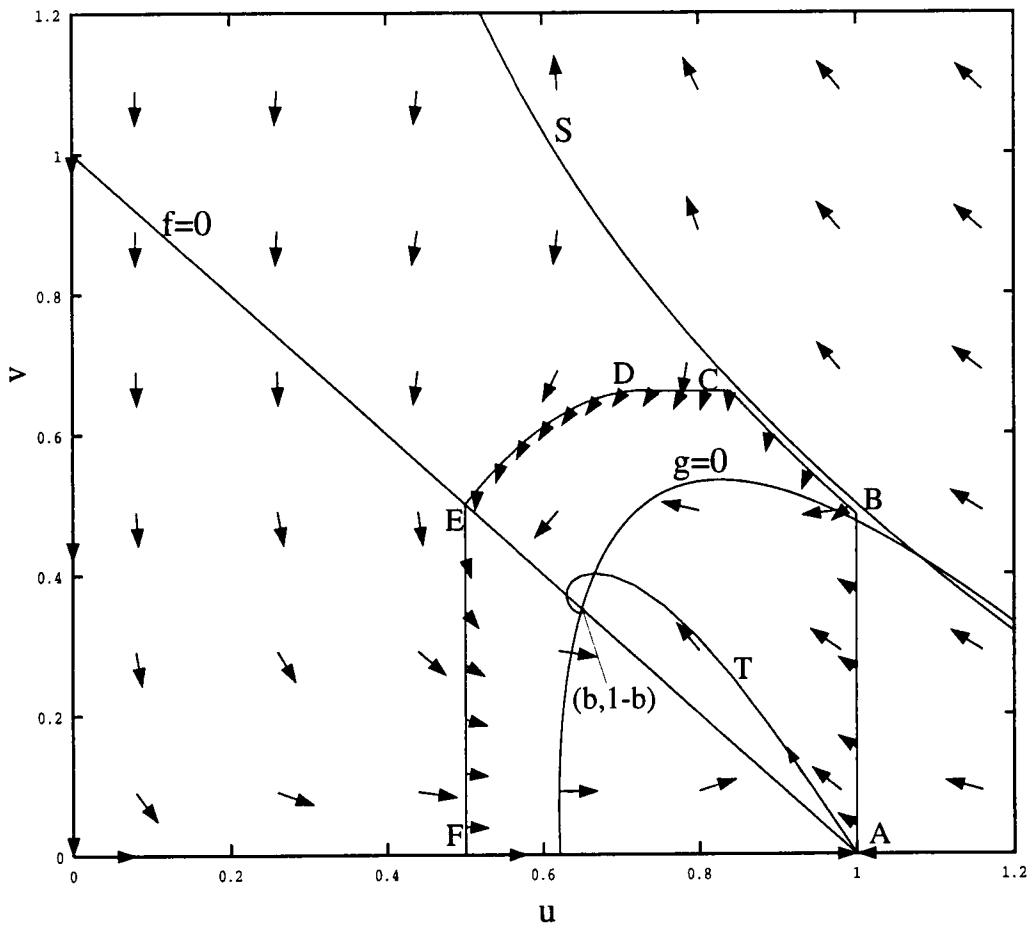



Figure 18: Typical phase plane portrait for system (I) when $b > \frac{1}{2}$, $c > \frac{1}{2}$, $c^2 > 4a(1-b) - 2$, and $ac^2 > b^2$. $ABCDEF$ is the boundary of the invariant set about $(b, 1-b)$. Parameters are $a = 2$, $b = 0.65$, and $c = 1$.

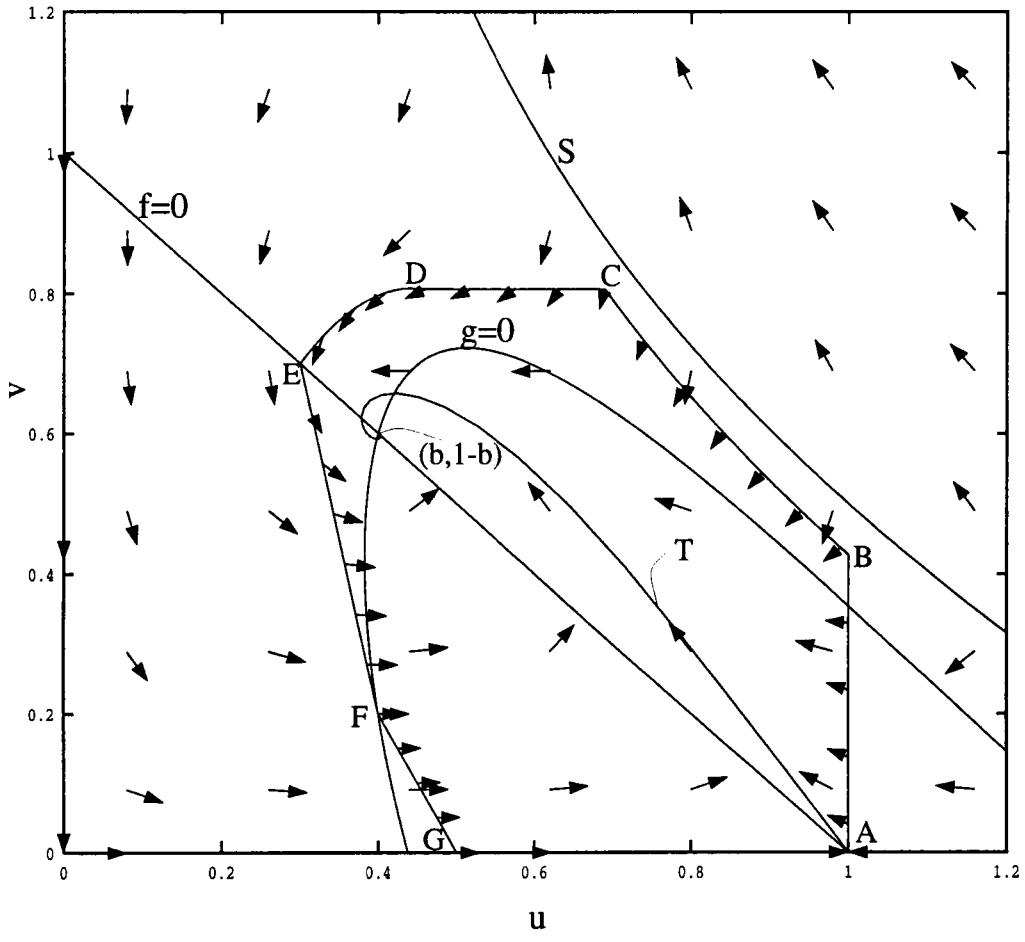
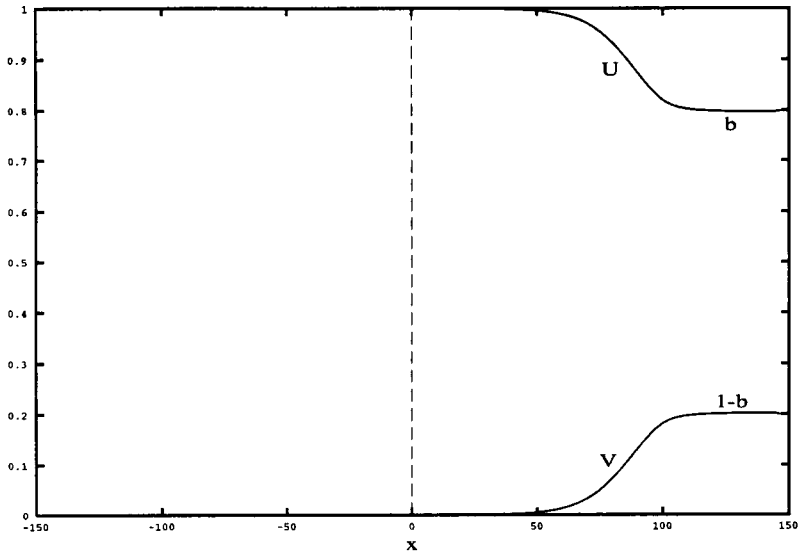
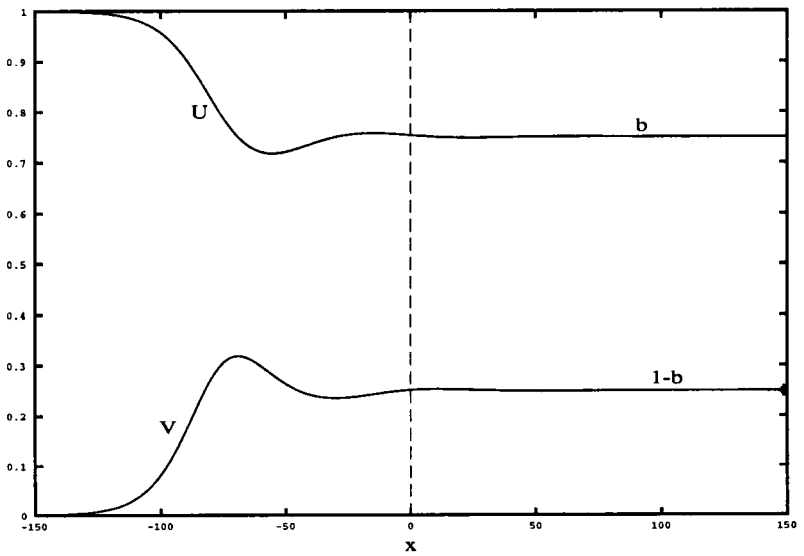



Figure 19: Typical phase plane portrait for system (I) when $b \leq \frac{1}{2}$, $c > \frac{1}{2}$, $c^2 > 4a(1-b) - 2$, and $ac^2 > b^2$. $ABCDEFG$ is the boundary of the invariant set about $(b, 1-b)$. Parameters are $a = 0.8$, $b = 0.4$, and $c = 1$.




(a)




(b)

Figure 20: Solutions of the predator ($V$)–prey ($U$) system (15) with initial conditions (26) at time $t = 20$. Parameters are: (a) $A = 0.1$, $\alpha = 0.1$, $a = 0.5$, and $b = 0.8$. (b) $A = 0.1$, $\alpha = 0.1$, $a = 4$, and $b = 0.75$. Note the damped oscillations about $b$, $1 - b$.

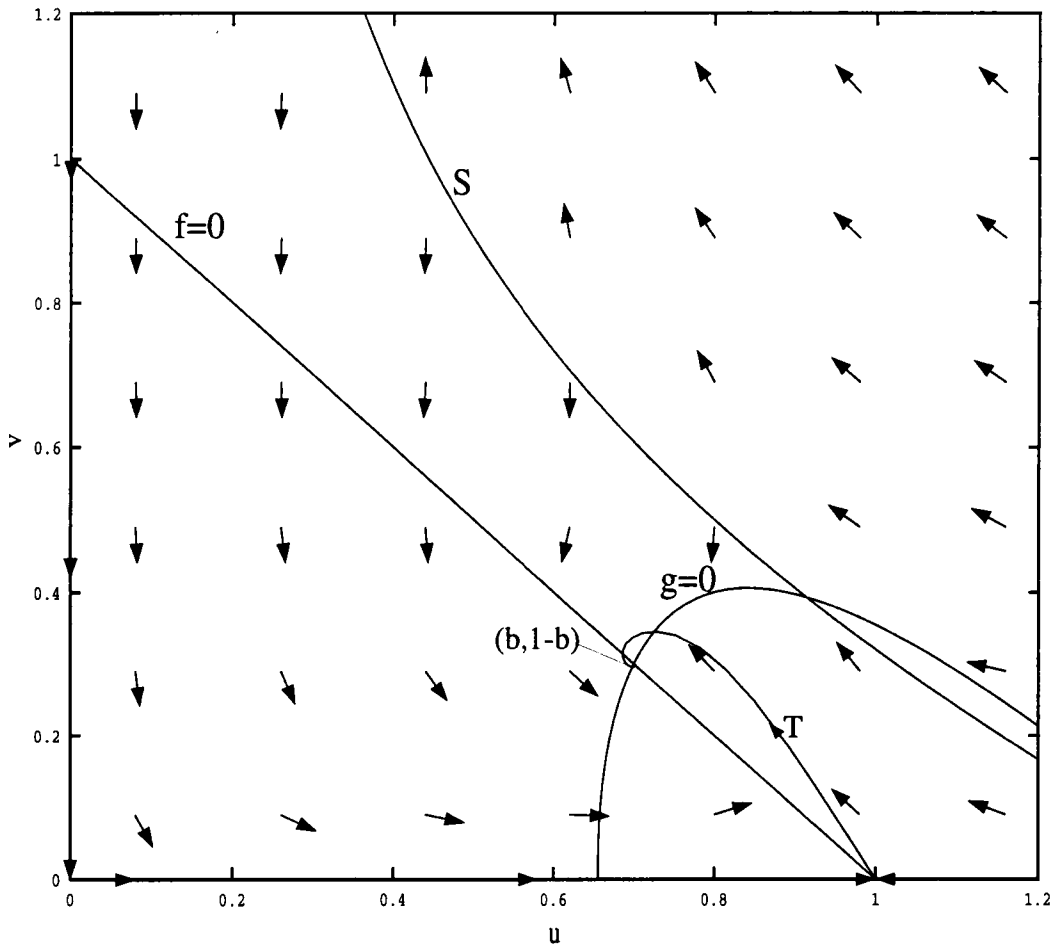



Figure 21: The vector field for system (I) and the heteroclinic connection, $T$, between $(1,0)$ and $(b,1-b)$ with $a=2.5$, $b=0.7$, and $c=0.8$.

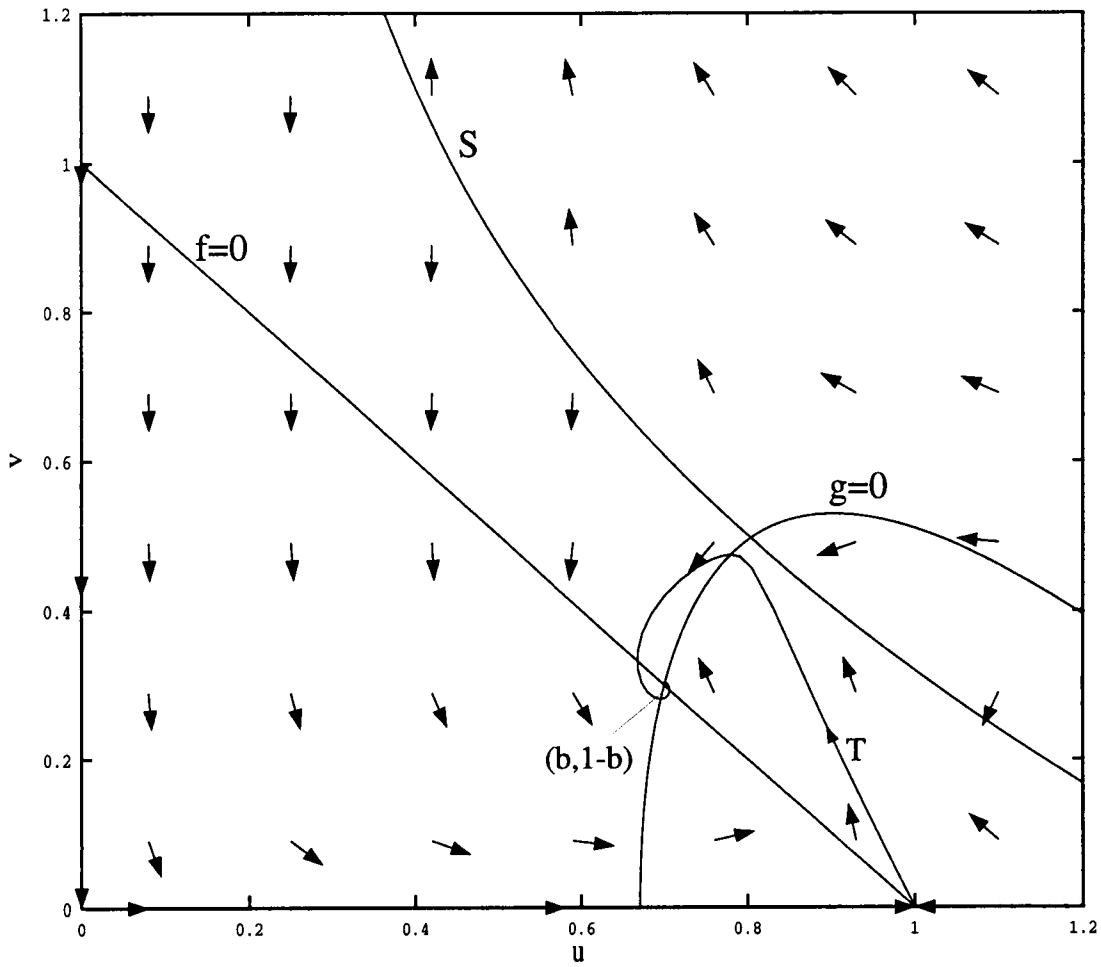



Figure 22: The vector field for system (I) and the heteroclinic connection, $T$, between $(1,0)$ and $(b,1-b)$ with $a=4$, $b=0.7$, and $c=0.8$.

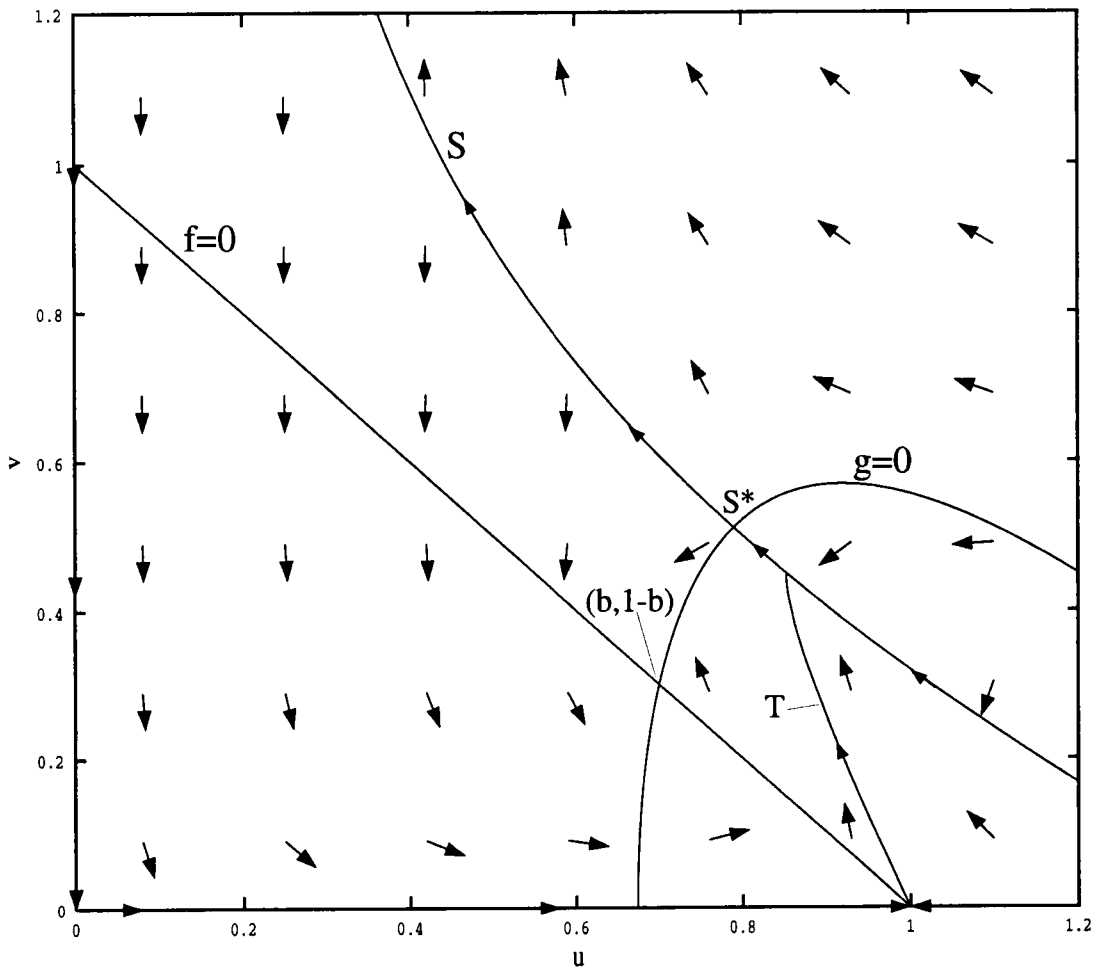
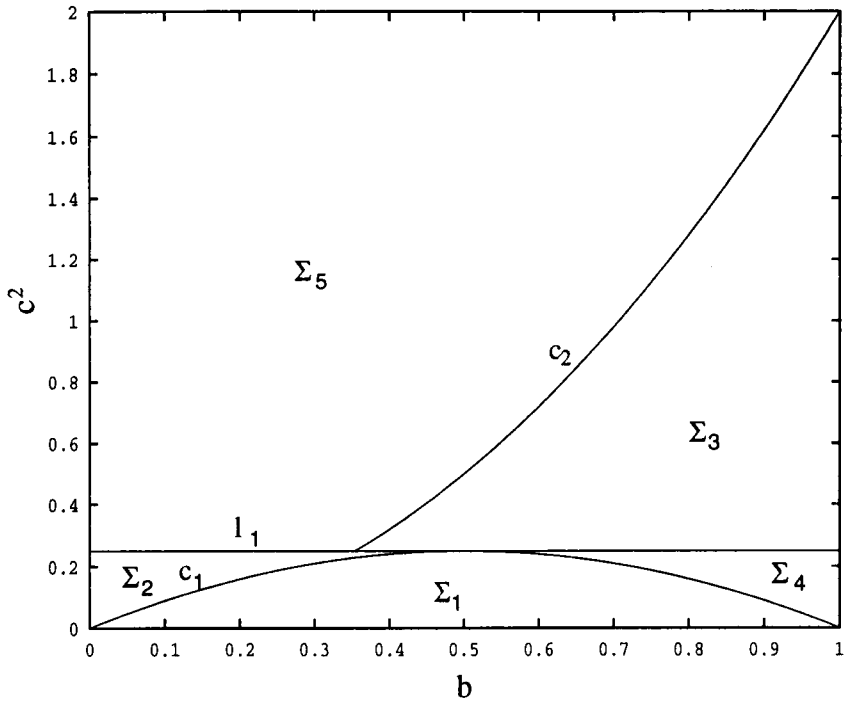
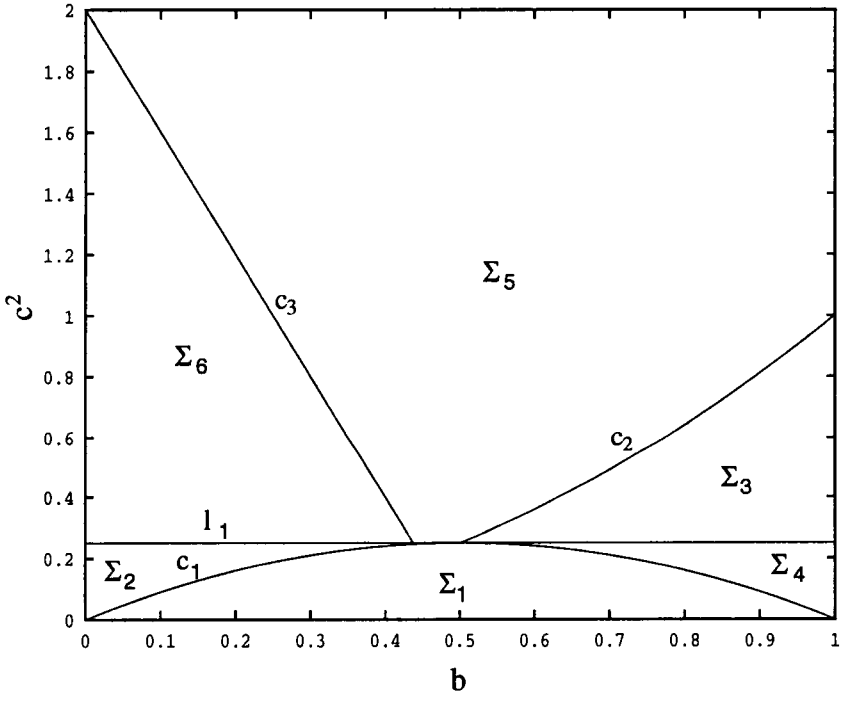


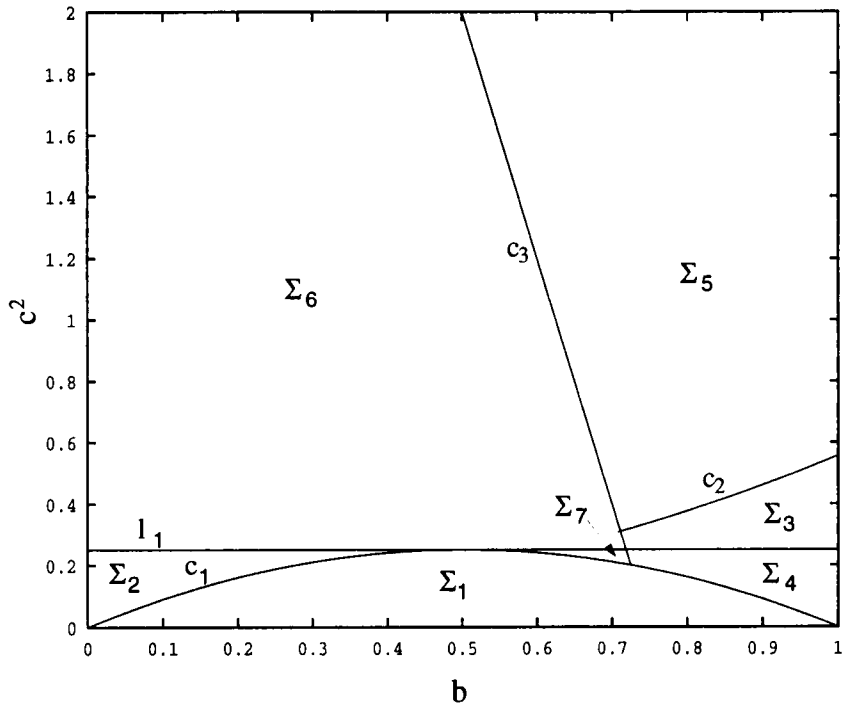

Figure 23: The vector field for system (I) with $(b, 1-b)$ with $a = 4.5$, $b = 0.7$, and $c = 0.8$. The trajectory $T$ that leaves the saddle point $(1, 0)$ hits the singularity curve in finite time.


$c^2$
b
$\Sigma_5$
$\Sigma_3$
$\Sigma_2$
$\Sigma_1$
$\Sigma_4$
$c_1$
$c_2$
$l_1$

(a)


$c^2$
b
$\Sigma_5$
$\Sigma_6$
$\Sigma_3$
$\Sigma_2$
$\Sigma_1$
$\Sigma_4$
$c_1$
$c_2$
$c_3$
$l_1$

(b)




(c)

Figure 24: Parameter domains for existence/nonexistence of traveling wave solutions of system (I). $l_1$ represents the line $c^2 = \frac{1}{4}$; $c_1$ represents the curve $c^2 = b(1-b)$; $c_2$ represents the curve $c^2 = \frac{b^2}{a}$; and $c_3$ represents the curve $c^2 = 4a(1-b) - 2$. (See text for details). (a) $a = 0.5$, (b) $a = 1$, and (c) $a = 2$.

# PART II

# PREY–DIRECTED MOVEMENT FOR A STRUCTURED FISH POPULATION

# 1 Introduction

In the interest of analytic tractability, many spatial models (see [23, 28] for a review) assume that individuals are identical. In part I of this dissertation we analyzed a simple aggregated predator–prey model in which the prey are immobile, predators move in the direction of increasing prey density, and each individual predator responds identically to changes in the prey density. In natural populations, individuals of different age and size often display differences in their movement behavior and in the velocities at which they move. Differences among individuals within a population due to demographic, genetic or environmental processes may force consideration of an individual-based approach instead of an aggregated one when a more faithful representation is desired.

In [17], Hallam et al. used an equation of extended McKendrick-von Foerster type to model dynamics of fish populations. This partial differential equation allows incorporation of individual dynamics into a dynamic population formulation, and contains explicit representation of physiological variables. While developing a protocol to assess the effects of lipophilic toxicants on a population, they found it necessary to include measures of the physiological variables age, lipid and structure (protein and carbohydrates). The use of an individual model that has lipid density as a compartment is necessary for studies in ecotoxicology because lipid variations can determine the bioaccumulation of lipophilic toxicants. From an ecological perspective, lipid is essential for reproduction and also serves as an energy resource while structure is necessary for reproduction and growth.

Even though the classical single extended McKendrick-von Foerster model allows the incorporation of individual dynamics into a population, individual organisms can

differ only by age and initial birth sizes. All individuals of the same age and same initial size have the same genetic, physiological and environmental constraints, and hence grow according to the same dynamics. To introduce individual variability in the population model, Hallam et al. [17, 19, 18] coupled several equations of extended McKendrick-von Foerster type where each equation models subpopulations that have different physiological and environmental characteristics (as reflected by different parameter values in the individual model). In the *Daphnia* and fish models [17, 18], three parameters have been used to introduce individual variability; two environmental parameters (the resource density and the fraction of lipid in the resource) and one physiological parameter (the daphnid filtering rate and the fish gut clearance rate). In both cases, each of the three parameters was varied through three levels, introducing a total of 27 ecotypes. This led to metapopulations that exhibit variation in both initial individual size and physiological structure.

A primary aim of this study has been to introduce individual variability due to environmental processes by incorporating spatial heterogeneity and a varying food supply in the physiologically–based fish model introduced by Hallam et al. [17].

For the prey population, we assume that all individuals are essentially identical and do not move, or move very slowly relative to the predator's speed of movement. Hence, the prey population is unstructured and sessile. Its dynamics are assumed to be governed by an ordinary differential equation.

Fish are assumed to live and move in a closed bounded habitat; that is, migration into or out of the habitat is not allowed. Births and deaths are the only contributions to the changes of the fish population in the habitat. In our model, all individuals are assumed to be female and reproduction is clonal. Movement behavior of the fish within the habitat might be very complicated. Because later in this work effects of lipophilic nonpolar narcotic chemicals on fish populations in a heterogeneous environment are studied, attention is given to the foraging behavior of the fish. It is reasonable to assume that an individual fish moves in the direction where food density

is higher because all prey are identical. Although all individuals alter their movement in response to the local changes of the food density, their movement velocities depend on the size of the individual. Because we structure the fish population in terms of lipid and structural mass, a model that describes the dynamics of lipid and structure of an individual has to be employed.

# 2 Individual Model

The model that we use for the dynamic behavior of an individual fish is based on the physiologically-based individual model introduced by Hallam et al. [17]. It has been developed to deal with rainbow trout, *Oncorhynchus mykiss*, but because of the generality of the energetics approach, it can be used for other species of fish with some necessary modifications. The model for an individual fish features two components: lipid, $m_l$, and structure, $m_s$. Each of these components consists of a labile and nonlabile portion. The nonlabile portion is the mass of lipid and structure bound in somatic tissue that cannot be mobilized even under conditions of starvation. The labile portion of lipid and structure is available for growth and reproduction.

The rates of change of the lipid and structure are the differences in growth rates (measured by the assimilated lipid and structure) and loss rates. The losses represent lipid and structural matter allocation to egg production, energy allocation to maintenance, specific dynamic action (SDA), activity and reproduction. We assume that the losses due to maintenance, SDA and activity occur on a continuous time scale and that the reproductive losses occur periodically on a discrete time scale.

The dynamics of lipid and structural mass of an individual fry (young trout before it starts feeding) are represented only by the cost of differentiation and maintenance, which is assumed to be proportional to the size of the components, and are modeled

by the equations

$$\frac{dm_l}{dt} = -B_1 m_l \,,$$

(1)

$$\frac{dm_s}{dt} = -B_2 m_s \,,$$

with initial conditions $m_l(0) = m_{l0}$ and $m_s(0) = m_{s0}$, the lipid and structure content of an egg. Rainbow trout eggs hatch 34–36 days after fertilization at $10°C$ ([33]), the yolk sac is depleted 3–7 days later, and the fry begin feeding about 15 days after hatching ([29]).

After an organism commences feeding, $Y$ days after fertilization, the dynamics of the lipid and structural mass are modeled by the ordinary differential equations

$$\frac{dm_l}{dt} = g_l(m_l, m_s, X) = \frac{a_{0l} X_l}{X} F - a_1 (m_l - \epsilon m_{ps}) \frac{E_d}{E_a} \,,$$

(2)

$$\frac{dm_s}{dt} = g_s(m_l, m_s, X) = \frac{a_{0s} X_s}{X} F - a_2 (m_s - m_{ps}) \frac{E_d}{E_a} \,.$$

with initial conditions given by the final values $m_l(Y)$ and $m_s(Y)$ obtained from (1).

**The Loss Terms.** The terms $(m_l - \epsilon m_{ps})$ ($\epsilon$ is nondimensional: mass of lipid / mass of structure) and $(m_s - m_{ps})$ represent the labile portions of lipid and structural mass of an individual. The variable $m_{ps}$ (mass of protected structure) is assumed to be nondecreasing with age and is computed as a fraction $\beta m_s$ of the structural mass. $E_a$ denotes the energetic equivalent of the mass that an individual utilizes in order to maintain basal metabolism. This energy is derived from the labile lipid and labile structure using the function

$$E_a = 3.768 \cdot 10^4 a_1 (m_l - \epsilon m_{ps}) + 1.675 \cdot 10^4 a_2 (m_s - m_{ps}) \,,$$

where $a_1$ and $a_2$ are the rates $(1/d)$ at which lipid and structure are mobilized to maintain basal metabolism, and the numbers in each term are the energetic values in *joules* of 1 $g$ of lipid and structure, respectively.

The rates at which the labile lipid and structure are utilized depend on the energy demands, $E_d$, of the organism. This is accomplished via supply energy that is

apportioned by the fraction $E_d/E_a$.

The total energy demand, $E_d$, is comprised of a number of subcomponents: maintenance, SDA which represents work associated with feeding, and activity which represents the work associated with swimming.

*Maintenance.* Maintenance demand is the energy utilization by animal organs and tissues at complete rest, also referred to as standard metabolism. Brett et al. ([5]) estimate the standard metabolism of rainbow trout to be 100 $mg\, O_2/Kg \cdot hr$, and list the respiratory energy equivalent for fish as 3.25 $cal/mg\, O_2$. This gives a standard metabolism of 32.5 $J/g \cdot d$. Thus, the energy needed by rainbow trout for maintenance is $32.5(m_l + m_s)\ J/d$.

*Specific Dynamic Action.* Another factor contributing to the total energy demands is the so–called specific dynamic action (SDA) of food. SDA is the increase in heat production following a meal and is associated with amino acid mobilization and biochemical processes associated with digestion [6, 24]. SDA is greater if the diet is rich in protein and less if the diet is rich in carbohydrates. Estimates vary between 6 and 30% of the ingested energy.

*Activity.* The energy cost for activities includes cost of cruising and cost of pursuit and capture of the daily food. Gerritsen's [12] activity formulation is used to calculate the energy required by a swimming fish :

$$P = 0.2376 \cdot 10^{-6}\, S\, v^{5/2}\, L_f^{-1/2}\, q^{-1}\,,$$

where $P$ is given in $J/d$. $L_f$ is the length of the fish in $m$, $S$ is the wetted surface area and given by $\beta_2\, L_f^2$, $v$ is the swimming velocity $(m/sec)$ (part of the time cruising and part of the time pursuing food), and $q$ is the swimming efficiency.

**Growth Terms.** We now return to equations (2) to describe the components associated with feeding. The feeding rate $F$ $(g/d)$ of an individual is governed by constraints imposed by processes associated with encounter, pursuit and digestion of a prey. These processes are implemented sequentially, i.e., the encounter, pursuit and digestion of a prey must be completed first before another prey may begin to be

processed. For a sequential process the feeding rate is given by the form (cf. [22])

$$F = \frac{1}{T_e + T_p + T_d}. \tag{3}$$

The terms in the denominator represent the characteristic times $(d/g)$ for encounter, pursuit, and digestion of prey.

The time an individual spends encountering one gram of food is expressed as $T_e = 1/a_d X$, where X is the density of the prey $(g/m^3)$ (dry weight) which is assumed to be immobile. The encounter rate coefficient, $a_d$ $(m^3/d)$, represents the volume swept per unit time by the foraging fish [13] and is given by

$$a_d = \pi\, s_d^2\, v_s\,,$$

where $s_d$ is the reactive distance $(m)$ of the fish [4] given by $s_d = [aL_p + b]L_f^{1/2}$; $L_p$ and $L_f$ denote the lengths of the prey and fish in $m$, and $a$ and $b$ are constants with units $m^{-1/2}$ and $m^{1/2}$ respectively. The length of the fish $L_f$ is given by the allometric relationship $L_f = \sqrt[3]{m_{ps}/\beta_1}$. The fish searches for food at a velocity characteristic of its species and body size. From a modeling perspective, the assumption made to implement this is that a fish searches for food at a velocity directly proportional to its length, $v_s = 8.64 \cdot 10^4\, s\, L_f$ $(m/d)$, where $s$ denotes the body lengths per second of the fish while searching and is characteristic of the species. A fish searching for food might alter its swimming speed in space and time depending on the local feeding opportunity. Predators might increase their speed in response to the gradient of the prey. The latter possibility is not entirely a speculation as Magnuson [26] found that skipjack tuna increased their swimming speed above the basal level when food extracts were injected into the water. The way we model this case is discussed in the next section.

The time an individual spends to pursue and capture one gram of food is $T_p = D/v_p M_p$, where $v_p = 8.64 \cdot 10^4\, s_p\, L_f$ $(m/d)$ is the pursuit velocity of the fish which is usually different from the searching velocity; $M_p$ is the mass of a prey $(g)$; and $D$ is the distance between the fish and a neighboring prey $(m)$. If we assume that the

resource is composed of discrete particles (prey) of mass $M_p$, uniformly distributed in the unit volume, the variable $D$ is assumed to be half the distance between two prey and is computed by $D = \frac{\sqrt{3}}{2} \sqrt[3]{\frac{M_p}{X}}$.

The time an individual spends digesting one gram of food is given by $T_d = 1/kM_g$, where $M_g$ is the mass capacity of the fish's gut ($g$) calculated from the volume $V_g$ of the fish's gut and the body density of the prey $d_p$. $V_g$ is a linear function of fish mass [14] given by $V_g = c\, m_{ps}$. The constant $c$ has units of $cm^3/g$ . $m_{ps}$ is used in this representation so that the volume of the gut is nondecreasing. The gut clearing rate coefficient $k$ ($1/d$) depends on several factors. The most significant of these are fish size and temperature [14]. Since in this formulation of the model we do not consider temperature variations, we take $k$ to depend only on the size of the fish. To find a representation for $k$, Hallam et al. [17] used the following gut clearance model

$$\frac{dm_g}{dt} = -km_g$$

where $m_g$ ($g$) is the mass of the food at time $t$. Solving this equation, we observe that $k$ is proportional to (gut clearance time)$^{-1}$. In general, gut clearance time is proportional to (fish mass)$^{k_1}$, and, thus, $k = k_0 m_{ps}^{-k_1}$, where $k_1$ is nondimensional, and $k_0$ is a constant with units $g^{k_1}/d$. For rainbow trout, $k_1 = 0.7$ [14].

If $X_l$ and $X_s$ are the densities of (dry) resource lipid and structure and if a constant proportion $a_{0l}$ of the ingested lipid, $\frac{X_l}{X}F$, and a constant proportion $a_{0s}$ of the ingested structure, $\frac{X_s}{X}F$, is assimilated, then

$$\frac{a_{0l}X_l}{X}F\,, \quad \frac{a_{0s}X_s}{X}F$$

represent the mass of lipid and the mass of structure gained by consumption per unit time.

**Reproduction and Mortality.** Fish are assumed to reproduce periodically after attaining maturation size (Brown [7] indicates that seasonal periodicity in egg production is characteristic of many fish species; the reproductive time interval $P$ is

taken as 365 days in our computations). Reproduction occurs in a time window to represent seasonal aspects of reproduction. The organism grows according to equations (1) and (2) until reproduction occurs at the first reproductive window at age $A$. At this time losses associated with reproduction are computed, and the initial conditions of (2) are reset. The individual again grows according to (2) until it reproduces again at age $A + P$. This process is repeated periodically with period $P$ until the individual dies. An organism dies either because it reaches the prescribed maximum age or because its structural mass, $m_s$, decreases below the protected structural mass $m_{ps}$. The latter may happen due to losses associated with reproduction and/or due to shortage of food.

Losses associated with reproduction represent lipid and structural mass needed for egg formation as well as the energy utilized to accomplish this transfer of mass. These allocations obviously do not occur instantaneously. Because there is little specific information on the time scales of these processes and they are short relative to population time scales, we treat them as discrete events.

The number of eggs produced by an individual will be constrained by both lipid and structural mass available for reproduction. Although variation in egg size is probably controlled by many factors, we assume here that only lipid constrains this process. Therefore, the egg is assumed to be composed of a fixed amount of structural material and a variable amount of lipid. The governing factors for allocation of lipid to eggs are assumed to be labile lipid, $m_l - \epsilon m_{ps}$, and a counteractive coupling with labile structure. If $E_s$ is the maximum number of eggs for available labile structure, the lipid allocated to each egg is defined by

$$\frac{(e_M - e_m)(m_l - \epsilon m_{ps})}{A_1 E_s + (m_l - \epsilon m_{ps})} + e_m \,,$$

where $e_m$ and $e_M$ are the minimum and maximum amount of lipid contained per egg, respectively. Although this hyperbolic function assumes values in the interval $[e_m, e_M)$, the maximum $e_M$ is only attained asymptotically as labile lipid is large. The maximum number of eggs for available labile structure, $E_s$, regulates the egg

lipid, since for fixed labile lipid, egg lipid decreases as $E_S$ increases. The constant $A_1$ $(g/egg)$ determines, in some sense, the relative importance the female places on the amount of lipid in the eggs, and consequently, the initial size of the eggs. The maximum number of eggs per available lipid, $E_l$, is the total labile lipid, $m_l - \epsilon m_{ps}$, divided by the lipid per egg.

A constraint to set the maximum number of eggs that can be produced from labile structure is also needed. Weatherley [38], using data from Allen [1], found that the number of eggs laid by trout in the Horokiwi stream can be determined, at least in a restricted range, as a linear function of body length. Using this information, we define the maximum number of eggs, $E_s$, produced per available protein and carbohydrate by a female of length $L_f$ as

$$\min \{\sigma(L_f - \eta),\ (m_s - m_{ps})/e_s\}\ .$$

The first expression gives the number of eggs per clutch as a linear function of organism length. The positive number $\eta$ $(length)$ is chosen to be the length at which the organism first reproduces. Thus, the expression results in a positive number of eggs. The slope, $\sigma$, is generally a function of resource availability. The second expression is the structural material available for reproduction, $m_s - m_{ps}$, divided by a prescribed amount of structure, $e_s$, in each egg. Weatherley [38] argues that the size at reproduction is a governing factor for reproduction. We have imposed the size constraint for reproduction and also require that there be sufficient lipid and structure to make eggs.

The total number of eggs per female is $\min\{E_l,\ E_s\}$. The egg composition, assumed to be a fixed amount of structural material, $e_s$, and a variable amount of lipid, fluctuates according to labile lipid reserves.

The energy required to support the mass transfer of lipid and structure to reproduction is modeled by $A_2 S_e + A_3 L_e$, where $S_e$ and $L_e$ are the total structure and lipid in eggs, respectively.

Table 1 summarizes the model parameters and gives the default values used in the simulations [1].

# 3 The Dynamic Predator–Prey Model

Let $\rho(t, a, m_l, m_s, x)$ $(numbers/d \cdot g^2 \cdot m)$ be the population density function which depends upon time, the physiological variables $a$, representing age $(d)$; $m_l$, representing the mass of lipid $(g)$; $m_s$, representing the mass of structure $(g)$; and the spatial variable $x$, representing the spatial location of an individual in a bounded linear habitat $I$. Then an equation that incorporates the growth of these physiological variables and the movement of an individual into the population is

$$\frac{\partial \rho}{\partial t} + \frac{\partial \rho}{\partial a} + \frac{\partial(\rho\, g_l)}{\partial m_l} + \frac{\partial(\rho\, g_s)}{\partial m_s} + \frac{\partial(\rho\, q)}{\partial x} = -\mu\rho\,. \tag{4}$$

A derivation of this model may be found in Appendix I. For simplicity, we assume that individuals live in a linear habitat, i.e., $I \subset R$. For instance, a linear habitat might be a coastline or a river. In equation (4), $g_l = g_l(m_l, m_s, X)$ and $g_s = g_s(m_l, m_s, X)$ are the growth rates $(g/d)$ of the lipid and structural components of an individual respectively, and are given in formulae (1) and (2). Here, $X = X(t, m_l, m_s, x)$ is the prey density to which a predator with lipid content $m_l$ and structure content $m_s$ responds. Since resource is limited, predators which are assumed to forage in social groups divide the resource by an intraspecific competitive mechanism with larger predators receiving larger shares. If $r(t, x)$ is the prey density $(g/m^3)$ at location $x$, then a predator with mass of lipid $m_l$ and mass of structure $m_s$ located at $x$ responds to a density $(g/m^3)$ of

$$X(m_l, m_s, x, \Delta x) = r(t, x)\frac{m_l + m_s}{\int_{x-\Delta x}^{x+\Delta x}\int_0^\infty\int_0^\infty\int_0^\infty (m_l + m_s)\rho(t, a, m_l, m_s, y)\, da\, dm_l\, dm_s\, dy}\,,$$

where the denominator represents the total predator biomass in a small interval $(x - \Delta x, x + \Delta x)$ around $x$.

[1] All Figures and Tables appear in Appendix III.

The mortality function $\mu$ is assumed to have the form

$$\mu = \mu_a + \mu_d,$$

where $\mu_a$ represents the mortality in the population due to age and $\mu_d$ represents a density dependent mortality. The age-dependent mortality is assessed uniformly along cohorts born at the same time, whereas the density-dependent mortality is assessed uniformly across the population with age in the interval $[a_0, a_J]$; where $a_0$ and $a_J$ represent the beginning and ending of the juvenile period, respectively. Density-dependent mortality might be caused by predation or overcrowding. The specific forms of these mortalities are given in Table 2.

The function $q = q(m_l, m_s, x)$ is the movement velocity $(m/d)$ and describes how an individual of age $a$, lipid mass $m_l$ and structure mass $m_s$ at location $x$ alters its movement in response to environmental heterogeneity and energetic constraints. We assume that individuals tend to move towards neighboring areas with higher prey densities. The resource-directed movement velocity of an individual will depend on the size of the individual, the energy gained, and the gradient of the resource at the position where the individual is located.

In our illustrations we implement two movement behaviors

$$q = \kappa v_s \frac{\partial r}{\partial x}, \tag{5}$$

$$q = \begin{cases} 0 & if \;\; E_g > E_d \\ \kappa v_s \frac{\partial r}{\partial x} & if \;\; E_g \leq E_d \end{cases}, \tag{6}$$

where $\kappa$ is a positive constant that measures the tendency of predators to pursue prey and represents the distance covered by the foraging predator per unit change in the prey density. $\frac{\partial r}{\partial x}$ denotes the derivative of $r$ with respect to the variable $x$ and represents the change of the resource at $x$. $v_s$ is an average swimming velocity $(m/d)$ of an individual with length $L_f(m)$ and is given by $v_s = 8.64 \cdot 10^4 s L_f$ where $s$ denotes the body lengths per second of the predator while performing sustained cruising.

Movement behavior (5) represents the case in which predators change location continuously in the direction of increasing prey. Movement behavior (6) represents the case in which predators do not change location when the energy gained, $E_g$, while foraging around location $x$, exceeds the energy demands, $E_d$, even if there are local changes in the prey density. In both cases, $q$ determines the spatial movement of individuals relative to their location. If there are no local changes of the prey density, or if $E_g > E_d$, then predators do not change foraging location and the speed at which predators encounter prey is determined only from physiological constraints. Therefore, an individual fish of length $L_f$ foraging at location $x$ encounters prey at a rate given by $\max\{q, v_s\}$.

Because we do not discriminate between prey individuals, we will treat the density of the prey at location $x$ as a single dynamically varying quantity. The prey population at location $x$ is modeled by the differential equation

$$\frac{dr}{dt} = R(r) - \int_0^\infty \int_0^\infty \int_0^\infty F(m_l, m_s, X)\rho(t, a, m_l, m_s, x) da dm_l dm_s \,, \tag{7}$$

where $R(r)$ describes the growth of the prey in the absence of predators and the integral term describes the prey mortality due to predation with the food intake rate $F(m_l, m_s, X)$ given by equation (3).

In addition to the balance law equation (4) and the dynamical equation (7), we adjoin the initial conditions

$$\rho(0, a, m_l, m_s, x) = \rho_0(a, m_l, m_p, x) \,, \tag{8}$$

$$r(0, x) = r_0(x) \,, \tag{9}$$

the boundary condition

$$q\rho = 0 \quad x \in \partial I \,, \tag{10}$$

which asserts that there is no flow of the population across the boundary of the habitat, and the boundary condition or renewal equation

$$\rho(t, 0, m_{l0}, m_{s0}, x) = \int_0^\infty \int_0^\infty \int_0^\infty \beta\rho(t, a, m_l, m_s, x)\, da\, dm_l\, dm_s \,, \tag{11}$$

where $m_{l0}$ is the mass of the lipid and $m_{s0}$ is the mass of the structure at $a = 0$ and $\beta = \beta(t, a, m_{l0}, m_{s0}, m_l, m_s)$ represents the expected number of eggs with lipid content $m_{l0}$ and structure content $m_{s0}$ born to an individual of age $a$ with lipid content $m_l$ and structure content $m_s$ at time $t$.

# 4 Numerical Procedure

The approach utilized to compute the predator density function, $\rho$, is the method of characteristics. The characteristic curves of (4) in $(t, a, m_l, m_s, x, \rho)$-space are given by the system of ordinary differential equations

$$
\begin{aligned}
\frac{dt}{d\tau} &= 1\,, \\
\frac{da}{d\tau} &= 1\,, \\
\frac{dm_l}{d\tau} &= g_l\,, \\
\frac{dm_s}{d\tau} &= g_s\,, \\
\frac{dx}{d\tau} &= q\,, \\
\frac{d\rho}{d\tau} &= -(\mu + \frac{\partial}{\partial m_l} g_l + \frac{\partial}{\partial m_s} g_s + \frac{\partial}{\partial x} q)\rho\,.
\end{aligned}
\tag{12}
$$

Along a characteristic in $(t, a, m_l, m_s, x)$–space, the density function $\rho$ can change, according to the last of the characteristic equations in (12), not only when mortality acts but also when the growth rates $g_l, g_s$ and the movement rate $q$ of the individuals change. For purposes of interpretation, it is convenient to transform the problem to the setting where the computations along characteristics indicate effects of mortality only.

Because of the assumption that the growth and movement of an individual are deterministic, all individuals that are born at the same time and place with the same lipid and structural content will stay together as a cohort during their entire lives. This assumption implies that for $a < t$ (after the initial population has died out), instead of a representation by means of one density function $\rho(t, a, m_l, m_s, x)$, the fish population is equivalently characterized (locally) by a density function $u(t, a)$, which

describes the age distribution of the population, and the relations $m_l = m_l(t,a)$, $m_s = m_s(t,a)$ and $x = x(t,a)$ which represent respectively the mass of lipid, the mass of structure and the location of an individual of age $a$ at time $t$.

The equations for the dynamics of $u = u(t,a)$, $m_l = m_l(t,a), m_s = m_s(t,a)$ and $x = x(t,a)$ can be derived by following one cohort of identical individuals through time. In order to derive the new equations, we use a technique that has been called the "Murphy trick" [27].

Let $\Delta t$ be a time increment. If we follow one cohort, then the average amount the mass of lipid of an individual of age $a$ at time $t$ grows during the time interval $(t, t+\Delta t)$ is

$$m_l(t+\Delta t, a+\Delta t) - m_l(t,a). \tag{13}$$

We have assumed that the growth rate $g_l$ of the lipid $m_l$ depends upon the mass vector $\mathbf{m} = (m_l, m_s)$, representing the mass of lipid and the mass of structure, of an individual and the resource density to which it responds. Then, the average amount the mass of lipid of an individual in the $(t,a)$–cohort grows during $(t, t+\Delta t)$ is given by

$$\int_0^{\Delta t} g_l(\mathbf{m}(t+\tau, a+\tau), X(\mathbf{m}(t+\tau, a+\tau), x(t+\tau, a+\tau))\, d\tau \tag{14}$$

If we equate (13) and (14), divide by $\Delta t$ and take the limit as $\Delta t \to 0$, we find, assuming sufficient smoothness

$$\frac{\partial m_l}{\partial t} + \frac{\partial m_l}{\partial a} = g_l(\mathbf{m}(t,a), X(\mathbf{m}(t,a), x(t,a)))\,. \tag{15}$$

Similarly, we derive the equations for $m_s$, $x$, and $u$, which eventually lead to the reformulated set of equations:

$$\frac{\partial u}{\partial t} + \frac{\partial u}{\partial a} = -\mu u(t,a)\,, \tag{16a}$$

$$\frac{\partial m_l}{\partial t} + \frac{\partial m_l}{\partial a} = g_l(\mathbf{m}(t,a), X(\mathbf{m}(t,a), x(t,a)))\,, \tag{16b}$$

$$\frac{\partial m_s}{\partial t} + \frac{\partial m_s}{\partial a} = g_s(\mathbf{m}(t,a), X(\mathbf{m}(t,a), x(t,a)))\,, \tag{16c}$$

(16d) $$\frac{\partial x}{\partial t} + \frac{\partial x}{\partial a} = q(\mathbf{m}, r_x(t, x(t,a)))\,,$$

(16e) $$\begin{aligned} m_l(t,0) &= m_{l0}, \quad m_s(t,0) = m_{s0}\,, \\ x(t,0) &= x_0, \qquad u(t,0) = \textstyle\int_0^\infty \beta(t,a,\mathbf{m}(t,a))u(t,a)da\,, \end{aligned}$$

(16f) $$\begin{aligned} u(0,a) &= U(a), \qquad x(0,a) = \Psi(a)\,, \\ m_l(0,a) &= \Phi_1(a), \quad m_s(0,a) = \Phi_2(a)\,, \end{aligned}$$

provided the initial state of the population is such that $\Psi(a)$, $\Phi_1(a)$ and $\Phi_2(a)$ are well–defined.

Because the food availability is a dynamically varying quantity, it is necessary to add equation (7) to the system (16). For the rate of change of the resource in the absence of fish, denoted by $R(r)$, we will choose a logistic type equation

(17) $$R(r) = \alpha\, r(1 - \frac{r}{K})$$

in which $\alpha$ $(d^{-1})$ is the maximum rate of increase and $K$ $(g/m^3)$ the carrying capacity of the resource.

# 5 Results

The simulations are conducted by numerically solving equations (7) and (16) with the logistic growth limitation (17) on the prey. The habitat in which the populations live is taken to be 1 $Km$ long and is divided into 10 equal length cells. The resource density is assumed to be uniform within the cells. Details about the numerical scheme are given in Appendix II. These simulations were carried out with many different combinations of the parameters $\alpha$, $K$, and $s$ the characteristic velocity of the fish population. We study the dynamics of the fish population and resource as they are viewed through the total fish biomass, the total resource biomass, and the age, lipid, and structural distributions of the fish, using the two movement behaviors of the fish given by equations (5) and (6).

*Case 1.* We will first discuss in more detail the dynamic behavior of the model in the case where fish move continuously in the direction of increasing food (equation (5)). This movement behavior results in the formation of groups of individuals of similar size. Due to the continuous movement of all individuals, there is no great variation in resource density.

We say a population is persistent if the density function $u$ is nonzero through the simulation run time. A population goes to extinction if $u = 0$ at some time during the simulation run time. This definition of persistence is clearly a function of the length of the simulation run time; however, we find that extinction is independent of simulation run time if it is sufficiently long, generally $> 5,000$ $d$. Figure 1 indicates the threshold boundary between extinction and persistence of both predator and prey for various values of $\alpha$ and $K$ and for fixed $s$. The threshold boundary depends on the structure of the population. Populations that consist of small individuals, in general, require less food for survival. As we will discuss later, the characteristic velocity, $s$, of the population affects the growth of individuals and indirectly changes the structure of the population. Hence, the threshold boundary will change as $s$ changes.

In Figure 2a, the dynamics of the total fish and resource biomass are shown for values of $\alpha$ and $K$ in the region of coexistence for $s = 0.1$. Both fish and resource biomass are asymptotically periodic with a period of 1 year, the same period as the reproductive period, $P$, of the fish. The decrease of the fish biomass is due to the deaths of individuals which reach the prescribed maximum age $A_{max}$ (here $A_{max} = 8$ years) and the juvenile density-dependent mortality applied to individuals between age 18 and 200 days. To explain the oscillations in the fish and resource biomass we focus on a small part of the time series data. Figure 2b shows a small part of Figure 2a and Figure 2c shows the total number of fish in the population with the same parameters. The death of the old individuals together with the fact that individuals do not feed immediately after they hatch, result in an increase of the resource biomass. When the newly formed cohorts start feeding in joint action

with the adults, they bring the resource down to a minimum level. Then the strong mortality of the juveniles reduces the number of individuals and, as a result, there is a compensatory growth on the part of the remaining individuals due to reduced competition for food and an increase in the resource biomass. As the new individuals grow, the competition for food increases and eventually they diminish the resource. The dynamics do not change qualitatively as we change the carrying capacity, $K$, but the amplitude of the oscillations and the total fish biomass decrease as we decrease $K$ (Figures 3a, 3b, and 3c). This is caused by a reduction in the growth of individuals due to the low level of food.

The described pattern of oscillations is characteristic for the dynamics of the model with parameter values from the region of coexistence of both populations and away from the threshold boundary. However, for parameter values very close to the threshold boundary the system might still exhibit persistent oscillations that take longer to occur (Figure 4a), or it might oscillate in an irregular pattern (Figure 4b).

The asymptotic periodicity observed in the total fish and resource biomass is also present in the total age, lipid and structural distributions of the fish population. Figures 5a, 5b, and 5c illustrate the dynamic distributions of the age, lipid, and structure. To further demonstrate the periodicity, Figure 6 shows the age distribution of fish at particular times of the simulation. In Figures 6a and 6b, the scaled age distribution is shown at time $t_0$ and $t_0 + 150$ days. Notice that one time period, $P$, later, the age distributions shown in Figures 6c and 6d are consistent with those of Figures 6a and 6b. Similarly, Figure 7 demonstrates the periodicity for lipid distributions.

From the numerical simulations of the predator–prey system, we observe that the asymptotic persistent oscillations occur when individuals do not die from starvation and the new individuals entering the population every year balance the total mortality in all age classes.

The characteristic velocity, $s$, of the population affects the energetic cost of swimming as well as feeding. Beamish [3] reports a range of sustained cruising speeds

between 0.01 to 0.7 *length/sec* for fish of length 42–59 *cm*. Webb [39] performed experiments on rainbow trout approximately 30 *cm* in length and found that the critical swimming speed (the speed that the fish could maintain for 45 minutes) was between 0.35 and 2.05 *length/sec*. Therefore, to determine the effects of the characteristic velocity $s$ on the fish population, we vary $s$ from 0.001 to 1.5 *length/sec* to demonstrate the effects that occur for normal and extreme values of $s$. At lower values of $s$, the rate at which individuals encounter food is small. On the other hand, for large values of $s$, the energetic cost of swimming is large, particularly for large individuals. Figures 8a, 8b, and 8c illustrate the structural mass distributions of the fish population for three different values of $s$ at the same time in the simulation. Large values of $s$ favor the smaller individuals while small values of $s$ favor the larger individuals; this is typical for fish [3]. Hence, through the cost of swimming and feeding, the parameter $s$ affects the growth of individuals in a counteractive way, and, as a consequence the population dynamics are also affected.

To study the effects of the characteristic velocity on the fish population, we compare the cumulative fish biomass over a period of a year for values of $\alpha$ and $K$ that result in persistent oscillations. Figure 9a shows that there is a value $s_{op}$ (indicated by $\bigcirc$), and possibly a small range of values around $s_{op}$, for which the fish population biomass is maximized. The optimal value $s_{op}$ depends directly on the structure of the population and indirectly on the resource density. The dependence of $s_{op}$ on the resource density is illustrated in Figures 9a-9d. Increasing the carrying capacity, $K$, results in an increase of the resource density which, in turn, causes $s_{op}$ to decrease. This can be explained by the fact that populations that live in an environment with high resource density consist of larger individuals which move slowly to optimize growth. A low mean speed of swimming may have adaptive ecological significance by increasing the energetic efficiency for growth.

*Case 2.* The dynamic behavior of the model is now discussed for the case where fish do not change foraging location when energy gained exceeds energy demands

even if there are local changes in the resource density (equation (6)). This movement behavior also results in the formation of groups of individuals of similar size, but in this case, the individuals stay in a cell until the energetic requirements are not met by the available resource. This case has the possibility of leaving some cells unoccupied for a large period of time which results in a greater variation of the resource density than the variation in *Case 1*.

The asymptotic periodicity that has been observed in the system, for certain values of the parameters, in *Case 1* is not characteristic of the system for *Case 2*. Large values of the characteristic velocity, $s$, in general result in asymptotically persistent oscillations of period 1 year. These oscillations are stable for small changes of the parameters. As $s$ decreases the system loses the periodic solutions. The value of $s$ at which this occurs depends on the parameters $\alpha$ and $K$; that is, it depends on the resource density. For example, for $\alpha = 2$, $K = 10^3$ and $s = 1.5$ the system exhibits the asymptotic persistent oscillations (Figure 10), while for $s = 0.1$ the system oscillates aperiodically (Figure 11). For higher resource density ($\alpha = 0.5$ and $K = 10^4$) and $s = 0.1$ the system still exhibits persistent oscillations (Figure 12) and loses them for lower values of $s$. This change in the dynamic behavior of the system is due to the underlying movement behavior and not due to the fact that values are close to the threshold boundary of extinction.

There is no clear-cut movement behavior which results in the maximization of fish biomass. From Figures 13a and 13b, it is clear that continuous movement with large values of $s$ relative to the resource density is not favorable for the individuals because that results in high energetic cost for swimming. For lower values of $s$, continuous movement on average is better than the movement based on energetic constraints (Figure 13c).

# 6 Discussion and future work

We have indicated a method to introduce individual variability due to environmental processes by coupling a heterogeneous spatial environment and a dynamic resource with physiological processes of a fish population. We have studied the dynamics of the population using two movement behaviors and tried to disentangle the influences of the physiological and movement mechanisms of individuals that we incorporated in the model upon the population dynamics. It is not always possible to distinguish those mechanisms because they are intricately coupled.

We have compared two extreme movement behaviors, one in which individuals move continuously in the direction of increasing prey and another in which energetic constraints are imposed. These movement behaviors used are by no means well established. Neither of them take into account crowding effects directly.

Other model modifications that merit consideration in determining effects on population dynamics are the following two cases: 1) The constraints to determine the number of eggs that can be produced depend not only on physiological factors of the individual but also on resource availability; and 2) The juvenile density-dependent mortality is a function of size of individuals rather than age. Both cases will change the dynamics of the population especially when the resource density is low. The number of eggs produced will decrease if the food availability is low and as a result individuals may have better chances to grow larger. On the other hand, if juvenile mortality depends on the size of individuals, mortality may cease earlier when resource density is high and later when resource density is low. This mortality might be viewed as predation affecting the smaller individuals.

In the present study of the model, all individuals were assumed to have the same physiological characteristics. This is not a restriction in the model. We may introduce more variability in the population by varying certain parameters in the individual model such as the gut clearance rate (see Hallam et al. [17]).

# References


[1] K. R. ALLEN, *The Horokiwi Stream. A study of a trout population*, Fish. Bull. N. Z., No 10 (1951).

[2] F. W. H. BEAMISH, *Ration size and digestion in largemouth bass, Micropterus salmoides, Lacepede*, Can. J. Zool., 50 (1972), pp. 153–164.

[3] ——, *Swimming capacity*, in Fish Physiology Vol. VII, W. S. Hoar and D. J. Randall, eds., Academic Press, New York, 1978.

[4] J. E. BRECK AND M. J. GITTER, *Effect of fish size on the reactive distance of bluegill (lepomis macrochirus) sunfish*, Can. J. Fish. Aquat. Sci., 40 (1983), pp. 162–167.

[5] J. R. BRETT AND T. D. GROVES, *Physiological energetics*, in Fish Physiology, W. S. Hoar, D. J. Randall, and J. R. Brett, eds., vol. VIII, Academic Press, New York, 1979.

[6] S. BRODY, *Bioenergetics and Growth*, Reinhold, New York, 1945.

[7] M. E. BROWN, *Experimental studies on growth*, in Physiology of fishes, M. E. Brown, ed., Academic Press, New York, 1957.

[8] K. D. CARLANDER, *Handbook of Freshwater Fishery Biology*, vol. I, Iowa State University Press, Ames, Iowa, 1969.

[9] J. M. ELLIOT, *Body composition of brown trout (Salmo trutta l.) in relation to temperature and ration size*, J. Animal Ecol., 45 (1976), pp. 273–289.

[10] S. D. GERKING, *Revized food consumption estimate of a bluegill sunfish population in Wyland Lake, Indiana, U.S.A.*, J. Fish. Biol., 4 (1972), pp. 301–308.

[11] ——, *Ecology of fresh water fish production*, John Wiley & Sons, New York, 1978.

[12] J. GERRITTSEN, *Size efficiency reconsidered: A general foraging model for free swimming aquatic animals*, Am. Nat., 123 (1984), pp. 450–467.

[13] J. GERRITTSEN AND J. R. STRICKLER, *Encounter probabilities and community structure in zooplankton: a mathematical model*, J. Fish. Res. Board Can., 34 (1977), pp. 73–82.

[14] D. J. GROVE, L. G. LOIZIDES, AND J. NOTT, *Satiation amount, frequency of feeding and gastric emptying rate in salmo gairdneri*, J. Fish Biol., 12 (1978), pp. 707–516.

[15] W. S. C. GURNEY AND R. M. NISBET, *The regulation of inhomogeneous populations*, J. Theor. Biol., 52 (1975), pp. 441–457.

[16] M. E. GURTIN AND R. C. MACCAMY, *On the diffusion of biological populations*, Mathematical Biosciences, 33 (1977), pp. 35–49.

[17] T. G. HALLAM, R. LASSITER, AND S. M. HENSON, *Modelling fish population dynamics: a physiologically based perspective*, Manuscript, (1996).

[18] T. G. HALLAM, R. LASSITER, J. LI, AND W. MCKINNEY, *Toxicant-induced mortality in models of daphnia populations*, Environ. Toxicol. Chem., 9 (1990), pp. 597–621.

[19] ——, *An approach for modeling populations with continuous structured models*, in Individual-based models and approaches in Ecology, D. L. DeAngelis and L. J. Gross, eds., Chapman & Hall, 1992, pp. 312–337.

[20] M. HARTMANN, F. G. MEDEM, R. KUHN, AND H. BIELIG, *Untersuchungen uber die befruchtungsstoffe der Regenbogenforelle*, Z. Naturforsch, 26 (1947), pp. 330–349.

[21] R. J. HENDERSON AND D. R. TOCHER, *The lipid composition and biochemistry of freshwater fish*, Prog. Lipid Res., 26 (1987), pp. 281–347.

[22] S. M. HENSON AND T. G. HALLAM, *Constraints to feeding: A mechanistic approach*, J. Theor. Biology, To appear (1996).

[23] E. E. HOLMES, J. BANKS, M. LEWIS, AND R. R. VEIT, *Partial differential equations in ecology: spatial interactions and population dynamics*, Ecology, 75 (1994), pp. 17–29.

[24] M. KLEIBER, *The Fire of Life*, Wiley, New York, 1961.

[25] S. A. L. M. KOOIJMAN, *Population dynamics on basis of budgets*, in The Dynamics of Physiologically Structured Populations, J. A. J. Metz and O. Dikmann, eds., vol. 68 of Lecture Notes in Biomathematics, Berlin, West Germany, 1986, Springer-Verlag.

[26] J. J. MAGNUSON, *Swimming activity of the scombrid fish euthynmus affinis as related to search for food*, in FAO Conf. on Fish Behaviour in Relation to Fishing Techniques and Tactics, vol. 3, Bergen, Norway. Exper. Pap., 1967, pp. 439–451.

[27] L. F. MURPHY, *A nonlinear growth mechanism in size-structured population dynamics*, J. Theor. Biol., 104 (1983), pp. 493–506.

[28] J. D. MURRAY, *Mathematical Biology*, Springer-Verlag, Berlin, Germany, 1989.

[29] W. B. SCOTT AND E. J. CROSSMAN, *Freshwater fishes of Canada*, Bull. Fish. Res. Board Can., No 184 (1973).

[30] N. SHIGESADA, K. KAWASAKI, AND E. TERAMOTO, *Spatial segregation of interacting species*, J. Theor. Biol., 79 (1979), pp. 83–99.

[31] J. W. SINKO AND W. STREIFER, *A new model for age-size structure of a population*, Ecology, 48 (1967), pp. 910–918.

[32] S. SMITH, *Studies in the development of the rainbow trout (Salmo irideus). I. the heat production and nitrogenous excretion*, J. Exptl. Biol., 23 (1947), pp. 357–373.

[33] ——, *Studies in the development of the rainbow trout (Salmo irideus). II. the metabolism of carbohydrates and fats*, J. Exptl. Biol., 29 (1952), pp. 650–666.

[34] D. J. STAPLES AND M. NOMURA, *Influence of body size and food ration on the energy budget of rainbow trout salmo gairdneri richardson*, J. Fish. Biol., 9 (1976), pp. 29–43.

[35] P. TYTLER AND P. CALOW, *Fish Energetics: New Perspectives*, John Hopkins University Press, Baltimore, Maryland, 1985.

[36] D. M. WARE, *Predation by rainbow trout (Salmo gairdneri): the effect of experience*, J. Fish. Res. Board Can., 28 (1971), pp. 1847–1852.

[37] ——, *Risk of epibenthic prey to predation by rainbow trout (Salmo gairdneri)*, J. Fish. Res. Board Can., 30 (1973), pp. 787–797.

[38] A. H. WEATHERLEY, *Growth and Ecology of Fish Populations*, Academic Press, New York, 1972.

[39] P. W. WEBB, *The swimming energetics for trout I. thrust and power output at cruising speeds*, J. Exptl. Biol., 55 (1971), pp. 489–520.

# Appendix I

In this Appendix we will present the derivation of the equation which governs the fish dynamics. The following derivation can be applied to any species that moves continuously in a bounded habitat.

Consider a single species population (predator), sufficiently dense so that a continuum theory is applicable, and assume that it is moving in a bounded environment $\Omega \subset R^N$ (in physical applications $N \leq 3$).

Let $\rho(t, a, m, \mathbf{x})$ be the number of the predators – per unit age, size and volume – of age $a$, size $m$ (a variable which may represent mass, volume, length, mass of lipid, mass of protein, or any other variable that characterizes the physiological behavior of an individual) which occupy the spatial location $\mathbf{x}$ at time $t$. The integral of $\rho(t, a, m, \mathbf{x})$ over all ages and sizes yields the spatial distribution

$$u(t, \mathbf{x}) = \int_0^\infty \int_0^\infty \rho(t, a, m, \mathbf{x})\, da\, dm\,. \tag{18}$$

Clearly, when $B$ is a subset of $\Omega$ with a piecewise smooth boundary $\partial B$,

$$n(t, a, m) = \int_B \rho(t, a, m, \mathbf{x})\, d\mathbf{x} \tag{19}$$

gives the number of individuals of age $a$ and size $m$ in $B$ at time $t$. The rate at which the age–size density $n$ changes in time is given by

$$Dn = \frac{\partial n}{\partial t} + \frac{\partial n}{\partial a} + \frac{\partial (ng)}{\partial m}\,, \tag{20}$$

(cf. [31]), where $g$ is the growth rate of the structure variable $m$ and is, in general, a function of $a, m, u$ and the food availability. If we have more than one structure variable, i.e., $\mathbf{m} = (m_1, \ldots, m_J)$, then equation (20) becomes

$$Dn = \frac{\partial n}{\partial t} + \frac{\partial n}{\partial a} + \sum_{i=1}^{J} \frac{\partial (ng_i)}{\partial m_i}\,,$$

where $g_i$ is the growth rate of the structure variable $m_i$.

Now let $\mathbf{q} = \mathbf{q}(t, a, m, \mathbf{x})$ be a vector in $R^N$ which denotes the movement velocity of an individual of age $a$, size $m$ at time $t$ and location $\mathbf{x}$. If $\mathbf{x}$ is a point on the boundary

$\partial B$, and if $\mathbf{n}(\mathbf{x})$ is the outward unit normal to $\partial B$ at $\mathbf{x}$, then $\rho\mathbf{q}\cdot\mathbf{n}$ represents the number of individuals, per unit area and time, of age $a$ and size $m$ who cross $\partial B$ at $\mathbf{x}$. Thus,

$$-\int_{\partial B}\rho\mathbf{q}\cdot\mathbf{n}\,ds \tag{21}$$

represents the number of individuals of age $a$ and size $m$ crossing the boundary of $B$. The minus sign reflects the fact that if more individuals go out of the region than in, the population density in $B$ decreases.

If $\mu=\mu(t,a,m,\mathbf{x})$ is the death rate and we assume that there is no migration into $\Omega$ from regions exterior to $\Omega$, conservation of population requires that the time rate of change of the population in $B$ is

$$D\int_B\rho d\mathbf{x}=-\int_{\partial B}\rho\mathbf{q}\cdot\mathbf{n}ds-\int_B\mu\rho d\mathbf{x}\,. \tag{22}$$

In words, this balance law asserts that the rate at which the number of individuals in a group of age $a$ and size $m$ changes in $B$ is equal to the number of individuals of this group crossing the boundary per unit time minus those that died per unit time.

By applying the Gauss Divergence Theorem to the integral over $\partial B$ in (22), using equations (19) and (20) and the fact that $B$ is an arbitrary subset of $\Omega$, we obtain

$$D\rho+\mathrm{div}(\rho\mathbf{q})+\mu\rho=0\,, \tag{23}$$

where

$$D\rho=\frac{\partial\rho}{\partial t}+\frac{\partial\rho}{\partial a}+\frac{\partial(g\,\rho)}{\partial m}\,.$$

The function $\mathbf{q}=\mathbf{q}(t,a,m,\mathbf{x})$ describes how animals of age $a$ and size $m$ alter their movement in response to conspecifics and/or environmental heterogeneity. For example, if animals tend to move away from one another, $\mathbf{q}$ takes the form $\mathbf{q}=-k(\rho)\nabla\rho$, where $k(\rho)>0$ measures the tendency to move away from conspecifics [15, 16]. Animals also might move to higher quality neighboring areas, or move based on the quality of the environment at their current location [30]. In particular,

if animals move to neighboring areas with higher prey density, then the function $\mathbf{q}(t, a, m, \mathbf{x})$ is given by

$$\mathbf{q} = \phi(a, m, u)\nabla r(t, \mathbf{x}), \tag{24}$$

where $\nabla r(t, \mathbf{x})$ is the gradient of the prey density at time $t$ and location $\mathbf{x}$, and $\phi(a, m, u)$ is a nonnegative function that may depend on the physiological characteristics of the individual and the density of the conspecifics at $\mathbf{x}$ and measures the tendency of predators to pursue prey.

# Appendix II

In this Appendix, we describe the scheme for the numerical solution of the system of equations (7) and (16). We assume that the predators move in the one dimensional habitat $I$ which has dimensions $1\,m \times 1\,m \times L\,m$. We discretize the habitat $I$ into $J$ cells with size $1\,m \times 1\,m \times h\,m$, where $h = \frac{L}{J}$. The resource is assumed to be uniformly distributed in each cell.

We define $r^{(j)}(t)$ to be the resource density in cell $j$ at time $t$ and $(u^{(j,i)}(t,a;s_0^i)$, $m_l^{(j,i)}(t,a;s_0^i)$, $m_s^{(j,i)}(t,a;s_0^i)$, $x^{(j,i)}(t,a;s_0^i))$ to be a cohort of age $a$ in cell $j$ at time $t$ with initial state $s_0^i = (m_{l0}^i, m_{s0}^i, x_0^i)$; that is, born in some cell $i$ at location $x_0^i$ with mass of lipid $m_{l0}^i$ and mass of structure $m_{s0}^i$. Suppose we start with some initial distribution of cohorts $(u^{(j,i)}(0,a;s_0^i)$, $m_l^{(j,i)}(0,a;s_0^i)$, $m_s^{(j,i)}(0,a;s_0^i)$, $x^{(j,i)}(0,a;s_0^i))$, for $j = 1,\ldots,J$ and $i \in \{1,2,\ldots,J\}$. Notice that in each cell $j$ there may be more than one cohort. Then for $j = 1,\ldots,J$ and $i \in \{1,2,\ldots,J\}$ the dynamics of the $(j,i)th$ subpopulation are described by

$$
\begin{aligned}
&\frac{\partial u^{(j,i)}}{\partial t} + \frac{\partial u^{(j,i)}}{\partial a} = -\mu u^{(j,i)},\\
&\frac{\partial m_l^{(j,i)}}{\partial t} + \frac{\partial m_l^{(j,i)}}{\partial a} = g_l(\mathbf{m}^{(j,i)}, X^{(j,i)}),\\
&\frac{\partial m_s^{(j,i)}}{\partial t} + \frac{\partial m_s^{(j,i)}}{\partial a} = g_s(\mathbf{m}^{(j,i)}, X^{(j,i)}),\\
&\frac{\partial x^{(j,i)}}{\partial t} + \frac{\partial x^{(j,i)}}{\partial a} = q(\mathbf{m}^{(j,i)}, r^{(j-1)}, r^{(j)}, r^{(j+1)}),\\
&\frac{dr^{(j)}}{dt} = R(r^{(j)}) - \frac{1}{h}\sum_i F(\mathbf{m}^{(j,i)}, u^{(j,i)}, r^{(j)})u^{(j,i)},
\end{aligned}
\tag{25}
$$

and the initiation of a new cohort is given by

$$\begin{aligned} u^{(j,j)}(t,0) &= \textstyle\sum_i \beta(a, \mathbf{m}^{(j,i)}) u^{(j,i)}, \\ m_l^{(j,j)}(t,0) &= m_{l0}^{(j)}, \\ m_s^{(j,j)}(t,0) &= m_{s0}^{(j)}, \\ x^{(j,j)}(t,0) &= x_0^{(j)}, \end{aligned}$$

where $X^{(j,i)} = r^{(j)} \dfrac{m_l^{(j,i)} + m_s^{(j,i)}}{\sum_i (m_l^{(j,i)} + m_s^{(j,i)}) u^{(j,i)}}$ is the resource density to which an individual of the cohort $i$ responds. The summation is taken over all the cohorts in cell $j$.

Since the first four equations of system (25) evolve along the characteristic $\frac{da}{dt} = 1$, they may be reduced to a system of ordinary differential equations. Therefore, system (25) takes the form

$$\frac{d\mathbf{Y}^{(j,i)}}{dt} = \mathbf{G}(\mathbf{Y}^{(j,i)}), \tag{26}$$

where $\mathbf{Y}^{(j,i)} = (a, m_l^{(j,i)}, m_s^{(j,i)}, x^{(j,i)}, r^{(j)})^T$ and $\mathbf{G}(\mathbf{Y}^{(j,i)})$ is a vector containing the right hand sides of the differential equations. System (26) can be solved using any numerical technique available for ordinary differential equations. The method we use is a corrected Euler method. Let $\tau$ be the (fixed) time step and let $t_n = n\tau$, $n = 0, 1, 2, \ldots$. If $Y_0^{(j,i)}$ is the initial vector for the $(j,i)th$ cohort, we compute $Y_n^{(j,i)}$, approximating $Y^{(j,i)}(t_n)$, $n = 0, 1, 2, \ldots$ from

$$\begin{aligned} \tilde{\mathbf{Y}}_{n+1}^{(j,i)} &= \mathbf{Y}_n^{(j,i)} + \tau \mathbf{G}(\mathbf{Y}_n^{(j,i)}), \\ \mathbf{Y}_{n+1}^{(j,i)} &= \mathbf{Y}_n^{(j,i)} + \frac{\tau}{2}(\mathbf{G}(\mathbf{Y}_n^{(j,i)}) + \mathbf{G}(\tilde{\mathbf{Y}}_{n+1}^{(j,i)})). \end{aligned}$$

# Appendix III

**Table 1.** Parameter values and units used in the individual model.

| *Symbol* | *Interpretation* | *Value (unit)* | *Source* |
|---|---|---|---|
| $a_{0l}$ | lipid assimilation efficiency | 0.85 (nondim) | Gerking 1972,1978 [10, 11]; Beamish 1972 [2]; Staples & Nomura 1976 [34] |
| $a_{0s}$ | structure assimilation efficiency | 0.684 (nondim) | " |
| $a_1$ | labile lipid mobilization rate | 0.013 ( $d^{-1}$) | Tytler & Calow 1985 [35] |
| $a_2$ | labile structure mobilization rate | 0.028 ($d^{-1}$) | " |
| $\epsilon$ | fraction lipid associated with nonlabile structure | 0.12 (nondim) | Staples & Nomura 1976 [34] |
| $M_p$ | mass of prey | $2.7 \times 10^{-4}$ ($g$) | Kooijman 1986 [25] |
| $L_p$ | length of prey | $0.34 \times 10{-}2$ ($m$) | " |
| $\beta$ | as in $m_{ps} = \beta m_s$ | 0.71 (nondim) | Staples & Nomura 1976 [34] |
| $\beta_2$ | proportionality constant for wetted surface area | 0.4 (nondim) | Webb 1971 [39] |
| $q$ | swimming efficiency | 0.2 (nondim) | Gerritsen 1984 [12] |
| $a$ | as in $s_d = [aL_p + b]L_f^{\frac{1}{2}}$ for reaction distance | 75 ($m^{-\frac{1}{2}}$) | Breck and Gittler 1983 [4]; Ware 1971,1973 [36, 37] |
| $b$ | as in $s_d = [aL_p + b]L_f^{\frac{1}{2}}$ for reaction distance | 0.52 ($m^{\frac{1}{2}}$) | " |
| $\beta_1$ | isometric constant relating weight to length | $17 \times 10^2$ ( $g\, m^{-3}$) | Webb 1971 [39]; Elliot 1976 [9] Staples & Nomura 1976 [34] |
| $s_p$ | burst swimming velocity | 4.0 ($length/sec$) | Beamish 1978 [3] |

**Table 1.** continued

| *Symbol* | *Interpretation* | *Value (unit)* | *Source* |
|---|---|---|---|
| $k_0$ | as in $k = k_0 m_{ps}^{k_1}$ | 16.5 $(g^{0.7} \cdot d^{-1})$ | Grove et al. 1978 [14]; Staples & Nomura 1976 [34] |
| $k_1$ | as in $k = k_0 m_{ps}^{k_1}$ | 0.7 (nondim) | Grove et al. 1978 [14] |
| $d_p$ | as in $M_g = d_p V_g$ density of prey (dry wt) | 0.052 $(g \cdot cm^{-3})$ | Kooijman (personal communication) |
| $c$ | as in $V_g = c\, m_{ps}$ for gut volume | 0.864 $(cm^3\, g^{-1})$ | Grove et al. 1978 [14]; Staples & Nomura 1976 [34] |
| $e_m$ | minimum lipid per egg | $3.2 \times 10^{-3}$ $(g)$ | Smith 1947 [32]; Henderson & Tocher 1987 [21] |
| $e_M$ | maximum lipid per egg | $1.02 \times 10^{-2}$ ( $g$) | " |
| $e_s$ | structure per egg | $2.38 \times 10^{-2}$ ( $g$) | Hartmann et al. 1947 [20]; Smith 1947 [32] |
| $\sigma$ | slope of egg equation | $67.2 \times 10^2$ $(m^{-1})$ | Carlander 1969 [8] |
| $\eta$ | minimum length for reproduction | $17.4 \times 10^{-2}$ $(m)$ | " |
| $P$ | reproductive period | 365 $(d)$ | Scott & Crossman 1973 [29] |
| $Y$ | time from fertilization until first feed | 51 $(d)$ | Scott & Crossman 1973 [29]; Smith 1952 [33] |
| $A_1$ | half saturation constant modulated by $E_s$ | $3.0 \times 10^{-4}$ $(g/egg)$ | created |
| $A_2$ | energy to mobilize labile structure for eggs | $2.0 \times 10^2$ $(J \cdot g^{-1})$ | " |
| $A_3$ | energy to mobilize labile lipid for eggs | $2.0 \times 10^2$ $(J \cdot g^{-1})$ | " |

**Table 2.** Mortality functions used in population model.

Age-dependent mortality:

$$\mu_a = \begin{cases} \kappa_a \ , & 0 \leq a \leq A_{max} \\ \infty \ , & a > A_{max} \end{cases}$$

where $\kappa_a$ is the mortality rate of individuals of age $a$.

Density-dependent mortality: $\mu_d = \mu_d(P_J, a)$, $P_J$ = total population with age in the interval $[a_0, a_J]$.

$$\mu_d = \begin{cases} \mu_J \dfrac{P_J}{P_c} \ , & 0 < P_J < P_c \quad \text{and} \quad a \in [a_0, a_J] \\ \mu_J \ , & P_J \geq P_c \qquad \text{and} \quad a \in [a_0, a_J] \end{cases}$$

where $\mu_J$ is a constant rate of mortality and $P_c$ is the largest number of juveniles the environment can support.

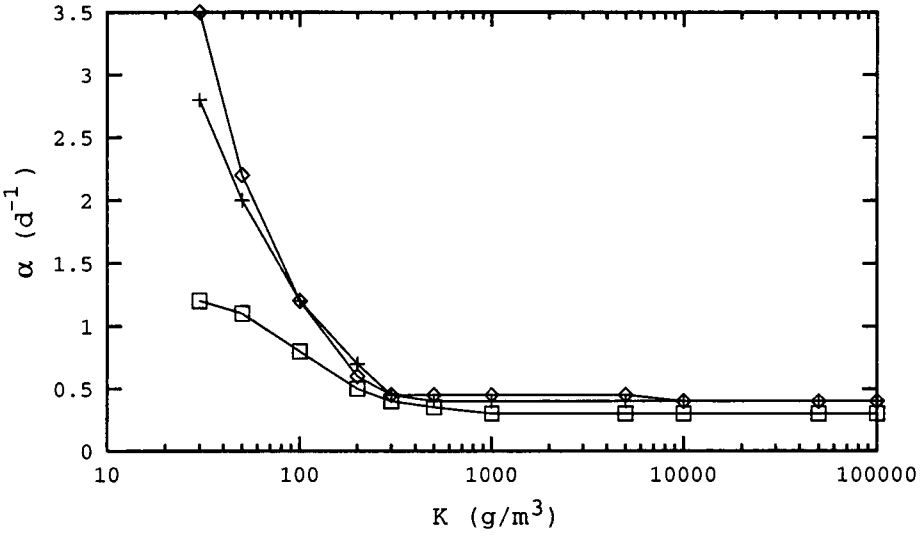
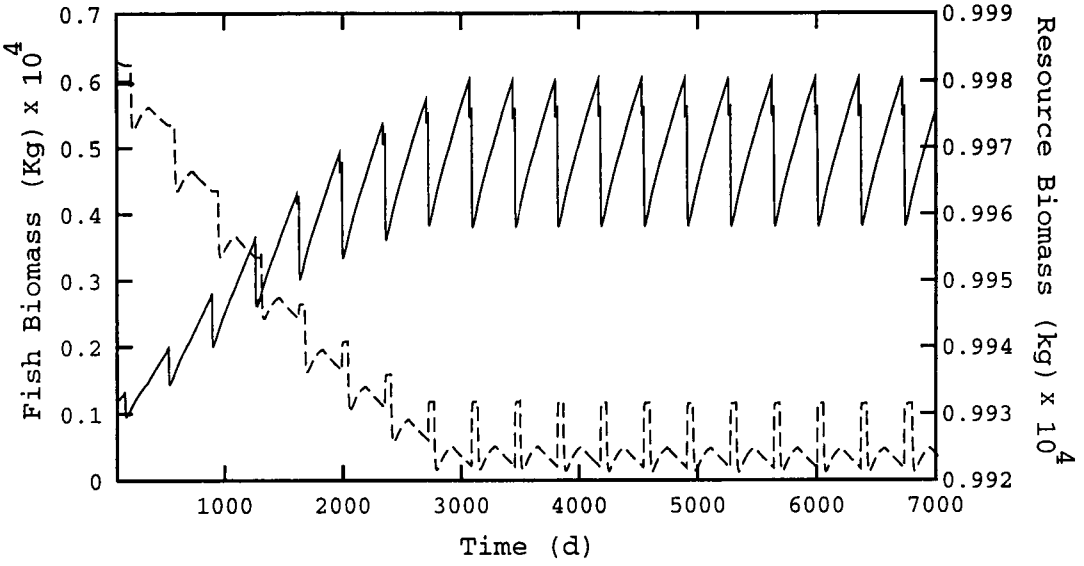
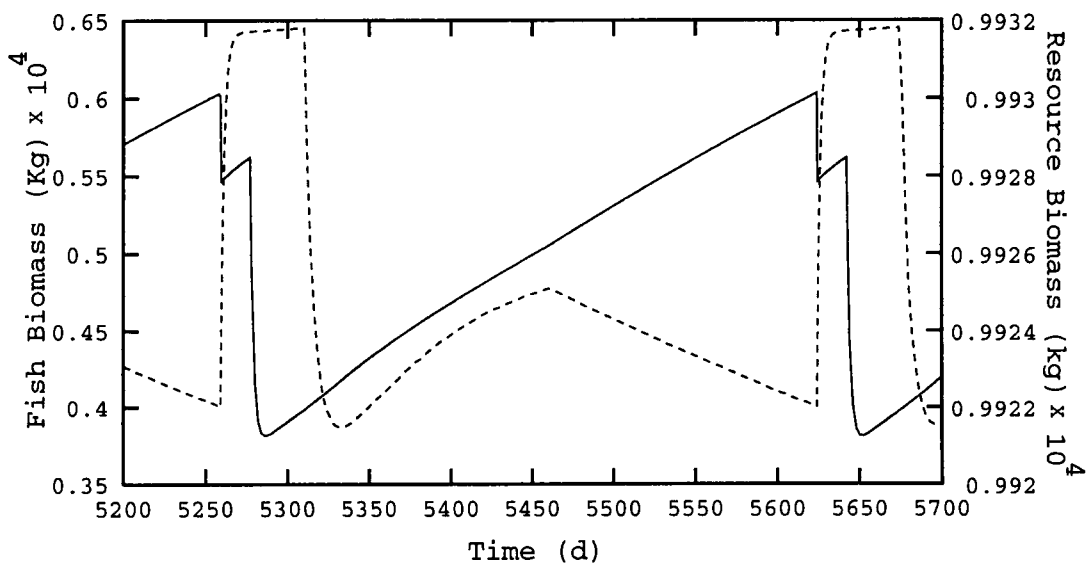



Figure 1: Threshold boundaries between extinction and persistence for the fish population and resource, for $s = 1.5$ ($\diamond$), $s = 0.1$ ($+$) and $s = 0.01$ ($\square$)

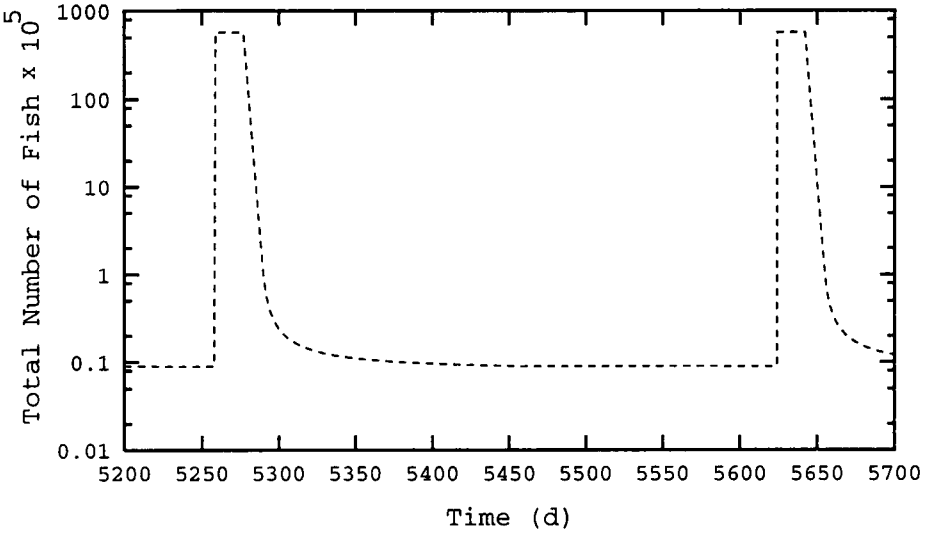
.


Fish Biomass (Kg) x 10^4
Resource Biomass (kg) x 10^4
Time (d)
0.7
0.6
0.5
0.4
0.3
0.2
0.1
0
0.999
0.998
0.997
0.996
0.995
0.994
0.993
0.992
1000
2000
3000
4000
5000
6000
7000

(a)

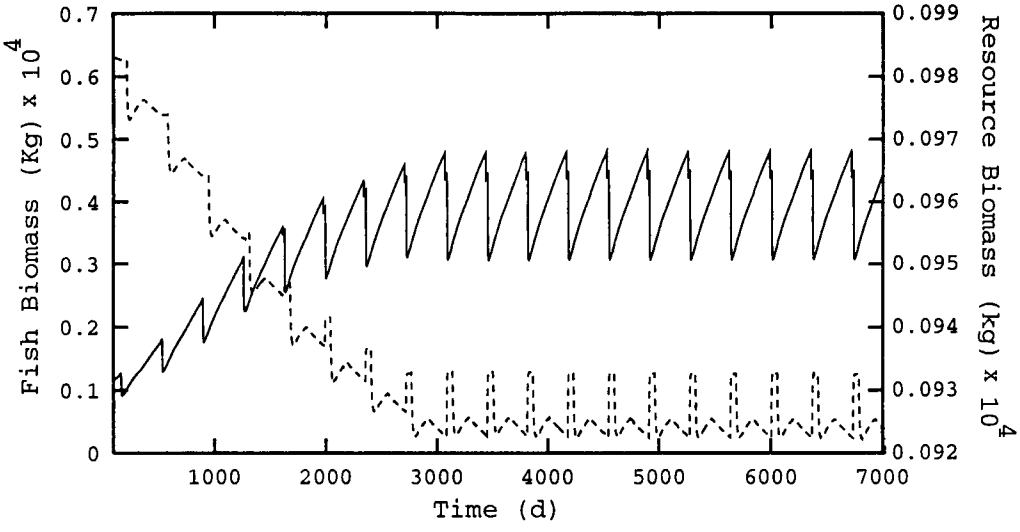

Fish Biomass (Kg) x 10^4
Resource Biomass (kg) x 10^4
Time (d)
0.65
0.6
0.55
0.5
0.45
0.4
0.35
0.9932
0.993
0.9928
0.9926
0.9924
0.9922
0.992
5200
5250
5300
5350
5400
5450
5500
5550
5600
5650
5700

(b)

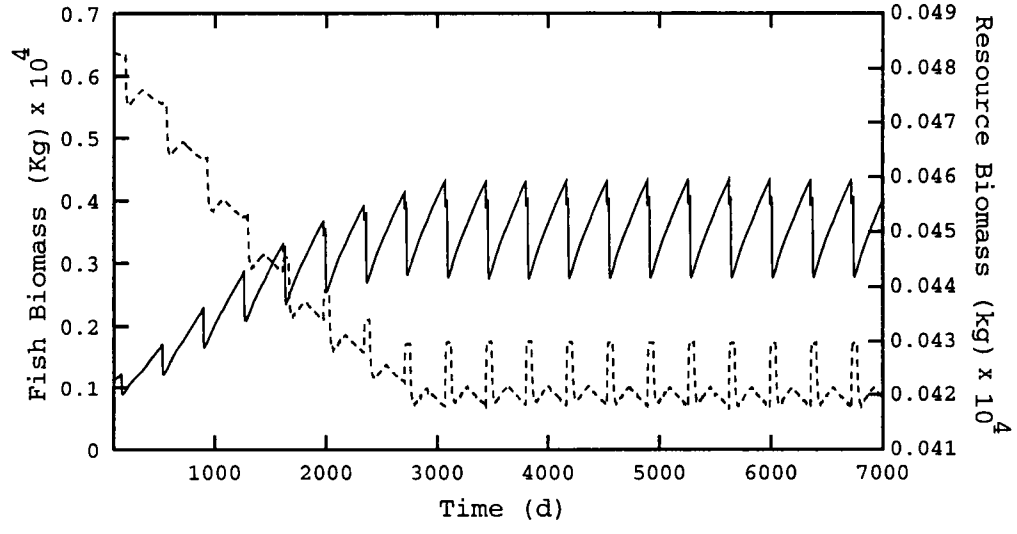



(c)

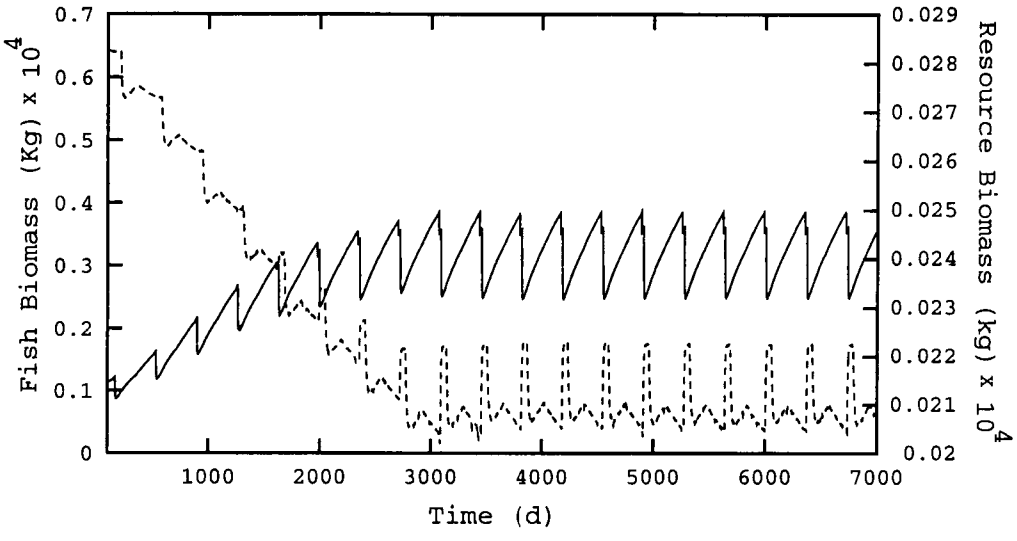
Figure 2: Dynamic behavior of the fish population and resource for $a = 0.5$, $K = 10^4$ and $s = 0.1$. (a) Total fish (—) and resource (– – –) biomass on the time interval from 100 to 7,000 d. (b) Total fish (—) and resource (– – –) biomass on the time interval from 5,200 to 5,700 d. (c) Total number of fish, on a semilogarithmic scale.


Fish Biomass (Kg) x 10^4
Resource Biomass (kg) x 10^4
Time (d)
0.7
0.6
0.5
0.4
0.3
0.2
0.1
0
0.099
0.098
0.097
0.096
0.095
0.094
0.093
0.092
1000
2000
3000
4000
5000
6000
7000

(a)

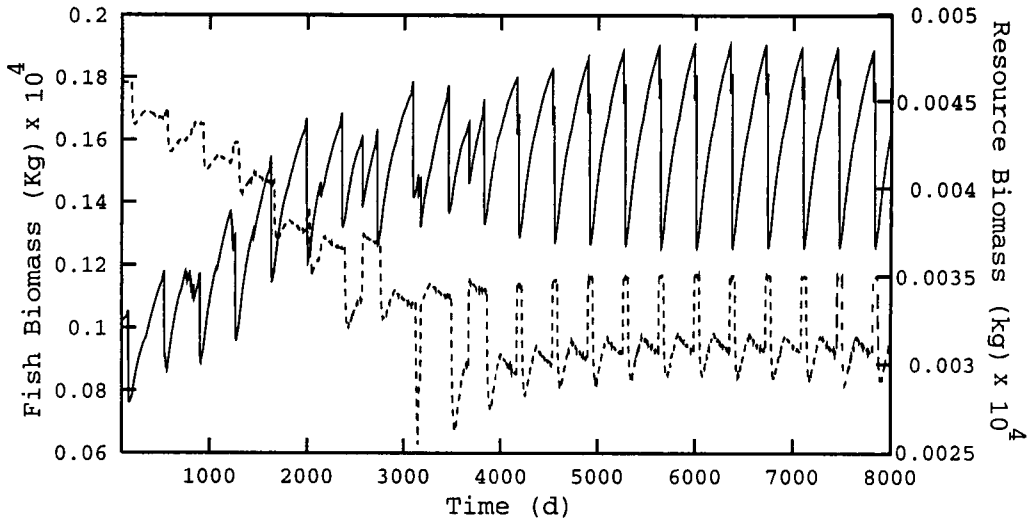

Fish Biomass (Kg) x 10^4
Resource Biomass (kg) x 10^4
Time (d)
0.7
0.6
0.5
0.4
0.3
0.2
0.1
0
0.049
0.048
0.047
0.046
0.045
0.044
0.043
0.042
0.041
1000
2000
3000
4000
5000
6000
7000

(b)

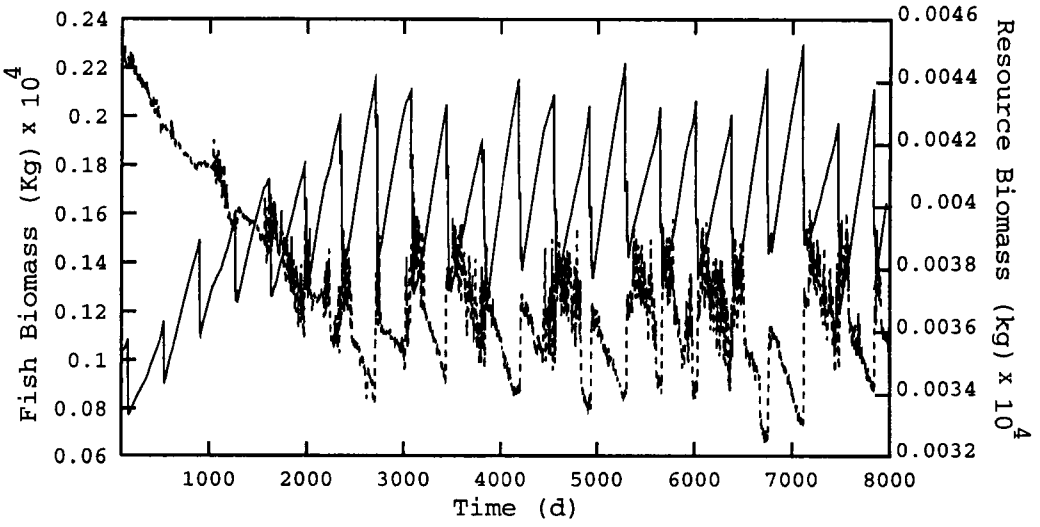



(c)

Figure 3: Dynamics of the total fish (—) and resource biomass (– – –) for $\alpha = 0.5$ and $s = 0.1$. (a) $K = 10^3$, (b) $K = 5 \times 10^2$, (c) $K = 3 \times 10^2$.

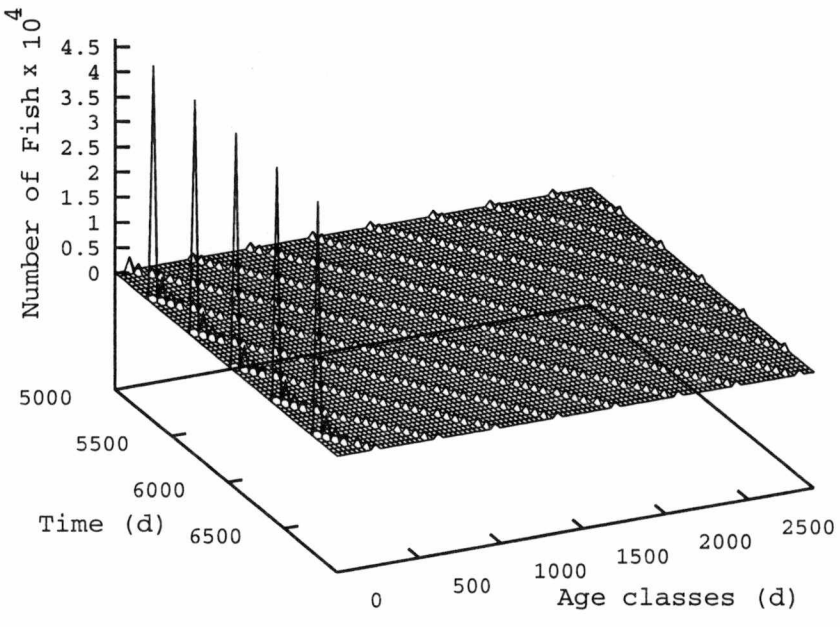



(a)

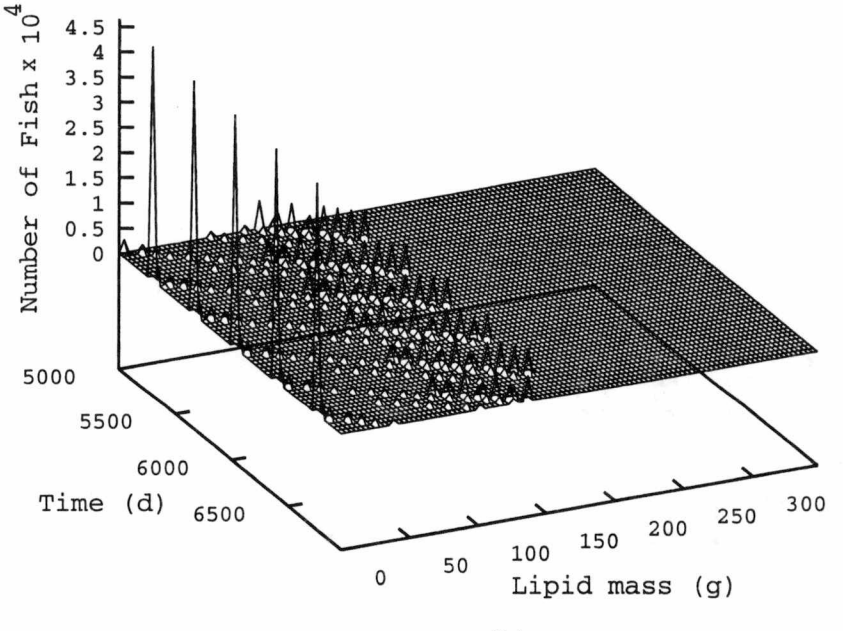



(b)

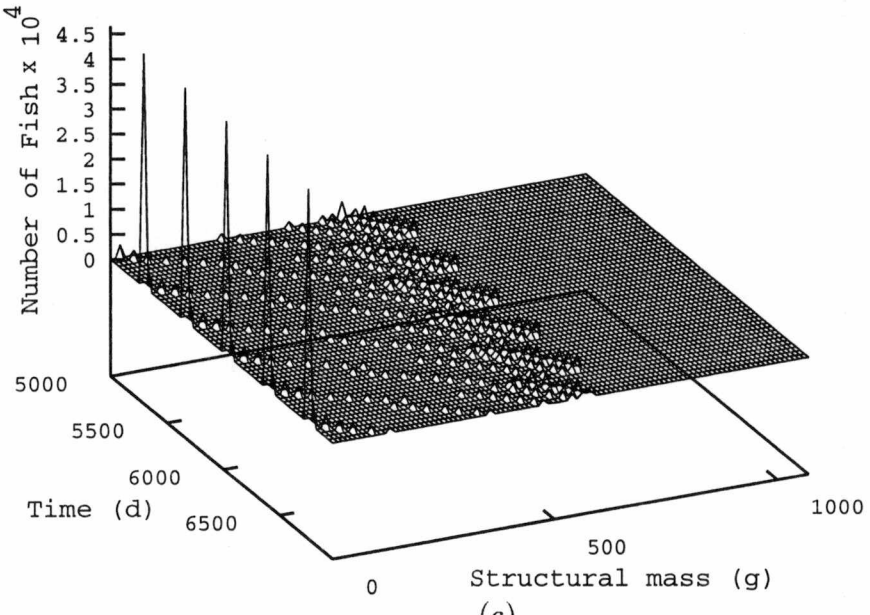
Figure 4: Dynamics of the total fish (—) and resource biomass (– – –) for $K = 50$. (a) $\alpha = 2.2$, $s = 1.5$, (b) $\alpha = 1.5$, $s = 0.01$.


Number of Fish x 10^4
4.5
4
3.5
3
2.5
2
1.5
1
0.5
0
5000
5500
6000
6500
Time (d)
0
500
1000
1500
2000
2500
Age classes (d)

(a)

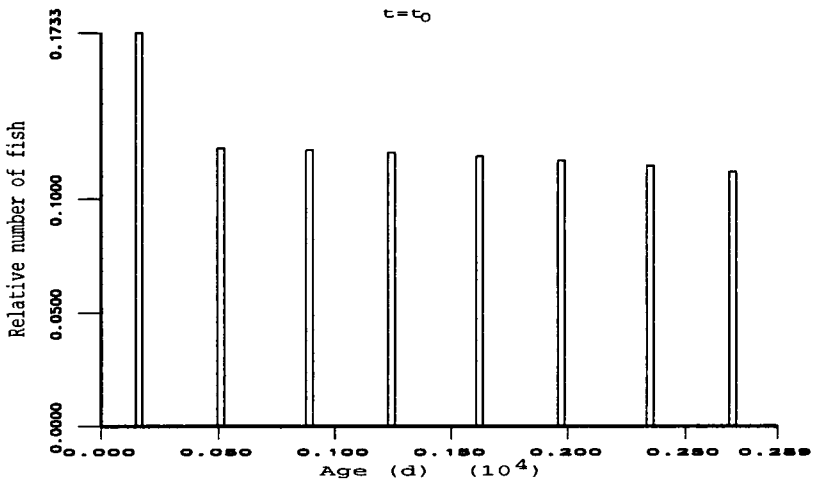

Number of Fish x 10^4
4.5
4
3.5
3
2.5
2
1.5
1
0.5
0
5000
5500
6000
6500
Time (d)
0
50
100
150
200
250
300
Lipid mass (g)

(b)

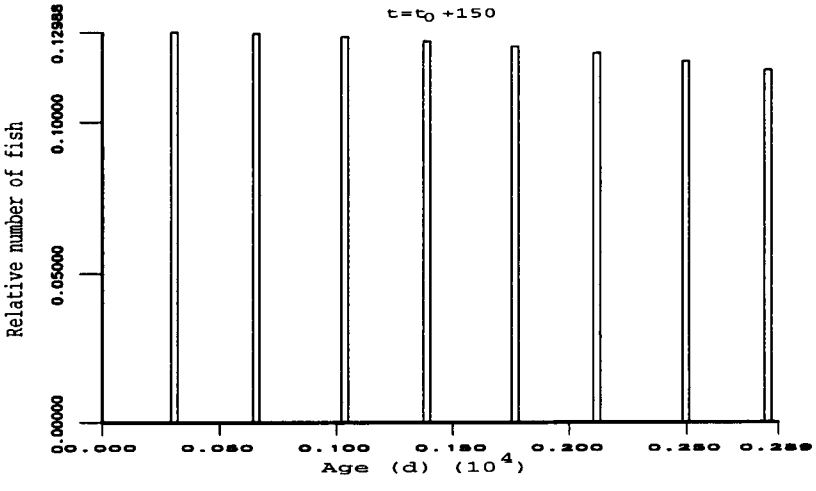


(c)

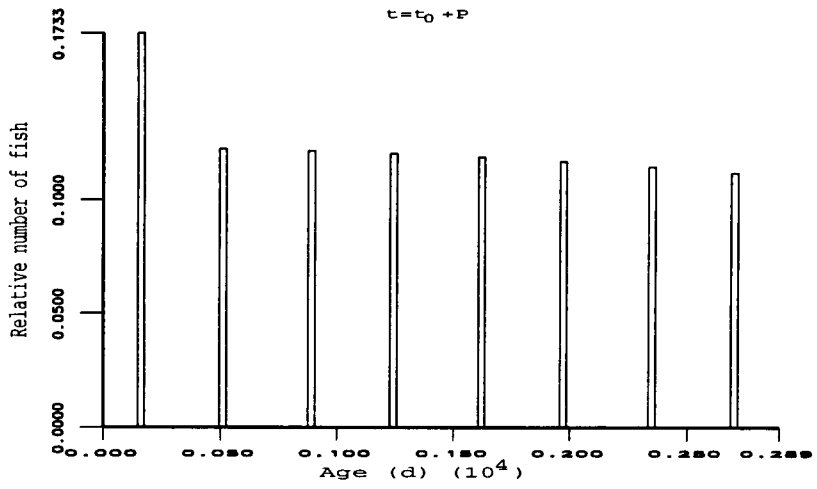
Figure 5: The dynamic fish population on the time interval from 5,000 to 7,000 $d$ as viewed through its (a) age distribution, (b) lipid distribution, and (c) structural distribution. Output every 36.5 $d$ with $\alpha = 0.5$, $K = 10^4$, and $s = 0.1$.


t=t0
Relative number of fish
0.1733
0.1000
0.0500
0.0000
0.000
0.050
0.100
0.150
0.200
0.250
0.289
Age (d) (10^4)

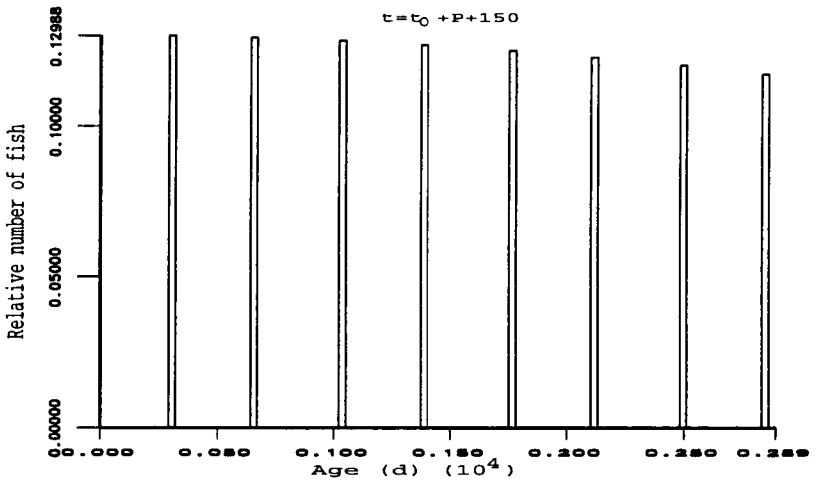
(a)


t=t0 +150
Relative number of fish
0.12988
0.10000
0.05000
0.00000
0.000
0.050
0.100
0.150
0.200
0.250
0.289
Age (d) (10^4)

(b)

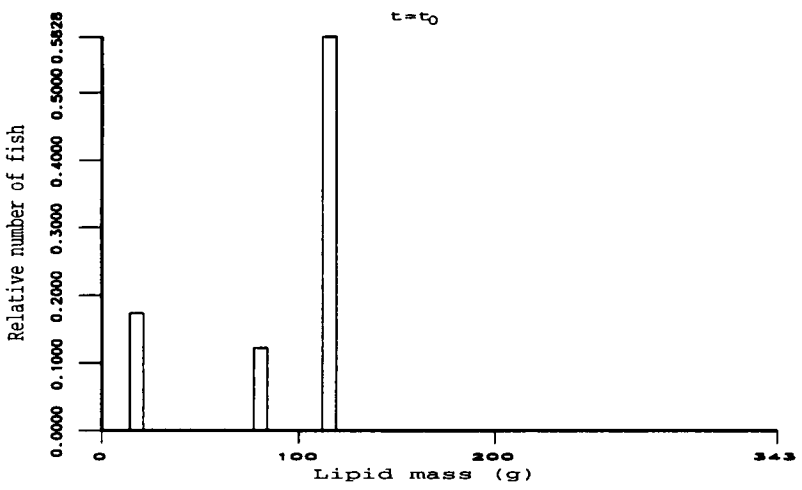



(c)

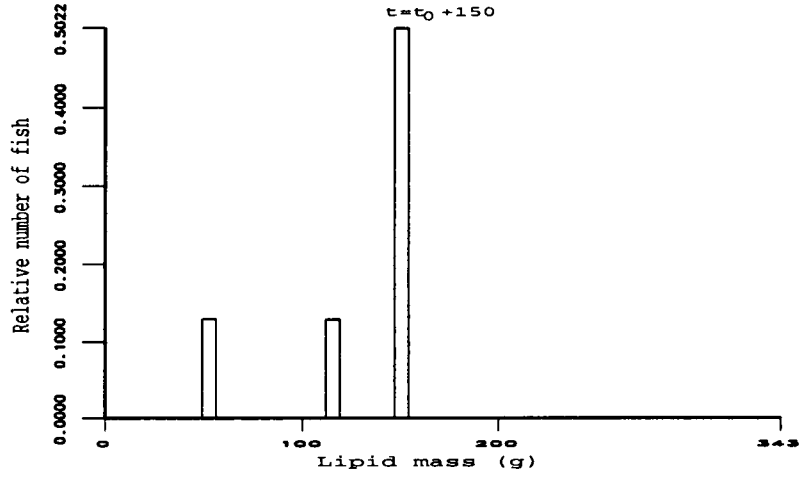



(d)

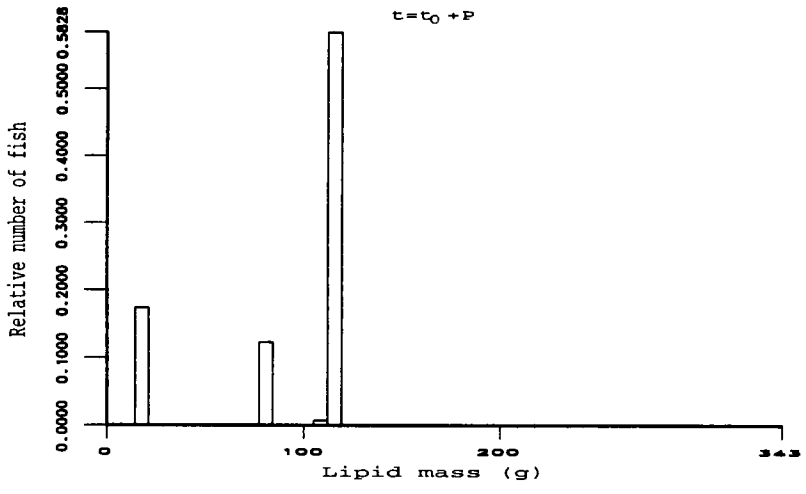
Figure 6: Age distribution of the fish population with $\alpha = 0.5$, $K = 10^4$, and $s = 0.1$ at times (a) $t = t_0$ , (b) $t = t_0 + 150$ , (c) $t = t_0 + P$, and (d) $t = t_0 + P + 150$.


t=t0
Relative number of fish
0.0000 0.1000 0.2000 0.3000 0.4000 0.5000 0.5828
0
100
200
343
Lipid mass (g)

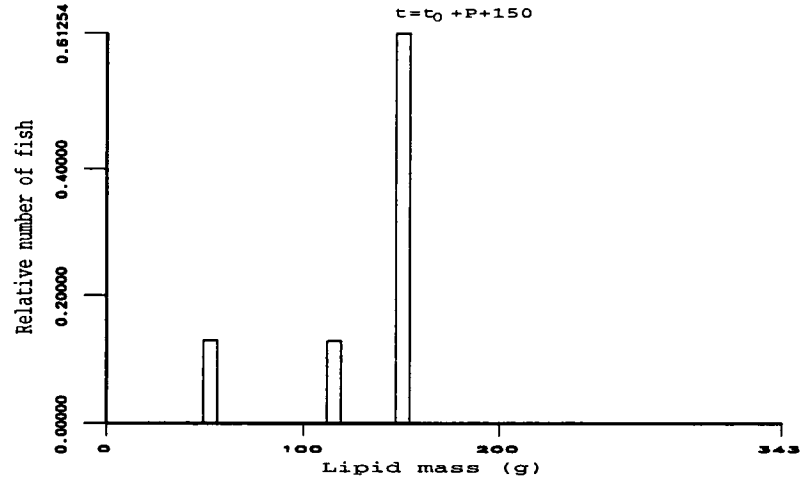
(a)


t=t0 +150
Relative number of fish
0.0000 0.1000 0.2000 0.3000 0.4000 0.5022
0
100
200
343
Lipid mass (g)

(b)

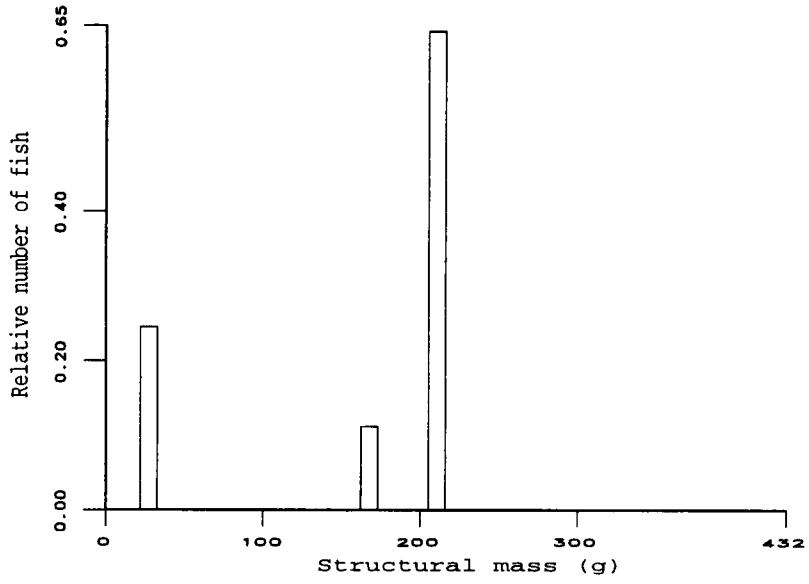



(c)

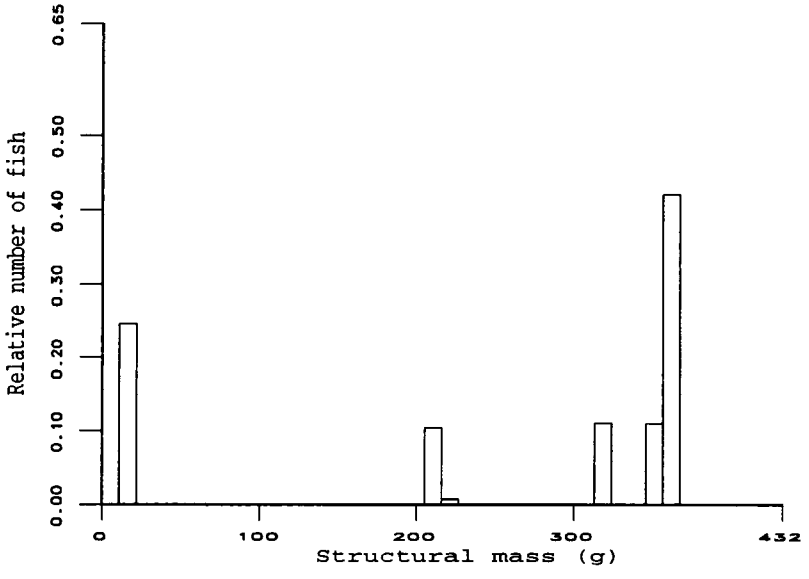



(d)

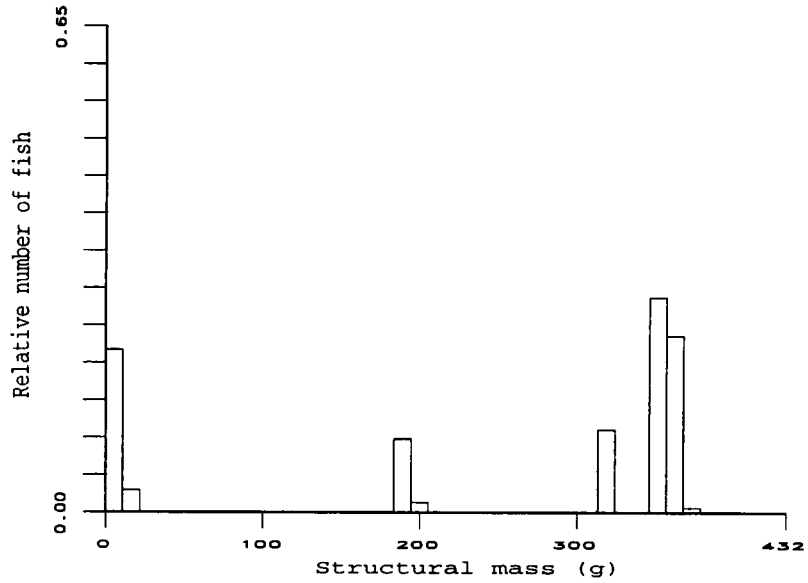
Figure 7: Lipid distribution of the fish population with $\alpha = 0.5$, $K = 10^4$, and $s = 0.1$ at times (a) $t = t_0$, (b) $t = t_0 + 150$, (c) $t = t_0 + P$, and (d) $t = t_0 + P + 150$.


Relative number of fish
0.00
0.20
0.40
0.65
0
100
200
300
432
Structural mass (g)

(a)

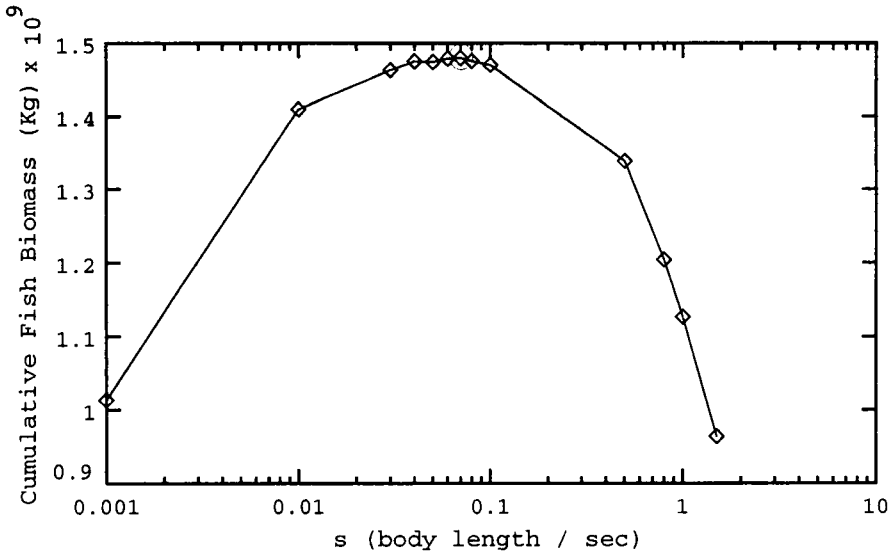

Relative number of fish
0.00
0.10
0.20
0.30
0.40
0.50
0.65
0
100
200
300
432
Structural mass (g)

(b)

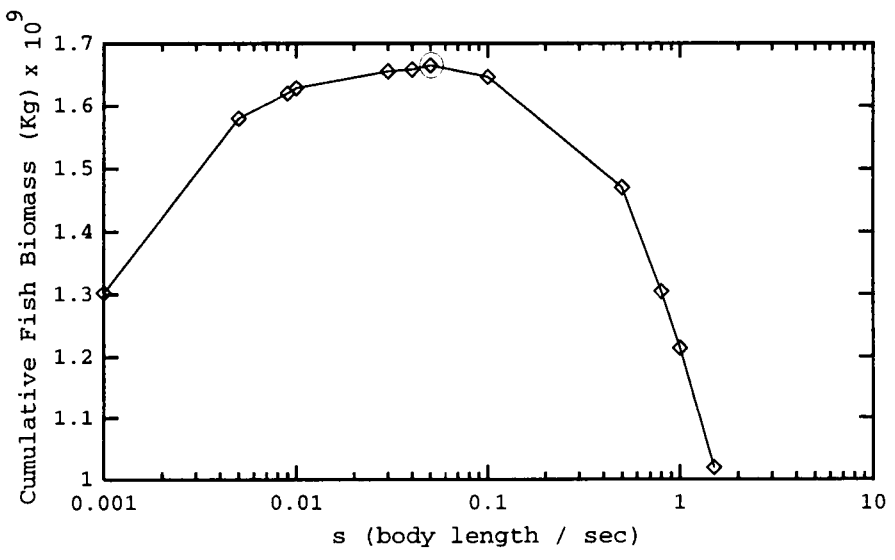



(c)

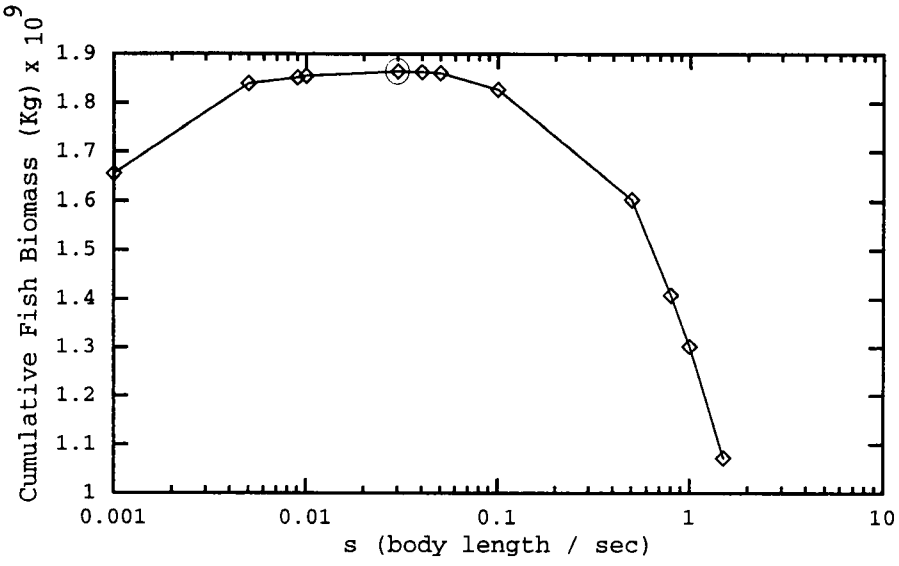
Figure 8: Structural distribution of fish at time $t = 5,000$ ($\alpha = 0.5$, $K = 5 \times 10^2$) (a) $s = 1.5$, (b) $s = 0.03$ and (c) $s = 0.009$.


Cumulative Fish Biomass (Kg) x 10^9
1.5
1.4
1.3
1.2
1.1
1
0.9
0.001
0.01
0.1
1
10
s (body length / sec)

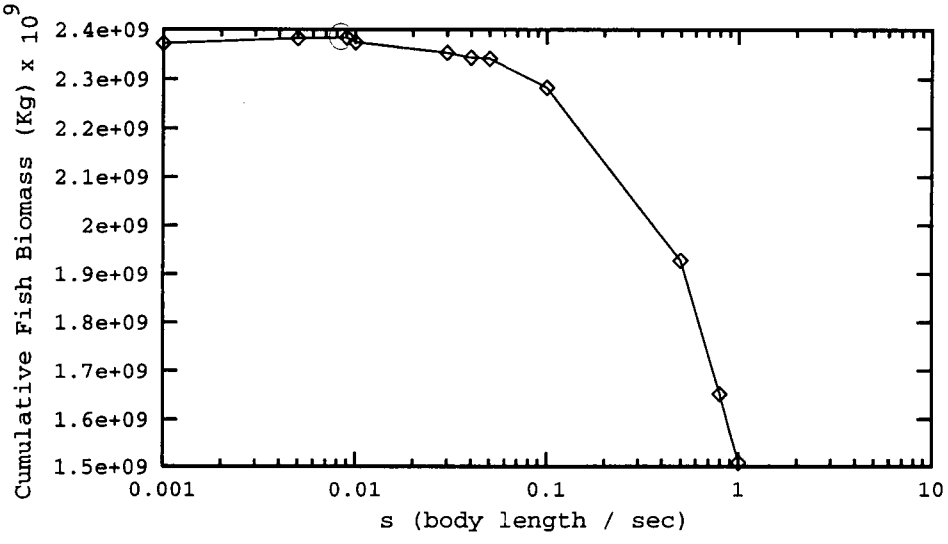
(a)


Cumulative Fish Biomass (Kg) x 10^9
1.7
1.6
1.5
1.4
1.3
1.2
1.1
1
0.001
0.01
0.1
1
10
s (body length / sec)

(b)




(c)




(d)

Figure 9: Cumulative fish biomass versus the characteristic velocity $s$ of the population ($\alpha = 0.5$). (a) $K = 3 \times 10^2$, (b) $K = 5 \times 10^2$, (c) $K = 10^3$, and (d) $K = 10^4$.

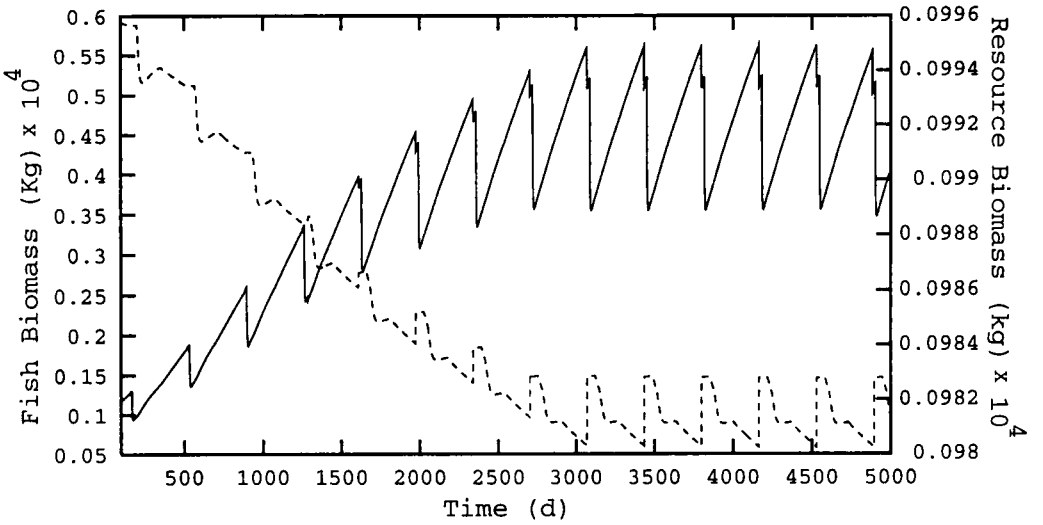
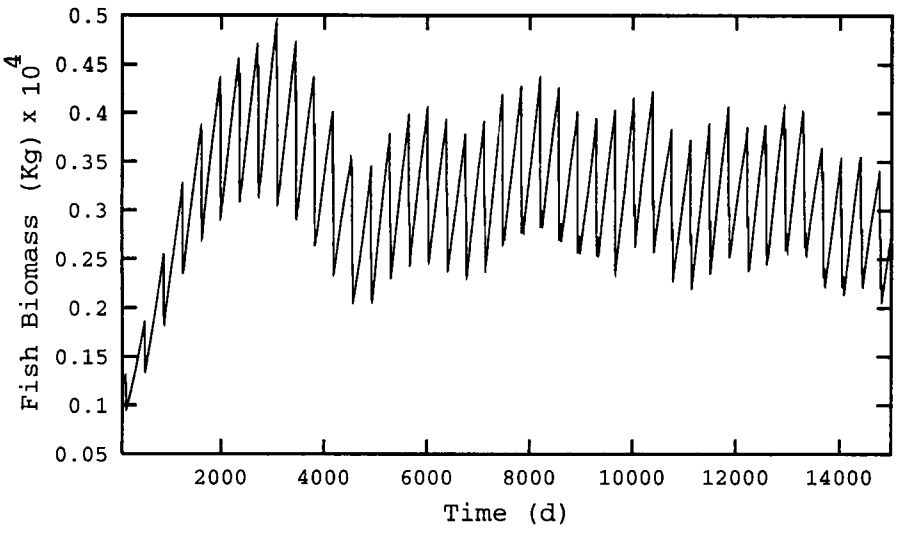
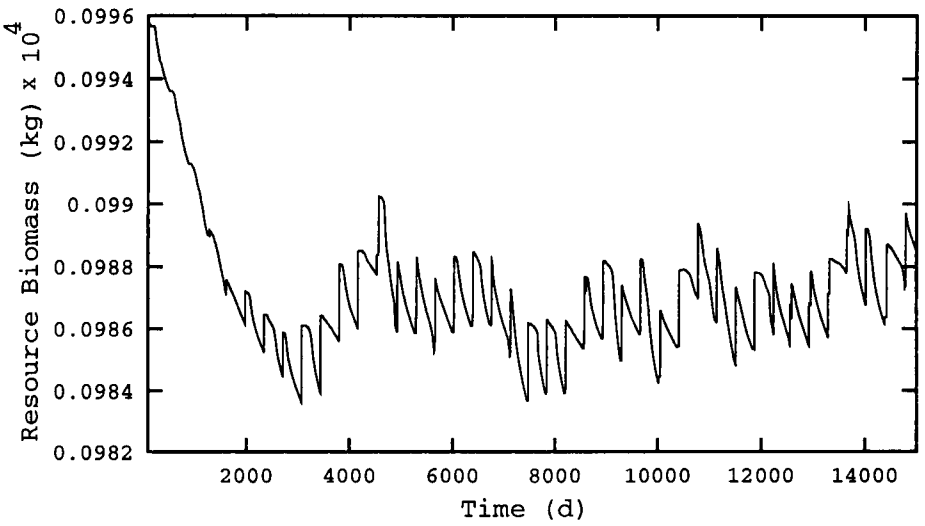



Figure 10: Dynamics of the total fish (—) and resource biomass (– – –) with $\alpha = 2$, $K = 10^3$, and $s = 1.5$.




(a)




(b)

Figure 11: (a) Dynamics of the total fish biomass for $\alpha = 2$, $K = 10^3$ and $s = 0.1$. (b) Dynamics of the total resource biomass for $\alpha = 2$, $K = 10^3$, and $s = 0.1$.

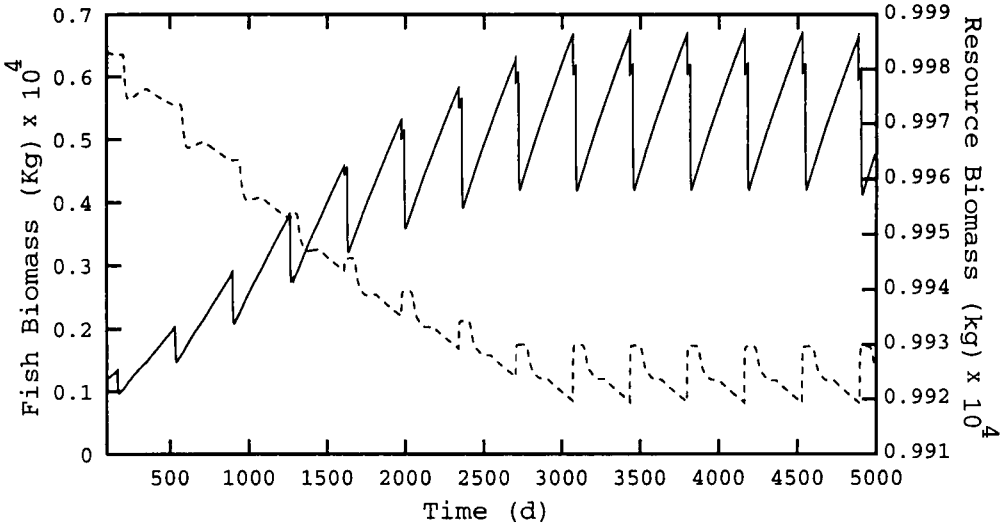
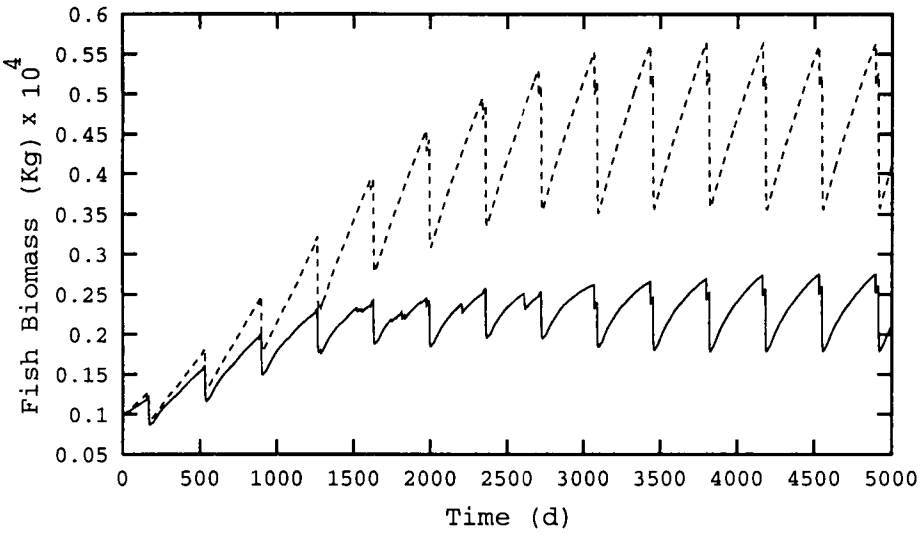
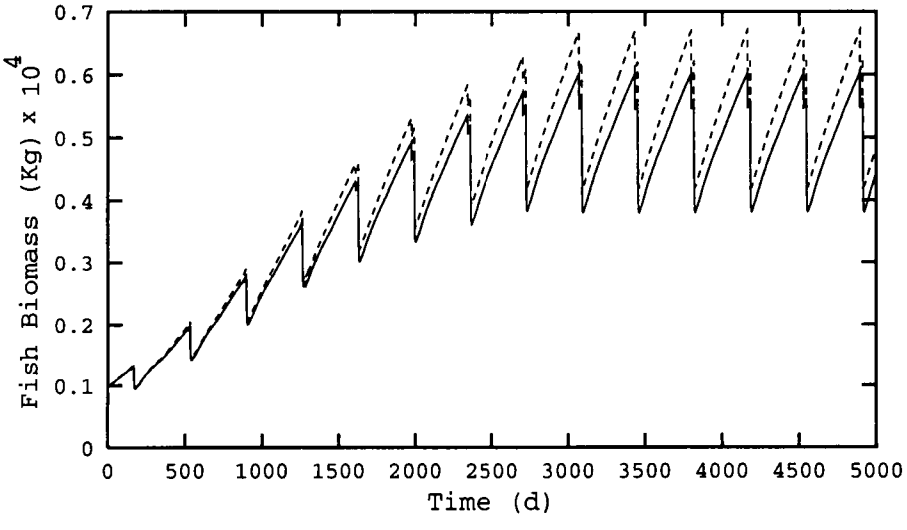


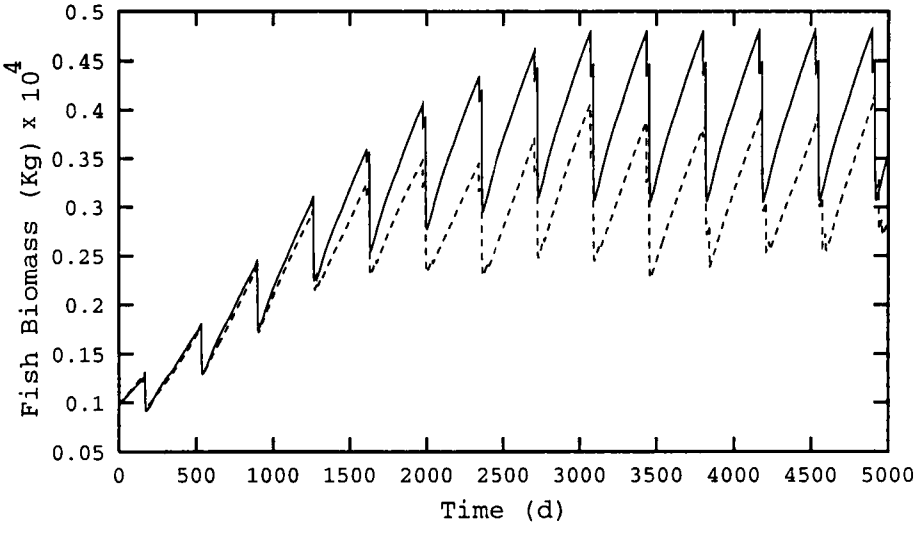

Figure 12: Dynamics of the total fish (—) and resource biomass (– – –) with $\alpha = 0.5$, $K = 10^4$, and $s = 0.1$.


Fish Biomass (Kg) x 10^4
0.6
0.55
0.5
0.45
0.4
0.35
0.3
0.25
0.2
0.15
0.1
0.05
0
500
1000
1500
2000
2500
3000
3500
4000
4500
5000
Time (d)

(a)


Fish Biomass (Kg) x 10^4
0.7
0.6
0.5
0.4
0.3
0.2
0.1
0
500
1000
1500
2000
2500
3000
3500
4000
4500
5000
Time (d)

(b)




(c)

Figure 13: Dynamics of the total fish biomass for continuous movement (eq. (5)) (—) and movement based on energetic constraints (eq. (6)) (– – –). (a) $\alpha = 0.5$, $K = 10^3$, and $s = 1.5$, (b) $\alpha = 0.5$, $K = 10^4$, and $s = 0.1$, and (c) $\alpha = 0.5$, $K = 10^3$, and $s = 0.1$.

# PART III

# MODELING THE EFFECTS OF TOXICANTS ON A FISH POPULATION IN A SPATIALLY HETEROGENEOUS ENVIRONMENT: LETHAL EFFECTS

# 1 Introduction

Risk assessment is primarily developed for the higher organizational levels of ecological systems such as populations and communities where there is a lack of biological information and toxicity evaluation. There are many reasons to base ecotoxicological models on an individually–based approach. Much toxicological and biological data are derived from short term experiments on individuals. Chemical impact occurs at the level of the individual, not at the population level, by affecting, directly or indirectly, individual processes such as the feeding rate, assimilation rate, maintenance, growth and reproduction or death of the individual. Even though the target site of a chemical may be specific tissues, the exposed, affected individual is the appropriate reference point for extrapolation to the population level. Hence, ecotoxicological models are best represented by using an individually–based approach, not an aggregated modeling technique.

Several research groups have developed individual–based models to determine chemical effects on aquatic organisms and populations [6, 7, 11, 12, 13, 14, 15]. The approaches utilized by the different research groups to model individual dynamics are based on energy budget techniques. The differences lie in the mechanisms employed to allocate energy for biological processes, the complexity of the models, and the approach followed to determine effects of chemicals on individuals.

Although structured models have been used to obtain a fairly good understanding of the qualitative response of aquatic systems to toxicant exposure, the effects of spatial heterogeneity on chemically stressed systems are generally unknown. The spatial component is very important for natural populations, but, generally, very hard to analyze in models.

Our initial project is to introduce space as a dimension in a physiologically–structured fish model introduced by Hallam et al. [4]. The spatial aspects of the model are limited to spatial variability of the resource and toxicant concentration. Fish are assumed to live and move in a closed bounded environment where spatial variation occurs in the toxicant concentration and temporal-spatial variation in the resource density which is assumed to consist of identical individuals that do not move. Because of the motility of the fish, the spatial variability in the toxicant, and the temporal-spatial variability in the resource, the toxicant exposure of an individual fish, which may occur through the environmental and food pathways, varies temporally.

The protocol used to study the effects of nonpolar narcotic toxicants on a fish population, which is exposed to a spatially varying toxicant and has a dynamic resource, when toxic exposure occurs through the environmental and/or the food pathways, utilizes the following components:

- individual model
- toxicant exposure–effect model
- population model coupling temporal–spatial processes with physiological processes of individuals and a dynamic resource.

The first and third model have been discussed in Part II and the basic ideas employed to assess chemical exposure and effects on individuals are discussed in [13]. A summary of these models is presented below to set the stage for this study on the effects of chemicals on populations living in spatially heterogeneous environments.

# 2 A Physiologically–based Individual Model

The individual model must allow for relevant interactions between the individual and the chemical and must also be able to account for toxicity. Appropriate model

components must be chosen with specific chemical and type of exposure in mind. For example, for lipophilic chemicals, the principal component of effect determination is the individual compartment of high affinity, the lipid compartment. The lipid in an individual acts as a buffer for lipophilic toxicants, allowing larger body burdens in fatter individuals than in less fat organisms. Lipid storage provides protection against stress from an acute exposure only if the organism does not mobilize stored lipid rapidly, such as during reproduction. Hence, to discuss the effects of toxicants, it is necessary to model the lipid content of an exposed organism. In addition to the lipid component, the individual model must consider a structure component to account for size related measurements such as weight or length of the organism. Structure is regarded as consisting primarily of protein and carbohydrates.

The model assumes that the only input to the lipid and structure compartments is obtained from the assimilated lipid and structure of the food; that is, no synthesis of lipid occurs from proteins and carbohydrates. This is not, in general, a valid hypothesis but because of the small amount of carbohydrates in the fish and its diet, lipogenesis may be ignored. The density of the resource is denoted by $X$ $(g/m^3)$ and we assume that $X = X_l + X_s$ where $X_l$ and $X_s$ are the lipid and structural portions of the resource.

The mass of lipid, $m_l$ (g), and the mass of structure, $m_s$ $(g)$, in an organism are assumed to have both labile and nonlabile portions. The nonlabile structure, $m_{ps}$, represents protein and carbohydrates bound in somatic tissues and is assumed to be nondecreasing with age; the nonlabile lipid, $\epsilon m_{ps}$, is the portion of the lipid associated with protein in cell membranes. The labile portion of lipid, $(m_l - \epsilon m_{ps})$, and the labile portion of structure, $(m_s - m_{ps})$, are utilized as energy sources to support the energy demands of the individual. Energetic demands, $E_d$, of the organism include maintenance, energy cost associated with ingested food (SDA), activity and reproduction. Reproduction consists of the transferring of mass from the individual for egg production and the associated energetic cost. The losses of energy due to

maintenance, SDA, and activity are assumed to occur on a continuous time scale and those due to reproduction occur periodically on a discrete time scale.

Hence, on intervals where there is no reproductive loss the dynamics of lipid and structural mass of an individual are modeled by the two coupled differential equations

$$\frac{dm_l}{dt} = g_l(m_l, m_s, X) = \frac{a_{0l}X_l}{X}F - a_1(m_l - \epsilon m_{ps})\frac{E_d}{E_a}\,,$$

(1)

$$\frac{dm_s}{dt} = g_s(m_l, m_s, X) = \frac{a_{0s}X_s}{X}F - a_2(m_s - m_{ps})\frac{E_d}{E_a}\,,$$

where $E_a$ denotes the energetic equivalent of the mass that an individual utilizes in order to maintain basal metabolism. This energy is derived from the labile lipid and labile structure using the function

$$E_a = 3.768 \cdot 10^4 a_1(m_l - \epsilon m_{ps}) + 1.675 \cdot 10^4 a_2(m_s - m_{ps})\,,$$

where $a_1$ and $a_2$ are the rates $(1/d)$ at which lipid and structure are mobilized to maintain basal metabolism, and the numbers in each term are the energetic values in $J$ of one *gram* of lipid and structure, respectively.

The feeding rate, $F$ $(g/d)$, of an individual is governed by constraints imposed by processes associated with encounter, pursuit and digestion of a prey and are implemented sequentially. The form of the feeding rate is

$$F = \frac{1}{T_e + T_p + T_d}\,,$$

(2)

where the terms in the denominator represent the characteristic times $(d/g)$ for encounter, pursuit, and digestion of prey.

For details on the feeding representation as well as the equations used to model maintenance, activity, and reproduction, refer to Part II.

# 3 Exposure–Effect Model

The uptake of chemical from the environment and food represents the chemical exchange between the aqueous environment and the individual fish across the gill mem-

branes and the chemical exchange between the fish and its intestinal food across the intestinal wall. The uptake model we use is a modification of FGETS, a model developed by Barber et al. [1] to handle exposure of fish to nonpolar, hydrophobic, reversible chemicals. The model was formulated based on the assumption that both environmental and food exposure are gradient-driven processes.

The mathematical model that describes the processes of chemical uptake from the environment and food and includes dilution of chemical due to organism growth is

$$\frac{dC_T}{dt} = k_1 C_w + \frac{F}{W_T} C_F - k_2 C_T - \frac{E k_E}{W_T} C_A - \frac{1}{V}\frac{dV}{dt} C_T \tag{3}$$

where $C_T$, $C_w$, $C_F$, and $C_A$ are respectively the concentrations of chemical in the whole fish, in the environment, in the food, and in the aqueous portion of the organism. $F$ is the weight of the food eaten per day and $E$ is the weight of material defecated per day. $k_E$ is the partition coefficient of chemical to excrement and is given by $k_E = \frac{C_E}{C_A}$, where $C_E$ is the concentration of the chemical in the feces. $k_1$ and $k_2$ are the uptake and depuration rates of the environmental chemical, respectively, and are specified by

$$k_1 = S_g k_w V^{-1}, \quad k_2 = S_g k_w V^{-1}(P_A + P_L K_L + P_S K_S)^{-1}.$$

$k_w$ measures the conductivity of the exposed surface area, $S_g$, and $V$ is the volume of the organism calculated by using the total weight, $W_T$, and the density of the organism. $P_A$, $P_L$, and $P_S$ are the aqueous, lipid, and structural fractions of the organism, respectively; $K_L$ is the partition coefficient of the chemical between the organismal lipid and water; $K_S$ is the partition coefficient of the chemical between the organismal structure and water. The last term in (3) represents the dilution of chemical due to organism growth. A summary of the variables and parameters used in the uptake model is given in Table 1 [1].

Hypotheses imposed in the model development include the following. An individual organism is assumed to be comprised of three chemical phases: aqueous, struc-

[1] All Figures and Tables appear in the Appendix.

tural, and lipid. The structural component is generally viewed as being composed of (physiologically active) protein and carbohydrates. A second hypothesis is that the time scales for the exchange across the exposed surface area, $S_g$, are regarded as being much slower than the distribution of chemical within the organism. Using this assumption, $C_A$ is expressed in terms of $C_T$ via

$$C_T = (P_A + P_L K_L + P_S K_S) C_A.$$

A third hypothesis was imposed to deal with difficulties of the transient events during digestive processes. The simplest assumption that avoids most of these difficulties is that of equilibration of chemical between the organism's body and the gut contents. This assumption, however, is not necessarily true. Hallam et al. [5] have indicated that this is the worst case assumption during increasing body concentration when exposed to contaminated food (i.e., no more chemical could be taken up under any thermodynamically consistent assumption than would be taken up when food and body equilibrate). During depuration, however, this assumption leads to predicted minimum depuration times; that is, any other thermodynamically consistent assumption would lead to longer predicted depuration times. For toxicity evaluations, this would usually not be considered the worst case scenario.

To calculate the concentration of the chemical in the food, we assume instantaneous chemical equilibration with the water and within the organism. The food, like the consumer, consists of the aqueous, lipid and structural phases and the chemical is distributed among them according to its affinity for these phases.

To model the effects of chemicals on individuals we need to couple the uptake model with models for the mode of action and models for concentration–response relations. Effects of chemicals on individuals focus on mortality but sublethal effects, such as reduction of growth rate, could be considered using a similar method [3, 9]. The assessment of mortality due to chemical action is implemented by utilizing formulations based upon quantitative structure–activity relations (QSARs). There are numerous QSARs in the literature for chemicals with different modes of action. We

utilize results of Veith et al. [17] and Konemann [10] developed for baseline narcotic chemicals and relate a chemical property, the octanol/water partition coefficient, $K_{ow}$, to mortality of individuals (see Figure 1). For a single individual, an effect occurs when concentration of chemical in the aqueous phase reaches a critical level, denoted by $LC_{50}$, and is calculated from the equation $\log LC_{50} = -0.8 - \log K_{ow}$.

The exposure–effect model is coupled with the physiologically–based individual model which yields expressions for the weight and surface area of the organism. This model of an individual fish includes lipid and structural components necessary for assessing effects of lipophilic chemicals on individuals. The aqueous component of an individual needed for the exposure model is assumed to be proportional to the structural mass of the individual.

# 4 A Dynamic Population Model

A dynamic population model based on physiological and movement behavioral aspects of individuals is needed so that effects of toxicants can be determined directly and the cumulative effect at the population level can be ascertained. An approach that allows incorporation of individual dynamics into a dynamic population formulation is the McKendrick–von Foerster equation.

The variables used to describe the physiological behavior of the individual are the age, $a$ $(d)$, mass of lipid, $m_l$ $(g)$, and mass of structure, $m_s$ $(g)$. Because of the environmental heterogeneity, a variable that denotes the spatial location of an individual is needed. The environment is assumed to be linear and the spatial location of an individual is denoted by $x$. The basic equations that model the fish and prey dynamics are:

$$\frac{\partial \rho}{\partial t} + \frac{\partial \rho}{\partial a} + \frac{\partial(\rho\, g_l)}{\partial m_l} + \frac{\partial(\rho\, g_s)}{\partial m_s} + \frac{\partial(\rho\, q)}{\partial x} = -\mu\rho\,. \tag{4}$$

$$\frac{dr}{dt} = \alpha\, r(1 - \frac{r}{K}) - \int_0^\infty \int_0^\infty \int_0^\infty F\ \rho\ da dm_l dm_s\,, \tag{5}$$

where $\rho = \rho(t, a, m_l, m_s, x)$ $(numbers/d{\cdot}g^2{\cdot}m)$ denotes the fish density and $r = r(t, x)$

$(g/m^3)$ the prey density. In addition to equations (4) and (5), we adjoin initial conditions, a boundary condition which asserts that there is no flow of population across the boundary of the habitat, and a renewal equation to describe the birth process.

Equation (4) incorporates the growth rates, $g_l$ and $g_s$, of the physiological variables $m_l$ and $m_s$, respectively, and the movement rate, $q$, of an individual into the population. The mortality function $\mu$ accounts for different types of mortalities. It includes mortality due to the physiological process of aging, mortality due to starvation, juvenile density dependent mortality and mortality due to toxicity. The addition of the toxicant leads to another type of mortality which is assessed at the individual level according to lipid content of the organism.

Equation (5) models the rate of change of the prey density at location $x$. The first term describes a logistic growth of the prey in the absence of fish with $\alpha$ $(d^{-1})$ denoting the maximum rate of increase and $K$ $(g/m^3)$ the carrying capacity of the prey. The integral term describes the prey eaten by fish and is determined by the feeding rate, $F = F(m_l, m_s, X)$, of each individual fish where $X$ is the resource density to which an individual fish with lipid content $m_l$ and structure content $m_s$ responds. Because resource is limited, predators which are assumed to forage in social groups, divide the resource by an intraspecific competitive mechanism with larger predators receiving larger shares. For the present study, we consider toxicants that do not affect the prey population; that is, predation is the only type of mortality assessed in the prey population.

Movement behavior of individuals can be very complicated. In Part II we discussed two movement behaviors, which both assume that individuals alter their movement in response to changes in resource density. In addition, exposed organisms may avoid contaminated media, may be attracted to contaminated media (e.g. pesticide–debilitated prey) or may lose their ability to detect contamination due to toxic effects [16]. If the contamination is local and of short duration, avoidance can prevent the

occurrence of effects on mobile organisms. However, avoidance of chronically contaminated media or food may result in lack of resource which can seriously affect the population. There is no standardized procedure for determining avoidance and preference behaviors largely because they depend on the chemical and its concentration as well as the species [2, 8]. Because behavioral data are lacking for most chemicals, in the present study, we assume that the presence of toxicants does not influence the movement behavior of individuals and continue to assume that individuals move into areas with higher prey density. In particular, our simulations are based on the following equation

$$q = \kappa v_s \frac{\partial r}{\partial x}, \tag{6}$$

where $\kappa$ is a positive constant that measures the tendency of predators to pursue prey and represents the distance covered by the foraging predator per unit change in the prey density. $\frac{\partial r}{\partial x}$ denotes the derivative of $r$ with respect to the variable $x$ and represents the rate of change of the resource at $x$. $v_s$ is an average swimming velocity $(m/d)$ of an individual with length $L_f$ $(m)$ and is given by $v_s = 8.64 \cdot 10^4 s L_f$ where $s$ denotes the body lengths per second of the predator while performing sustained cruising.

The toxicant-population model is formulated so that a toxicant may be released at different locations and at numerous times for arbitrary exposure length and as a result we may obtain a spatially explicit variation in toxicant concentration. We ignore movement and transformation of toxicants in the environment and concentrate on the effects of stress on biota. Our numerical procedure follows cohorts of individuals that move continuously in the heterogeneous habitat (heterogeneity results from both resource and toxicant distributions). This numerical procedure allows effects of spatially explicit toxicant exposure to be assessed at the individual level, but the overall effects can still be determined by an accumulation of individual effects.

# 5 Effects of Toxicants on Population

The population model is investigated numerically with the nominal, unstressed simulations compared to the simulations with toxicant stress to indicate effects. A characteristic behavior of the unstressed model is that the fish and resource biomass as well as the age, lipid and structural distributions, are asymptotically periodic with a period of one year, the same period as the reproductive period for parameter values that result in the coexistence of both populations.

Lassiter and Hallam [13] developed an approach to evaluate the effects of the lipid distribution in a population on population dynamics in response to an acute exposure of a lipophilic narcotic chemical. According to this theory, in an assessment of mortality, an individual with smaller lipid fraction content will die before another individual with a larger lipid fraction, given equal exposure. The theory of the survival of the fattest considers homogeneous toxic exposures to a static population that are necessarily acute. This theory is not valid when these assumptions are violated. In a dynamic setting, survival of the population after chronic exposure is determined not only by the lipid distribution, but also by the growth rate of the individuals in the population [7].

In addition to physiological aspects of the population, the response of a fish population to a toxicant exposure depends on the spatial pattern of the toxicant and resource as related to the distribution of individuals in time and space, the duration of the exposure, as well as the strength of the toxicant.

In many cases, the rate and the spatial–temporal pattern of release of chemicals from a source is the major source of uncertainty in an ecological risk assessment. We consider two simple scenarios for the release of a chemical: 1) point source release (inhomogeneous spatial distribution of the chemical) and 2) non–point source release (homogeneous spatial distribution of the chemical). We incorporate release of the chemical in our model by dividing the habitat into cells that are assumed chemically homogeneous. For the following simulations, the habitat in which the populations

live is taken to be 1 $Km$ long and is divided into 10 cells. The parameter values used in the simulations are given in PART II.

To demonstrate the effects of chemicals and the importance of chemical heterogeneity we stress the theoretical population employing the same chemical and we investigate the outcomes by varying the spatial distribution of the environmental chemical concentration and the initial time of exposure. The structure of the population is compared before and after the exposure and the time evolution of the stressed population is compared to the nominal, unstressed population.

*Toxicant exposure case 1.* The fact that exposure may come from both the environmental and the food pathways complicates determination of cause of death. First, in order to demonstrate the effects of spatial variation of the chemical we consider only environmental exposure.

We expose the theoretical populations, generated with $\alpha = 0.5$, $K = 5 \times 10^2$ and two different values of the characteristic velocity $s$ of the population ($s = 0.04$ and $s = 0.05$), to a chemical with $K_{ow} = 10^5$. The two populations for the different values of $s$ consist of almost identical individuals (compare Figure 2 to Figure 3). In both cases, a seven day homogeneous environmental exposure to a $3.57 \times 10^{-5}\ g/cm^3$ aqueous concentration initiated on day 5,000 (106 days after reproduction) affects only individuals of the first age class. These individuals are very small in size which implies a rapid uptake of chemical resulting in mortality.

When the environmental exposure is not homogeneous, the structure of the populations after the termination of the exposure is completely different. The spatial distribution of the environmental chemical concentration used to stress the population is shown in Figure 4. The chemical concentration varies from $0.45 \times 10^{-5}$ to $9.9 \times 10^{-5}\ g/cm^3$ and has an average value of $3.57 \times 10^{-5}\ g/cm^3$.

Figure 5 and Figure 6 show the age, lipid and structural distributions of the population with $s = 0.04$ and $s = 0.05$, respectively, after the termination of the exposure. The physiological distributions of the two populations are different after

the end of the exposure. For example, the one year old individuals of the population with $s = 0.05$ survive the exposure while the same individuals in the population with $s = 0.04$ do not survive the exposure. Therefore, because the two populations do not differ in physiological structure, any differences in their response are reflected by differences in the distribution of the population in time and space. To illustrate the distribution of the population in time and space requires a three dimensional graph; these graphs provide little information because the spatial distribution of the population changes without any apparent pattern.

The distribution of the population in time and space also determines the extinction or survival of the population when the exposure occurs via the contaminated food, even if the spatial distribution of the chemical is homogeneous. The response of the population to the chemical is governed by the amount of chemical uptake from the food which varies spatially and temporally, causing the exposure to vary between individuals.

*Toxicant exposure case 2.* The time that the exposure starts relative to the physiological state of the population will, generally, result in different population structures. The resulting population structure is determined by a trade-off between the physiological state of individuals and their spatial locations.

An interesting case to investigate is the response of the population to toxicant exposures during reproduction. We expose a theoretical population, generated with $\alpha = 0.5$, $K = 5 \times 10^2$ and $s = 0.05$, to a chemical with $K_{ow} = 10^5$ starting the exposure, which occurs through both the environmental and food pathways, at $5,257$ $d$ into the simulation (three days before reproduction). Figure 7 illustrates the age and lipid distributions of the population at this time.

A ten day exposure to a chemical concentration of $1.06 \times 10^{-5}$ $g/cm^3$ initiated three days before reproduction results in extinction of the population. Extinction occurs because the eggs do not survive the exposure due to environmental chemical concentration being much larger than the lethal concentration, and the mothers die

due to the rapid mobilization of lipid storage for reproduction which results in release of some of the chemical into the blood stream.

We now consider the case where the chemical is not uniformly distributed in space. The spatial distribution of the environmental chemical concentration used to stress the population is shown in Figure 8. The chemical concentration varies from $0.15 \times 10^{-5}$ to $2.0 \times 10^{-5}$ $g/cm^3$ and has an average value of $1.06 \times 10^{-5}$ $g/cm^3$. At the end of a ten day exposure, there is a cohort of newborns that survive the exposure (Figure 9). These individuals survive because they are born in a location where the chemical concentration is below the lethal concentration and because the exposure has been terminated by the time the eggs hatch. Figures 10a-b show the dynamics of the fish and resource biomass before and after the exposure which is compared with the dynamics of the unstressed population. Because the chemical mode of action is reversible and there is no shortage of food, the population ultimately recovers and evolves in the same way as the unstressed population. Hence, spatial heterogeneity might save a population that otherwise would go to extinction.

Because the chemical mode of action is reversible, in all the exposure scenarios discussed here, when the simulation is continued after the termination of the toxicant exposure, the population ultimately recovers and has structure identical to the structure of the unstressed population.

# 6 Discussion

We have indicated a method to study the effects of nonpolar narcotic chemicals on a fish population exposed to a spatially varying chemical and a dynamic resource. We have demonstrated in the assessment of mortality that the spatial pattern of the toxicant and resource, as related to the distribution of individuals in time and space, can influence the physiological structure of the population and determine the survival or extinction of the population. An implication of the current study is that,

in addition to the biological attributes of the population, spatial heterogeneity is essential to determine the effects of a toxicant on the population.

Although we have assumed that the movement behavior of individuals is not influenced by the presence of toxicants, the model can easily be modified to take into account avoidance of contaminated media. However, prior to any modification, knowledge of the behavioral responses of the species to specific chemicals and concentrations is needed.

Because the prey population is unstructured, assessment of mortality cannot be implemented using similar formulations as for the fish population. The addition of a specific amount of chemical would have the same effect on the whole prey population; that is, either the whole population will survive or it will die. A structured prey population is needed to adequately assess mortality due to toxicants in the community.

The model developed here can be used to study effects of exposures to sublethal concentrations on individual processes such as swimming activity, feeding rate and reproduction, and the cumulative effects on the population.

# References


[1] M. C. BARBER, L. A. SUAREZ, AND R. R. LASSITER, *Modeling bioconcentration of nonpolar organic pollutant by fish*, Environ. Toxicol. Chem., 7 (1988), pp. 545–558.

[2] R. H. GRAY, *Fish behavior and environmental assessment*, Environ. Toxicol. Chem., 9 (1990), pp. 53–67.

[3] T. G. HALLAM, G. A. CANZIANI, AND R. R. LASSITER, *Sublethal narcosis and population persistence: A modeling study on growth effects*, Environ. Toxicol. and Chem., 12 (1993), pp. 947–954.

[4] T. G. HALLAM, R. LASSITER, AND S. M. HENSON, *Modelling fish population dynamics: a physiologically based perspective*, Manuscript, (1996).

[5] T. G. HALLAM, R. LASSITER, AND S. A. L. M. KOOIJMAN, *Effects of toxicants on aquatic populations*, in Applied Mathematical Ecology, S. A. Levin, T. G. Hallam, and L. J. Gross, eds., vol. 18, Berlin Heidelberg, 1992, Springer-Verlag, pp. 352–382.

[6] T. G. HALLAM, R. LASSITER, J. LI, AND W. MCKINNEY, *Modeling the effects of toxicants on fish populations*, in Proceeding of the conference on Fish Physiology, Fish Toxicology and Fisheries Management, Guangzhou, PRC, Athens, Georgia, 1988, U. S. Environmental Protection Agency, pp. 299–320.

[7] ——, *Toxicant-induced mortality in models of daphnia populations*, Environ. Toxicol. Chem., 9 (1990), pp. 597–621.

[8] J. M. HELLAWELL, *Biological Indicators of Freshwater Pollution and Environmental Management*, Elsevier Applied Science Publishers, London, 1986.

[9] J. JAWORSKA, T. G. HALLAM, AND T. W. SCHULTZ, *Chronic effects of nonpolar narcotics on a model microbial community*, Environ. Toxicol. and Chem., 15 (1996), pp. 1049–1056.

[10] H. KONEMANN, *Quantitative structure activity relationships in fish toxicity studies. Part I. Relationship for 50 industrial pollutants*, Toxicology, 19 (1981), pp. 209–221.

[11] S. A. L. M. KOOIJMAN, *Dynamic energy budgets in biological systems*, Cambridge University Press, Great Britain, 1993.

[12] ——, *The analysis of aquatic toxicity data*, VU University Press, Amsterdam, 1996.

[13] R. R. LASSITER AND T. G. HALLAM, *Survival of the fattest: Implications for acute effects of lipophilic chemicals on aquatic populations*, Environ. Toxicol. and Chem., 9 (1990), pp. 585–595.

[14] E. B. MULLER AND R. M. NISBET, *Modeling the effects of toxicants on the parameters of dynamic energy budget models*, in 6th Symposium on Environmental Toxicology and Risk Assessment, J. Dwyer, T. Doane, and M. Hinman, eds., Philadelphia, 1996, American Society for Testing and Materials.

[15] R. M. NISBET, A. H. ROSS, AND A. J. BROOKS, *Empirically–based dynamic energy budget models: theory and an application to ecotoxicology*, Nonlinear World, 3 (1996), pp. 85–106.

[16] G. W. SUTER II, *Ecological Risk Assessment*, Lewis Publishers, 1993.

[17] G. D. VEITH, D. J. CALL, AND L. T. BROOKE, *Structure toxicity relationships for the fathead minnow, Pimephales promelas: Narcotic industrial chemicals*, Can. J. Fish. Aquat. Sci., 40 (1983), pp. 743–748.

# Appendix

**Table 1.** Symbol reference list for the variables and parameters used in the uptake model

| *Symbol* | *Default value* | *Interpretation* | *Units* |
|---|---|---|---|
| Variables | | | |
| $C_T$ | | Toxicant concentration in whole fish | $g/cm^3$ |
| $C_w$ | | Toxicant concentration in ambient water | $g/cm^3$ |
| $C_A$ | | Toxicant concentration in aqueous portion of the fish | $g/cm^3$ |
| $C_F$ | | Toxicant concentration in intestinal contents | $g/cm^3$ |
| $S_g$ | | Active exposure area | $cm^2$ |
| $F$ | | Weight of ingested food per day | $g/d$ |
| $E$ | | Weight of material defecated per day | $g/d$ |
| $V$ | | Volume of the organism | $cm^3$ |
| $W_T$ | | Weight of the organism | $g$ |
| $P_A$ | | Fraction of fish that is aqueous | nondim. |
| $P_L$ | | Fraction of fish that is lipid | nondim. |
| $P_S$ | | Fraction of fish that is structure | nondim. |
| Parameters | | | |
| $k_w$ | 530 | Conductivity:exposure | $cm^2/d$ |
| $k_E$ | 0.2 | Partition coefficient of chemical to excrement | nondim. |
| $K_L$ | 1 | Lipid/water partition coefficient | nondim. |
| $K_S$ | 0.2 | Structure/water partition coefficient | nondim. |

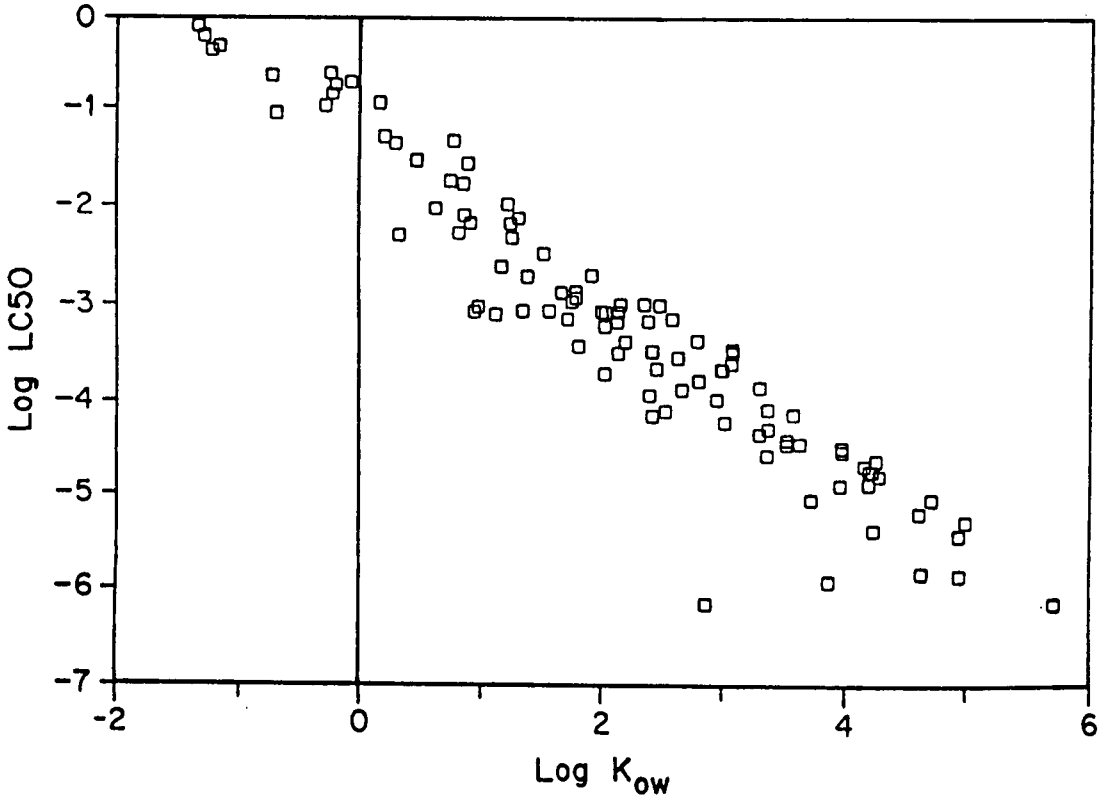
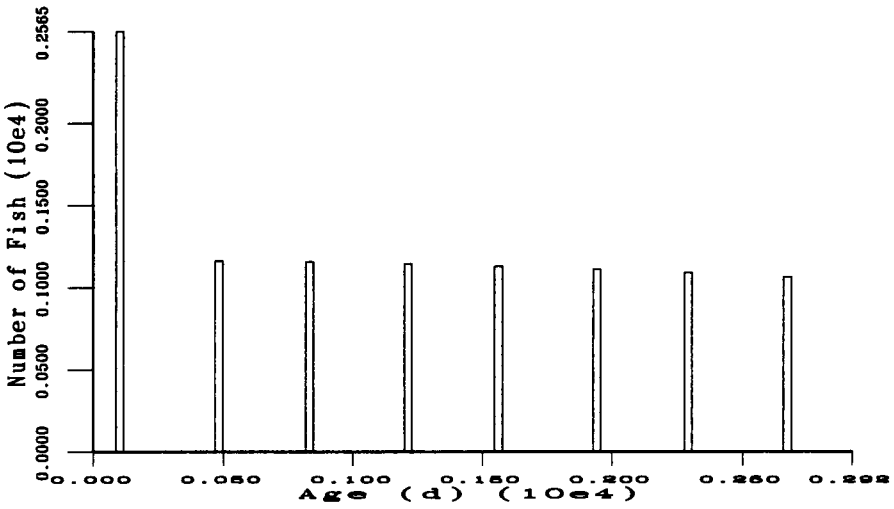
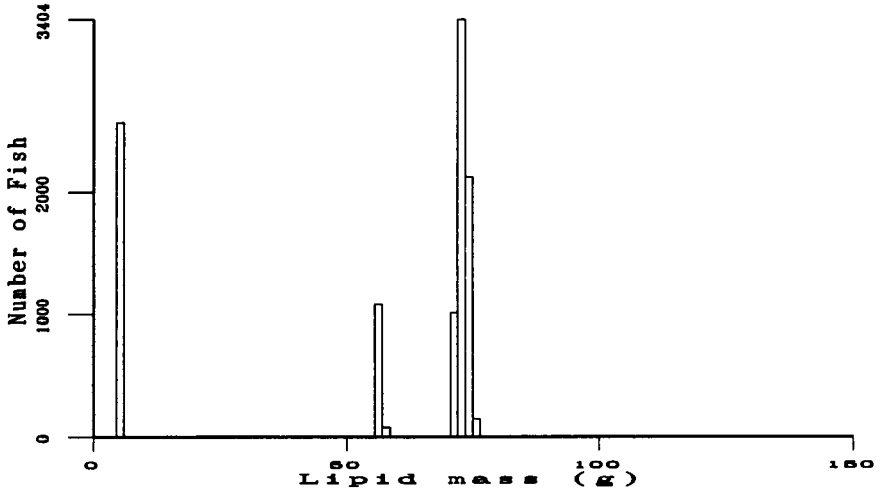


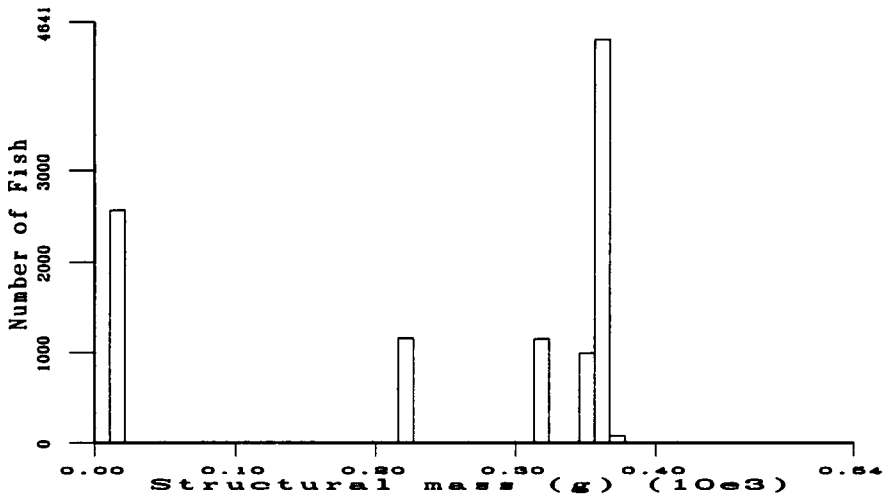

Figure 1: Relationship between $\log LC_{50}$ and $\log K_{ow}$. Fitted result is $\log LC_{50} = -0.8 - \log K_{ow}$. Data from Veith et al. [17] and Konemann [10].


Number of Fish (10e4)
0.0000
0.0500
0.1000
0.1500
0.2000
0.2565
0.000
0.050
0.100
0.150
0.200
0.250
0.292
Age (d) (10e4)

(a)

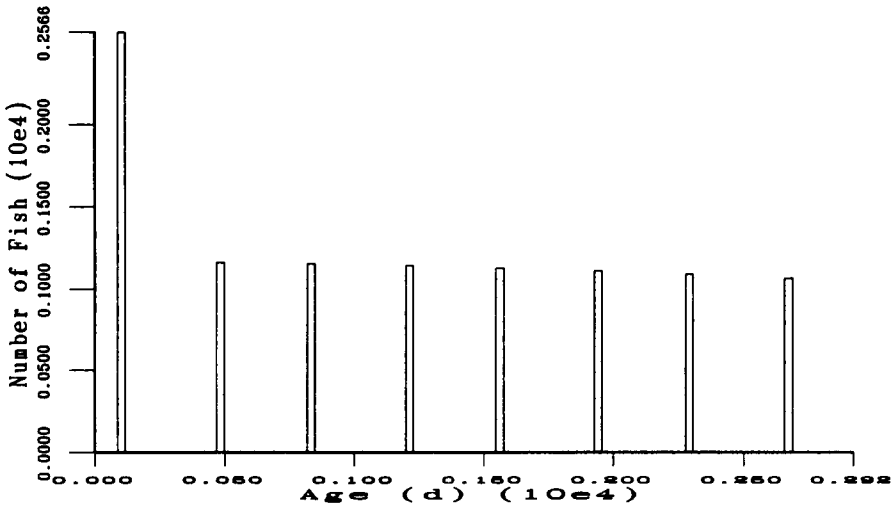

Number of Fish
0
1000
2000
3404
0
50
100
150
Lipid mass (g)

(b)

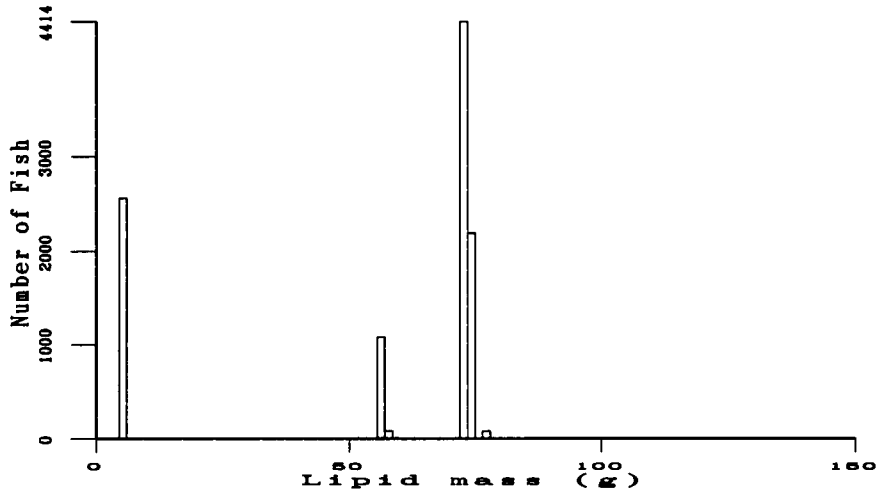



(c)

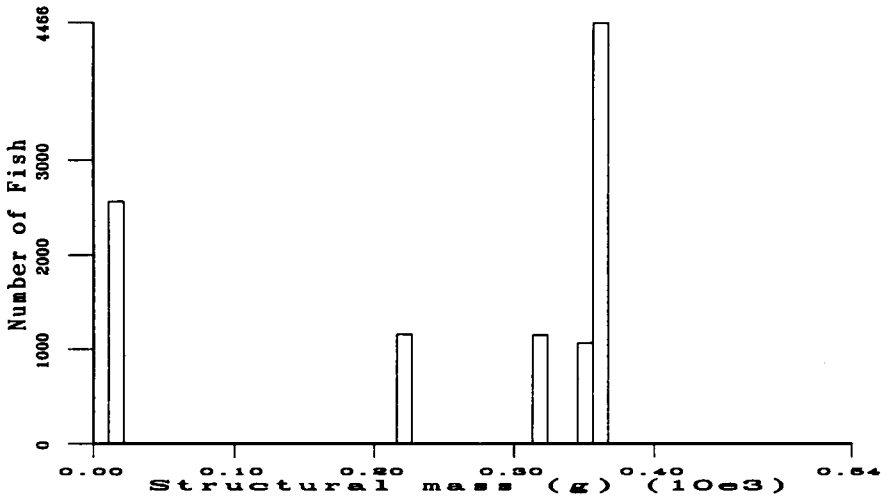
Figure 2: (a) Age, (b) lipid, and (c) structural distributions of the fish population with $\alpha = 0.5$, $K = 5 \times 10^2$, and $s = 0.04$ on day 5,000 of the simulation.


Number of Fish (10e4)
0.0000
0.0500
0.1000
0.1500
0.2000
0.2566
0.000
0.050
0.100
0.150
0.200
0.250
0.292
Age (d) (10e4)

(a)


Number of Fish
0
1000
2000
3000
4414
0
50
100
150
Lipid mass (g)

(b)




(c)

Figure 3: (a) Age, (b) lipid, and (c) structural distributions of the fish population with $\alpha = 0.5$, $K = 5 \times 10^2$, and $s = 0.05$ on day 5,000 of the simulation.

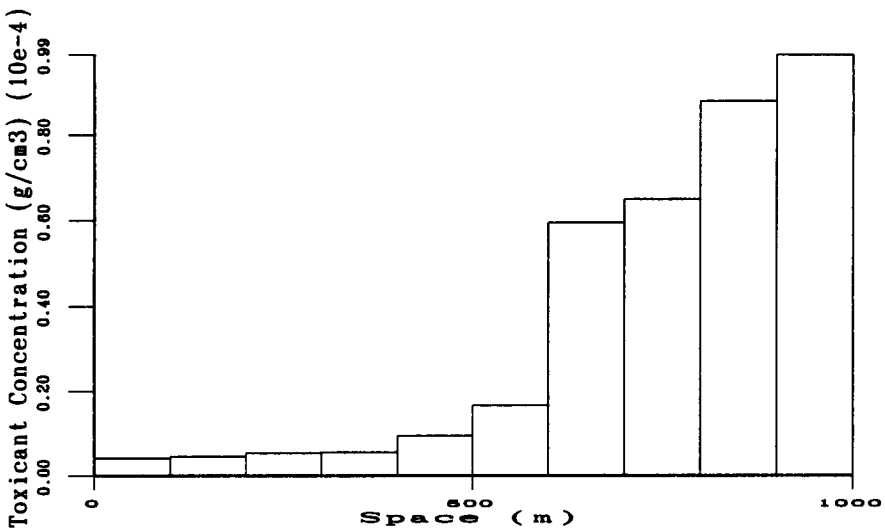
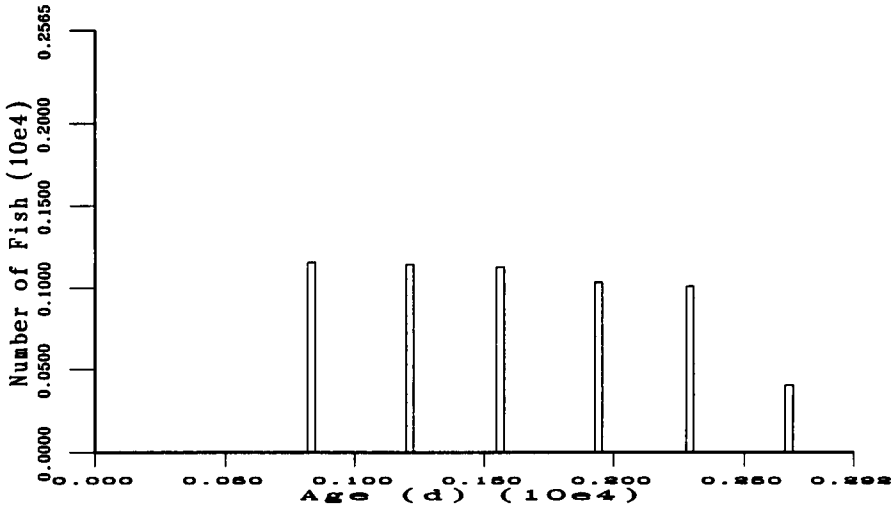
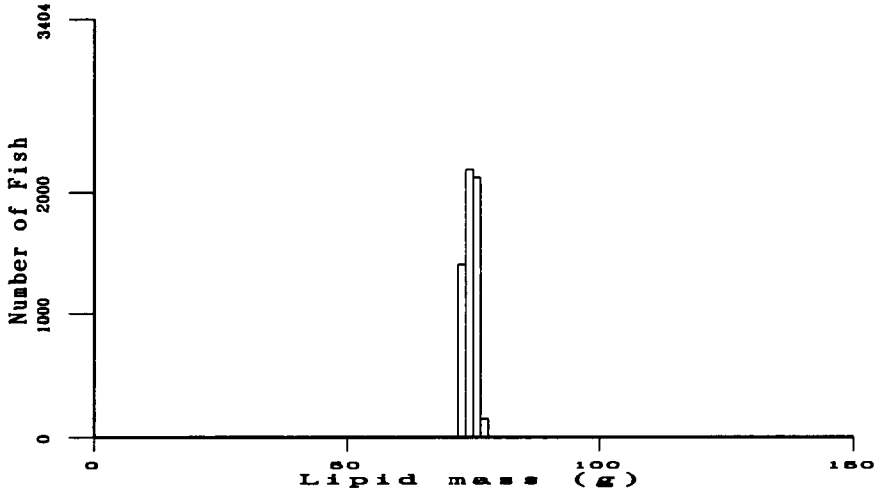


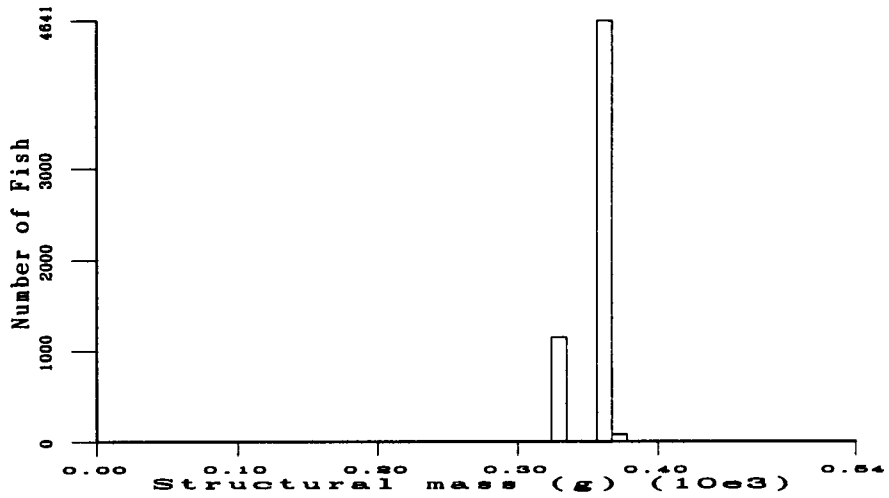

Figure 4: Spatial distribution of a chemical with $K_{ow} = 10^5$. Chemical concentration varies from $0.45 \times 10^{-5}$ to $9.9 \times 10^{-5}$ $g/cm^3$ with an average value of $3.57 \times 10^{-5}$ $g/cm^3$.


Number of Fish (10e4)
0.0000
0.0500
0.1000
0.1500
0.2000
0.2565
0.000
0.050
0.100
0.150
0.200
0.250
0.292
Age (d) (10e4)

(a)

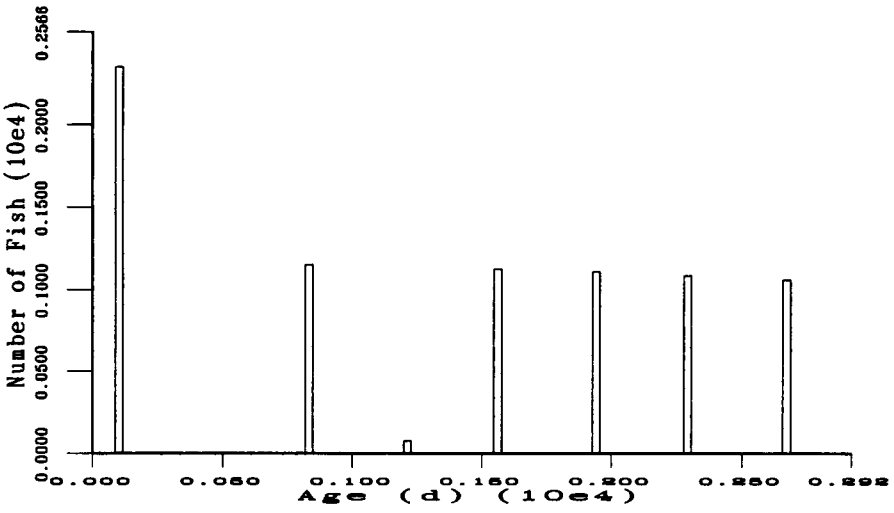

Number of Fish
0
1000
2000
3404
0
50
100
150
Lipid mass (g)

(b)

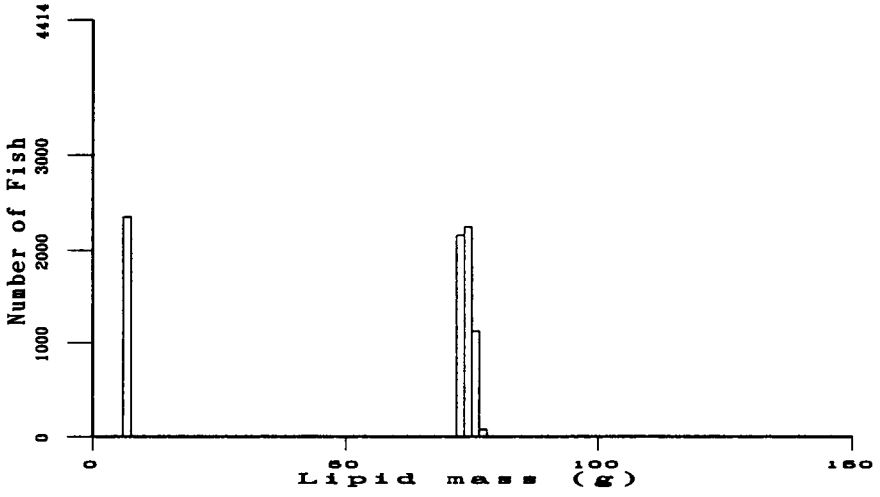



(c)

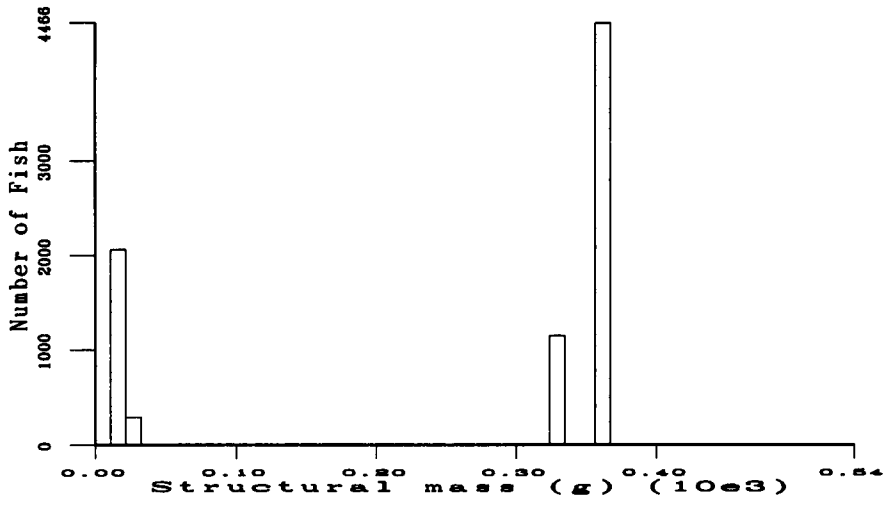
Figure 5: Toxicant exposure case 1 (see text for details). (a) The age, (b) lipid, and (c) structural distributions of the fish population with $s = 0.04$ after the termination of a 7–$d$ environmental exposure initiated on day $5,000$.


Number of Fish (10e4)
0.0000
0.0500
0.1000
0.1500
0.2000
0.2566
0.000
0.050
0.100
0.150
0.200
0.250
Age (d) (10e4)

(a)

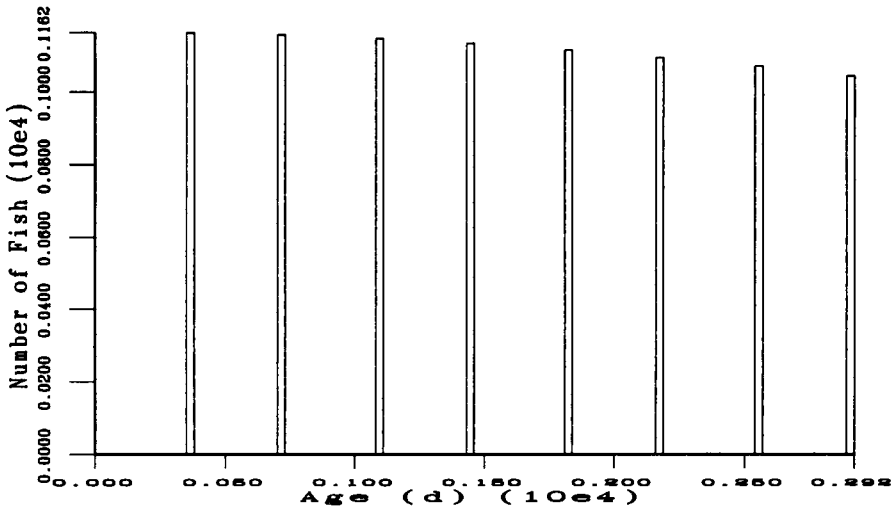

Number of Fish
0
1000
2000
3000
4414
0
50
100
150
Lipid mass (g)

(b)

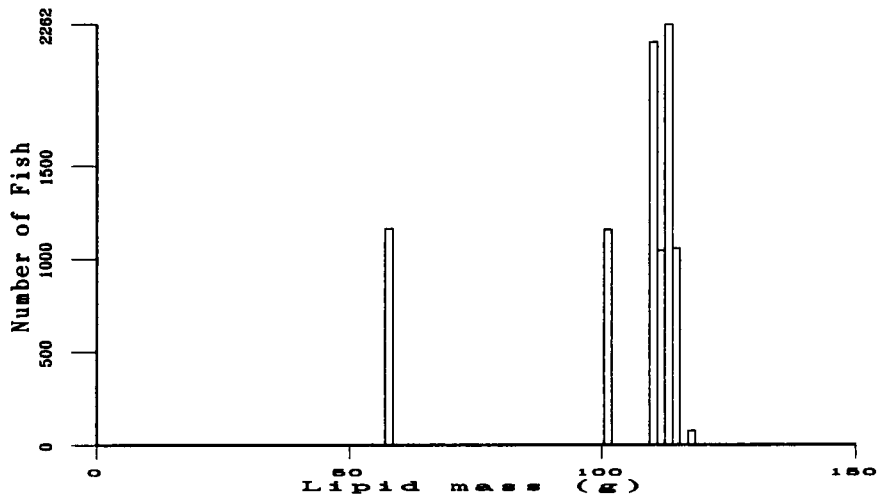



(c)

Figure 6: Toxicant exposure case 1 (see text for details). (a) The age, (b) lipid, and (c) structural distributions of the fish population with $s = 0.05$ after the termination of a 7–$d$ environmental exposure initiated on day 5,000.




(a)




(b)

Figure 7: (a) Age and (b) lipid distributions of the fish population with $\alpha = 0.5$, $K = 5 \times 10^2$, and $s = 0.05$ on day 5,256 of the simulation.

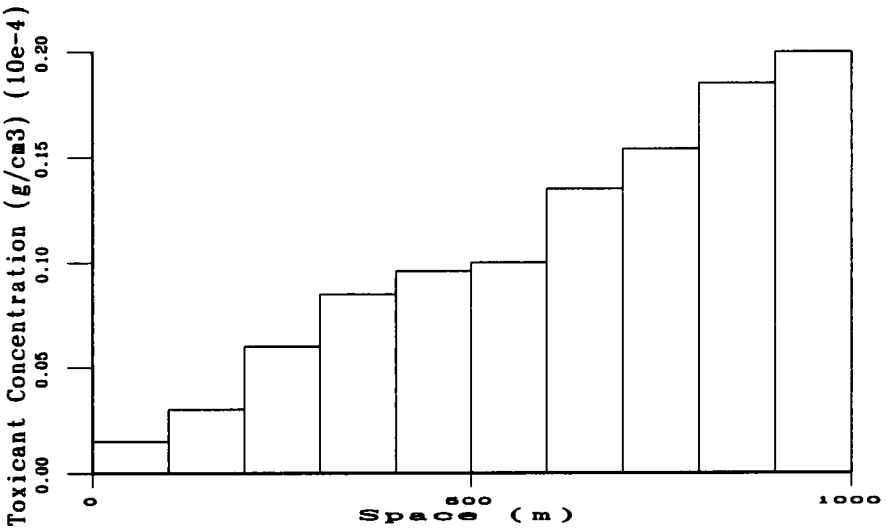
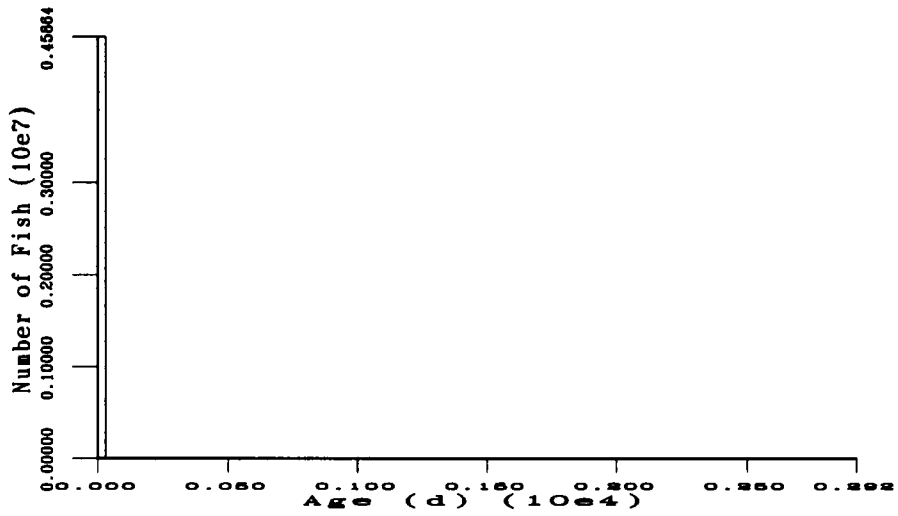
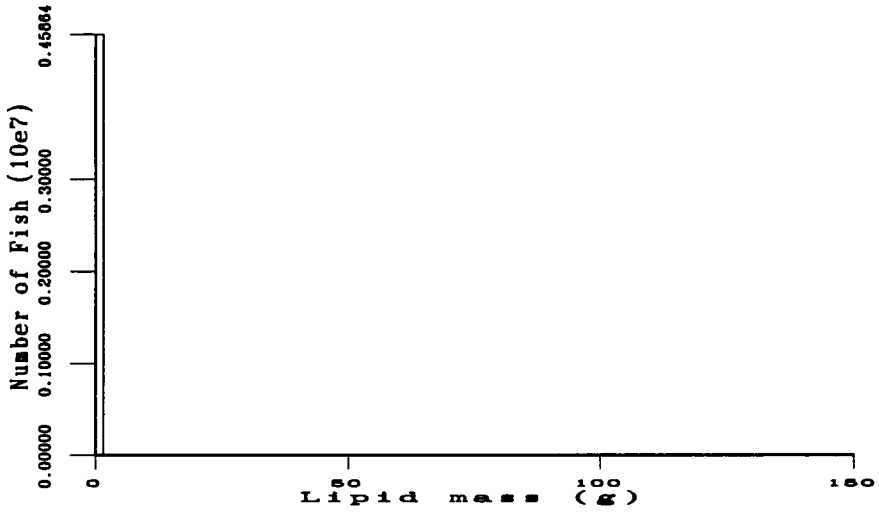



Figure 8: Spatial distribution of a chemical with $K_{ow} = 10^5$. Chemical concentration varies from $0.15 \times 10^{-5}$ to $2.0 \times 10^{-5}$ $g/cm^3$ with an average value of $1.06 \times 10^{-5}$ $g/cm^3$.

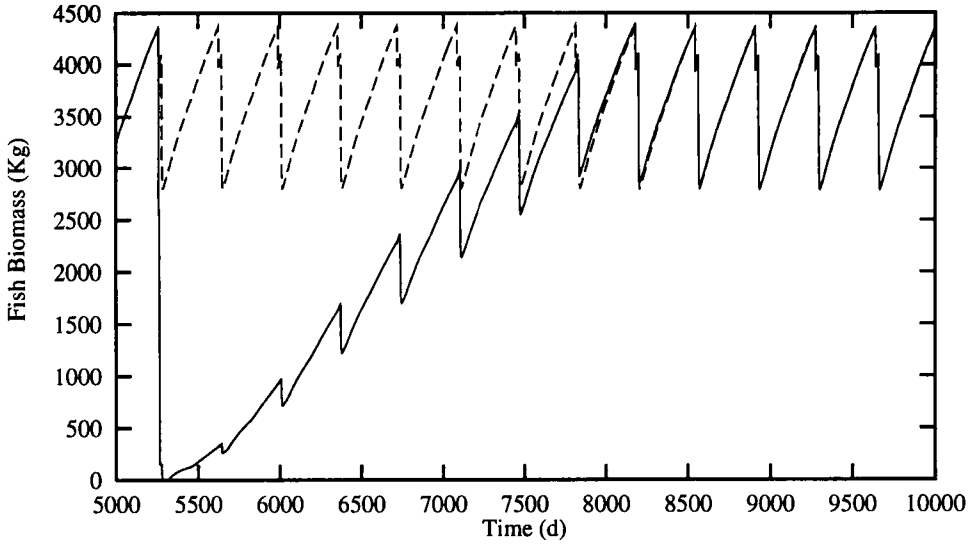



(a)

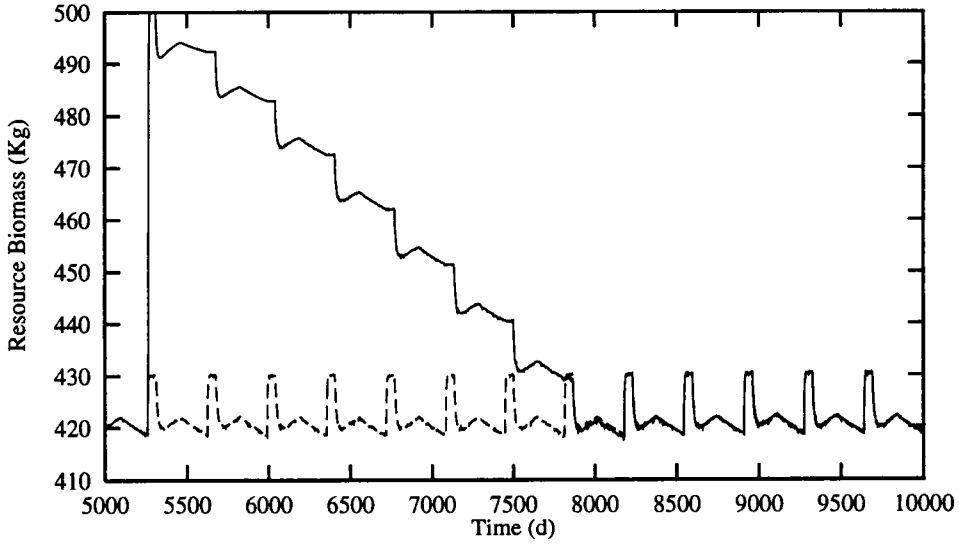



(b)

Figure 9: Toxicant exposure case 2 (see text for details). (a) The age and (b) lipid distributions of the fish population with $s = 0.05$ after the termination of a 10-$d$ exposure initiated on day 5,256.




(a)




(b)

Figure 10: Toxicant exposure case 2 (see text for details). Dynamic behavior of the fish population and resource for $a = 0.5$, $K = 5 \times 10^2$ and $s = 0.05$. (a) Total fish biomass (stressed —, unstressed ...). (b) Total resource biomass (stressed —, unstressed ...).

# VITA

Konstadia Lika was born in Karditsa, Greece, on September 28, 1964. She attended high school at the 2nd Lyceum of Nea Ionia, Athens and graduated in summer of 1982. In fall of 1983, she enrolled in the University of Crete at Heraklion, Greece, where she received a Bachelor of Science degree in Mathematics in summer of 1987. During her undergraduate studies she worked as a research assistant in the Institute of Applied and Computational Mathematics at Heraklion, Greece. From 1988 to 1989, she taught mathematics to high school students and in the following year she rejoined the Institute of Applied and Computational Mathematics as a research associate. In August 1990 she was accepted in the graduate program of the Mathematics Department at the University of Tennessee, Knoxville. She received a Master of Science degree in December 1992 and in December 1996 she graduated with a Doctor of Philosophy degree with major in Mathematics.

She currently has a postdoctoral position in the Department of Ecology, Evolution and Marine Biology at the University of California, Santa Barbara.